Inaugural dissertation

for

obtaining the doctoral degree

of the

Combined Faculty of Mathematics, Engineering and Natural Sciences

of the

Ruprecht - Karls - University

Heidelberg

Presented by

M.Sc. Jorge Lázaro Farré

born in Barcelona, Spain

Oral examination: 18th of October 2024

The regulation and scaling of developmental tempo across mammalian species

Referees:

Prof. Dr. Joachim Wittbrodt

Dr. Alexander Aulehla

Contents

Acknowledgements

First of all, I would like to thank Miki Ebisuya for these four years of guidance and support. Thank you for allowing me to fearlessly explore and develop my identity as a scientist.

I am grateful to all members of the Ebisuya lab, past and present, for their support and for making my PhD such a wonderful experience. Thanks to Mitsuhiro Matsuda for patiently teaching me and for our long scientific discussions, to Cassandra Villava for keeping the lab together and for the help with endless importations, to Maria Costanzo for being the best colleague I could have asked for. Our interactions, discussions and joyful fights always make my day. Thanks to Guillermo Martínez Ara for being a great desk mate and for bringing fresh perspectives into my project, to Abiram Eliab Olivares Resendiz for giving me advice on cell culture even after the lab split, to Marina Sanaki-Matsumiya for all the help in the tissue culture room, to Shuting Xu and Marina Marchenko for the time we spent together in Barcelona. Thanks to Maria Sintra for joining the Barcelona lab and making it so fun when we most needed it.

I am thankful to Vikas Trivedi for his continuous advice during this project. Thanks to the people of the Trivedi lab for their support, to Krisztina Arato for accommodating my crazy last-minute experiments and to Kristina Stapornwongkul for our insightful discussions and for the career advice.

Thanks to the members of my thesis advisory committee, Alexander Aulehla, Joachim Wittbrodt, Vikas Trivedi and Sean Megason, for their guidance and generous support. Thanks to Henrik Kaessmann for agreeing to serve on my defence committee.

I would like to thank our collaborators, Sebastian Diecke, Thomas B Hildebrandt, Giovanna Lazzari, Jun Wu, Stoyan Petkov and Rüdiger Behr, for providing us with the different stem cell lines and advice on how to culture them.

I am very grateful for the incredible work environment in EMBL Barcelona. Thank you all for creating such a welcoming and supportive community. Special thanks to Silvia Autet Balcells, Andra Aura Chirac and Alexandre Robert Moreno for making sure our science can happen in the best conditions.

I am thankful for the people I met at the MBL Embryology course, especially Matteo Fabbri and Ida Jentoft. Thank you for believing in me.

To Marc Duque Ramírez, thank you for always pushing me to do the best possible science.

None of this would have been possible without the support of my mother and sisters. Gracias!

To Júlia Charles Aymamí, thank you for your unconditional love, your overflowing patience and for illustrating my science. T’estimo.

Summary

The speed of embryonic development varies considerably across mammalian species. These differences in the tempo or duration of developmental processes are known to influence the final size and shape of organisms, serving as an important mechanism of evolutionary change. This thesis aims to understand how different mammals, despite using seemingly indistinguishable molecular toolkits, exhibit species-specific developmental rates. To this end, I have focused on investigating the timing of the vertebrate body axis segmentation.

The rate at which body segments form is controlled by the segmentation clock, the oscillatory gene expression found in the pre-somitic mesoderm (PSM) cells. The period of the segmentation clock oscillations differs greatly across vertebrates. However, investigating these temporal differences has proved challenging due to the difficulties in obtaining and quantitatively comparing embryos from different animal species. To overcome these challenges, I have used pluripotent stem cells (PSCs) from various mammals, a "stem cell zoo", to develop *in vitro* models of the segmentation clock. By differentiating PSCs into PSM cells, I have been able to study the developmental tempo of six mammalian species under similar experimental conditions. These species include humans, mice, rabbits, cattle, rhinoceros, and marmosets, which span a wide range of body sizes and morphologies.

Quantification of the segmentation clock oscillations revealed that their period scaled with the embryogenesis length rather than animal body weight. The biochemical kinetics of the core clock gene *HES7* showed clear scaling with the species-specific segmentation clock period. However, cellular metabolic rates did not exhibit a similar correlation. Instead, genes involved in biochemical reactions displayed expression patterns that scaled with the segmentation clock period, providing evidence of the transcriptional regulation of developmental tempo. To further explore this transcriptomic signature, I established a pipeline for screening genetic modifications affecting the segmentation clock period in human cells. By combining novel fluorescent reporters of biochemical kinetics with gene expression perturbations, I isolated human cell clones with accelerated or decelerated segmentation clock periods. Characterization of these clones revealed specific genes capable of modulating the segmentation clock period.

Overall, the stem cell zoo has uncovered general scaling laws governing developmental tempo at the cellular level. This research provides further insights into the mechanisms used by evolution to generate morphological diversity across species.

Zusammenfassung

Die Geschwindigkeit der embryonalen Entwicklung variiert erheblich zwischen den Säugetierarten. Diese Unterschiede in der Dauer der Entwicklungsprozesse beeinflussen die endgültige Größe und Form von Organismen und dienen als wichtiger Mechanismus der evolutionären Veränderung. Diese Dissertation zielt darauf ab, herauszufinden, wie verschiedene Säugetiere, trotz der Verwendung scheinbar nicht unterscheidbarer molekularer Toolkits, artspezifische Entwicklungsraten aufweisen. Zu diesem Zweck habe ich mich darauf konzentriert, die Segmentierungsgeschwindigkeit der Körperachse bei Wirbeltieren zu untersuchen.

Die Rate, mit der Körpersegmente gebildet werden, wird durch die Segmentierungsuhr gesteuert, die oszillatorische Genexpression in den Zellen des präsomitischen Mesoderms (PSM) aufweist. Die Periode der Segmentierungsoszillationen variiert stark zwischen verschiedenen Wirbeltieren. Allerdings war die Untersuchung dieser zeitlichen Unterschiede aufgrund schwerzugänglicher Embryonen und Mangels quantitativer Vergleiche schwierig. Um diese Herausforderungen zu überwinden, habe ich pluripotente Stammzellen (PSCs) von verschiedenen Säugetieren, einen sogenannten "Stammzellzoo", verwendet, um in vitro Modelle der Segmentierungsuhr zu entwickeln. Durch die Differenzierung von PSCs in PSM-Zellen konnte ich das Entwicklungstempo von sechs Säugetierarten unter ähnlichen experimentellen Bedingungen untersuchen. Zu diesen Arten gehören Mensch, Maus, Kaninchen, Rind, Nashorn und Marmosett, die eine breite Palette von Körpergrößen und Morphologien umfassen.

Die Quantifizierung der Segmentierungsoszillationen ergab, dass die Periode mit der Dauer der Embryogenese und nicht mit dem Körpergewicht der Tiere skaliert. Die biochemischen Kinetiken des Kernuhrgens HES7 zeigten eine klare Skalierung mit der artspezifischen Segmentierungsperiode. Allerdings zeigten die zellulären Stoffwechselraten keine ähnliche Korrelation. Stattdessen wiesen Gene, die an biochemischen Reaktionen beteiligt sind, Expressionsmuster auf, die mit der Segmentierungsperiode skalierten, was Hinweise auf die transkriptionelle Regulation des Entwicklungstempos liefert. Um diese transkriptomische Signatur weiter zu erforschen, habe ich eine Pipeline zur Untersuchung genetischer Modifikationen entwickelt, die die Segmentierungsperiode in menschlichen Zellen beeinflussen. Durch die Kombination neuartiger fluoreszierender Reporter für biochemische Kinetiken mit Veränderungen des Genexpressionsprofils, konnte ich menschliche Zellklone mit beschleunigten oder verlangsamten Segmentierungsperioden isolieren. Die Charakterisierung dieser Klone identifizierte spezifische Gene, die in der Lage sind, die Segmentierungsperiode zu modulieren.

Insgesamt hat der Stammzellzoo allgemeine Skalierungsgesetze aufgedeckt, die das Entwicklungstempo auf zellulärer Ebene regeln. Diese Forschung bietet weitere Einblicke in die Mechanismen, die von der Evolution genutzt werden, um morphologische Vielfalt über verschiedene Arten hinweg zu erzeugen.

To Júlia, for brightening my days

Preface

The research presented in this doctoral thesis was supported by the European Molecular Biology Laboratory (EMBL) International PhD programme and the Boehringer Ingelheim Fonds (BIF) PhD fellowship. It was carried out in the research group of Dr. Miki Ebisuya at EMBL Barcelona.

This thesis aims to determine why different animal species, despite using conserved molecular mechanisms, develop at different speeds. Using *in vitro* differentiation of pluripotent stem cells, I recapitulated the segmentation clocks of four novel mammalian species varying in body weight and taxa: marmoset, rabbit, cattle and rhinoceros. Together with mouse and human, I used this "stem cell zoo" to uncover general scaling laws governing species-specific developmental tempo.

This work has led to two published manuscripts. The following parts of this thesis have been adapted from those manuscripts.

Part I and II of Results

Lázaro, J., Costanzo, M., Sanaki-Matsumiya, M., Girardot, C., Hayashi, M., Hayashi, K., Diecke, S., Hildebrandt, T.B., Lazzari, G., Wu, J., Petkov, S., Behr, R., Trivedi, V., Matsuda, M., Ebisuya, M. (2023). *A stem cell zoo uncovers intracellular scaling of developmental tempo across mammals.* Cell Stem Cell, 30: 938-949.e7. https://doi.org/10.1016/j.stem.2023.05.014

Particular sections from the Introduction and Discussion

Lázaro, J., Sochacki, J., Ebisuya, M. (2024). *The stem cell zoo for comparative studies of developmental tempo*. Curr. Opin. Genet. Dev., 84. https://doi.org/10.1016/j.gde.2023.102149

1. Introduction

1.1 The evolution of animal form

Nature is beautiful. From the imposing blue whale to the delicate hummingbird, nature comes in a vast array of sizes, shapes, and colours. The origin of this animal diversity is arguably one of the most fascinating questions in biology. Evolutionary biologists have been trying for decades to address the problem of how morphology is altered during evolution. Given that adult morphology arises *de novo* in each generation, the evolution of new forms has to derive from changes in development [1]. Therefore, to understand the emergence of morphological diversity across species, one must look into the organisms' ontogeny.

Development is the process that gives rise to an adult animal starting from a zygote. During this time, all the different cell types in the body emerge and are organised in complex and functional tissues of various shapes and sizes. Therefore, a spatiotemporal coordination of developmental events is essential to achieve a correct morphology. We can understand development as a series of stereotypical events where correct order and timing are necessary for a defined output [2]. A classic example can be found in the early development of *Drosophila*. Gradients of maternally deposited effectors in the egg trigger a cascade of genetic events that, through the activation of various sets of zygotic genes, establish positional identity along the embryonic axes (reviewed in [3]). This ensures the expression of homeotic genes at the correct locations, which will later determine the regional characteristics of the embryo and control the formation of adult structures. The spatiotemporal coordination of this regulatory gene hierarchy allows the robust establishment of the *Drosophila* body plan [4]. Interestingly, comparative studies have revealed a great conservation of these regulatory genes across phyla [5]. Different species can reuse genetic elements to generate novel morphologies without having to establish new genetic strategies. For example, Hox genes containing similar homeobox domains as the ones found in the *Drosophila* homeotic genes are responsible for the axial specification of vertebrates and other phyla [6,7]. Evolution can tinker with regulatory elements, generating new modalities of development and, ultimately, new morphologies by using similar genes [8]. This requires the dissociation of different developmental processes, which are later reorganised and assembled into novel ontogenies [9]. The concept of developmental dissociability has had profound implications for understanding how development evolves. Apart from repurposing developmental modules, new ontogenies could be generated by simply shifting the timing of developmental events from one another. This change in the relative timing of developmental events is known as heterochrony [10], and constitutes a major mechanism in the evolution of animal form.

1.2 Heterochrony

The meaning of the term heterochrony has changed over the years (reviewed in [11]). It was first coined by Haeckel to describe exceptions to his universal Biogenetic Law, which stated that embryological stages reflect adult forms of evolutionary ancestors [12,13]. Heterochrony was found when a developmental event happened at a different time in the developmental sequence of an organism compared to its appearance in the phylogenetic sequence; hence, ontogeny was not recapitulating phylogeny. With the demise of the Biogenetic law, the term heterochrony was redefined by de Beer and Gould as a "*change to the timing or rate of developmental events, relative to the same events in the*

ancestor" [10,13]. Today, the most general definition of heterochrony applies to temporal shifts or changes in the rate of developmental processes across related taxa [11].

Heterochrony comprises a series of mechanisms that can lead to evolutionary change [10]. By prolonging, shortening or changing the rate of developmental events, evolution can modify the developmental trajectory of a species and alter its final morphology. Many examples of heterochrony have been documented over the years. Of note, a heterochronic event is thought to be responsible for the expanded brain size of humans compared to other primates [13]. During brain development, despite strong conservation of the developmental sequence across primates, humans prolong a defined developmental period of rapid neuronal growth, generating a greater number of neurons and, thus, bigger brains [14]. Understanding how these temporal changes can be encoded in the genome and deployed by cells and tissues is critical for understanding the mechanisms of evolution. Over the years, the field of Evolutionary Developmental biology (Evo-Devo) has offered a great framework to tackle these questions [15]. First, Evo-Devo studies have a clear comparative approach. Only by comparing ontogenies and phylogenies of multiple species will we uncover fundamental principles of development and describe how they changed throughout evolution. Second, the field's focus on the genetic and epigenetic players controlling developmental events is helping unveil the molecular mechanisms underlying evolutionary variation. The challenge remains in finding experimental systems that enable comparisons across a broad range of species while keeping the possibility of molecular-level analysis.

1.3 Somitogenesis, a system where timing controls morphology

Among the many processes in development where precise temporal control is necessary to obtain a defined morphology, somitogenesis might be one of the best examples. During early vertebrate development, somitogenesis segments the anterior-posterior body axis in chunks of mesodermal tissue known as somites (reviewed in [16]). These are precursor structures that will later give rise to various elements of the axial skeleton, including the vertebrae, back muscle, and dermis [17]. Somites are generated sequentially, with new pairs of segments separating from the precursor tissue, the pre-somitic mesoderm (PSM), at regular intervals. This results in the vertebrate embryo being developed in a head-to-tail sequence, with anterior structures being formed and patterned earlier than their posterior counterparts [7]. The pace at which somites are formed is controlled by the "segmentation clock", the oscillatory gene expression found in the cells of the PSM [18]. Tight temporal control of these signalling oscillations is essential to produce the correct number of segments in the embryo [19].

Somitogenesis occurs during the phylotypic period, a moment during embryogenesis when vertebrates manifest their canonical body plan [20]. That is, embryos of different species undergo identical organogenic events and converge to a similar morphology. The observation of this stage of high embryonic resemblance led to the formulation of the vertebrate hourglass model of development (**Fig. 1**). Vertebrate embryos, despite starting their development with various shapes, transition through a period of similarity and conserved gene expression before displaying species-specific characteristics [21]. The phylotypic period is characterized by high developmental constraints and low adaptability [22]. The two main processes at play during this period are the segmentation of the anteroposterior body axis via somitogenesis and the establishment of axial identity through the Hox timer (**Fig. 1**) [23]. Embryos are elongating, segmenting and regionalizing; therefore, variations at this stage can profoundly affect the body plan and final morphology. For example, a heterochronic acceleration of the segmentation clock with respect to the embryo elongation rate is responsible for the much larger number

of somites observed in snakes compared to other amniotes: around 300 somites in snakes versus 65 in mice [24]. Similarly, heterochronic shifts in the activation timing of Hox genes can change the position of limbs across species [25], or completely prevent their formation [26].

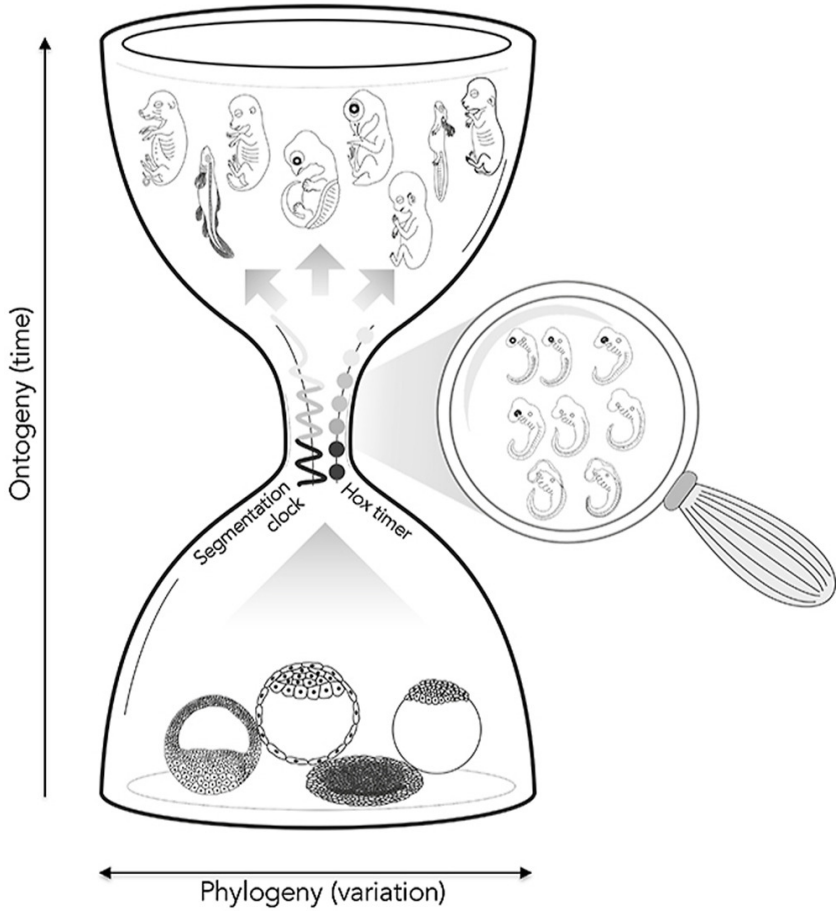

Figure 1: The developmental hourglass model.
In the hourglass model, the horizontal axis represents the variation between species (phylogeny), while the vertical axis represents the developmental progression (ontogeny). The bottleneck corresponds to the phylotypic period, a moment in development when embryos of different vertebrate species are most similar to one another (see drawings in the magnifying glass). It is during this time that the vertebrate body plan is established. The two main developmental processes acting at the phylotypic period are the segmentation clock and the Hox timer. Illustration extracted from Duboule [23].

1.4 The molecular identity of the segmentation clock

Changes in the rate of somitogenesis can affect animal morphology, but how is the pace of the segmentation clock established in the first place? The molecular identity of the segmentation clock has been linked to the Notch signalling pathway and its targets, members of the *Hes* (*Hairy* and enhancer of split) family of transcription factors, in a wide range of vertebrates, including chick [18], snake [24], mouse [27], zebrafish [28], *Xenopus* [29] and human [30,31]. The expression of these genes has been found to oscillate in the vertebrate PSM, with each oscillation controlling the formation of one somite.

In mouse, *Hes7* is considered to be the core oscillatory gene of the segmentation clock [32]. Cyclic *Hes7* expression is driven autonomously by a delayed autoregulatory negative feedback look. After being synthesized, the HES7 protein can bind to its own promoter and repress its expression [33]. When production ceases, fast HES7 degradation releases this inhibition and allows HES7 levels to increase once more, starting another oscillatory cycle. Mathematical models suggest that the delay in the feedback loop is critical in determining the period of the oscillations [34]. This delay is generated by the time taken to transcribe, splice, transport and translate the genetic product of *Hes7*. Experimentally removing two of the three *Hes7* introns has been shown to shorten the period of oscillations, accelerating the segmentation clock and producing embryos with more somites [35]. Similarly, stabilising the HES7 protein by disrupting its ubiquitination sites results in dampened oscillations [36]. This highlights the importance of molecular kinetics in establishing the pace of developmental processes.

Despite strong conservation in its oscillatory machinery, the period of the segmentation clock differs greatly across vertebrate species: around 30 min in zebrafish [37], 90 min in chicken [18], 100 min in snake [24], 2 hours in mouse [38], 4 hours in pig [39], and 5 hours in human [30,31]. How the species-specific segmentation clock period is determined has been a longstanding question in the field. Efforts have been made to characterise the parameters contributing to the feedback loop of *Hes* genes [36,40]. Quantification of the splicing and export dynamics of *Hes* transcripts has revealed differences across mouse, chicken and zebrafish embryos, suggesting that changes in these parameters might contribute to the species-specific segmentation clock periods [41]. However, interspecies comparisons have remained challenging due to the different body environments of each species. The strong dependence of the segmentation clock on molecular kinetics makes it very sensitive to temperature and external variation [37,42]. Therefore, in order to systematically compare the parameters controlling the speed of the segmentation clock across species, experimental conditions must be normalised. *In vitro* modelling of developmental processes using pluripotent stem cells (PSCs) has recently emerged as a way to overcome many of these issues [43]. These methods hold great promise for understanding the mechanisms underlying the species-specific differences in developmental time.

1.5 *In vitro* recapitulation of the segmentation clock using PSCs

PSCs have revolutionized the field of developmental biology, especially in the last two decades. Since the discovery of mouse PSCs in 1961 [44], researchers have been able to derive PSCs from several species and use them to generate a variety of tissues, organs and even complete organisms (reviewed in [45]). The two main properties of PSCs are their ability to self-renew and their potency. During development, inner cell mass PSCs, also known as Embryonic Stem Cells (ESCs), will give rise to all embryonic tissues. In the lab, PSCs can be maintained in culture for indefinite periods of time and, upon receiving the correct signals, differentiated into derivatives of the three germ layers: ectoderm, mesoderm and endoderm. These properties have made them very attractive for Developmental Biology studies. For example, *in vitro* differentiation of PSCs can provide a better understanding of the mechanisms behind embryonic cell fate specification and their necessary signals [46]. Also, with the right culture conditions, PSCs can generate complex 3D structures that contain various cell types and recapitulate morphogenetic events (reviewed in [47]). These mini-organs in a dish, known as organoids, have been used to model and study the development of various tissues, including kidney [48], brain [49] or intestine [50]. Finally, PSCs open the possibility of expanding developmental studies to animals whose embryos would be hard to obtain due to practical or ethical reasons, such as humans [43,51].

In vitro recapitulation of the segmentation clock has been achieved using mouse and human PSCs [30,31,52,53]. By mimicking the *in vivo* signalling environment, modulating the WNT, FGF, BMP and TGF-β pathways, PSCs are differentiated into PSM-like cells expressing the same markers as those found in the embryo. Segmentation clock oscillations can then be visualized using genetic reporters that allow fluorescent or luminescent quantifications [38,54]. In mice, these *in vitro* recapitulated oscillations have been found to have a period that closely matches that of the embryo [52]. The cell-autonomous nature of the segmentation clock makes it particularly suitable for these kinds of *in vitro* studies. Cells of the PSM interact with each other to produce tissue-level coordinated oscillations [55]. However, even when isolated, they can still oscillate autonomously at the right period [56]. Therefore, the question of how the segmentation clock period is determined should be framed at the cellular level. 2D *in vitro* models of development where cellular identity but not tissue architecture is recapitulated offer a simplified system to study these cell-autonomous processes. Stem cell models are also very amenable to genetic modification and precise quantitative measurements, allowing a detailed analysis of the molecular players involved in developmental processes.

1.6 Interspecies comparisons of developmental tempo

A recent study by Matsuda et al. [57] has recapitulated *in vitro* the segmentation clock of mice and humans to address the mechanisms behind their species-specific differences in developmental tempo. Consistent with *in vivo* measurements, murine and human induced PSM cells displayed HES7 oscillations with a period of 2-3h and 5-6h, respectively. This two to three-fold difference was not caused by the *HES7* sequence, as swapping the mouse *HES7* genomic locus for that of the human did not influence the oscillatory period of mouse embryos. Instead, changes in the biochemical reaction kinetics governing the *HES7* negative feedback loop were responsible for the period differences. *HES7* production rate, splicing delay and protein degradation were found to be approximately twice as fast in mouse induced PSM cells compared to those of human. Mathematical modelling confirmed that changes in those parameters were sufficient to recapitulate the observed differences in the segmentation clock period. Therefore, comparing mouse and human induced PSM cells under similar experimental conditions revealed that changes in the speed of biochemical reactions are responsible for the species-specific differences in developmental tempo (**Fig. 2A**).

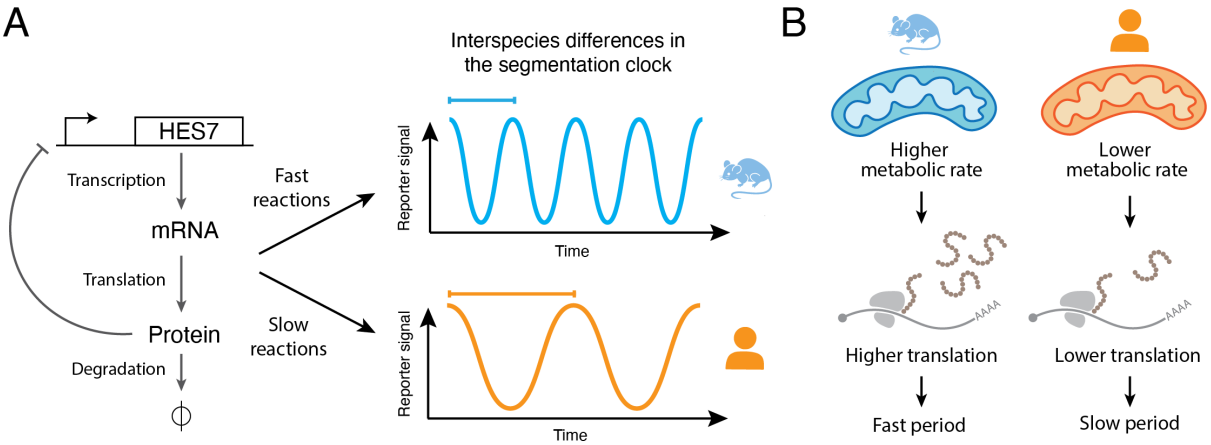

Figure 2: Interspecies comparisons of the segmentation clock tempo.
(A) Changes in the speed of biochemical reactions involving the HES7 negative feedback loop are responsible for the differences in period observed between mice and humans. (B) Variations in the rate of mitochondrial metabolism between mouse and human PSM cells lead to changes in the rate of protein translation, ultimately causing differences in their segmentation clock period. Adapted from Iwata et al. [58].

A parallel study by Rayon et al. [59] tackled a similar question using the developing spinal cord. The emergence of neuronal subtypes follows a species-specific temporal progression that can be modelled *in vitro* (reviewed in [60]). In mice, spinal cord motor neuron development occurs over 3-4 days, whereas in humans, it spans approximately 2 weeks [61]. When PSCs differentiate into motor neurons, this temporal difference is reflected, with the process taking about two to three times longer in humans compared to mice. The authors used this *in vitro* model to study the mechanisms governing the species-specific temporal scaling. Changes in the gene regulatory network, DNA sequence or signalling sensitivity failed to account for the differences in tempo. Instead, similar to what has been described for the segmentation clock, the faster progression in mice corresponded to an increased rate of protein degradation.

Overall, these results suggest a general cell-autonomous mechanism through which, by changes in their biochemical reaction speeds, different animal species can control the tempo of conserved gene regulatory developmental networks. However, two questions still remain: what is the underlying cause behind these interspecies differences in biochemical kinetics, and how did they first emerge at the genetic level? Limiting the comparisons to mice and humans has made it challenging to examine general relationships between developmental tempo and other cellular parameters. Only expanding these studies to more species covering a wider range of phylogenies will allow a better understanding of how developmental tempo changes throughout evolution.

Both mentioned studies are great examples of how stem cell-based models can be used to study developmental timing. Species-specific developmental rates can be precisely recapitulated *in vitro* using PSCs, suggesting that developmental tempo is a cell-intrinsic parameter. This is supported by several xenotransplantation experiments where injecting human PSC-derived teratomas or cortical neurons into a mouse host did not alter their developmental pace [62,63]. Similarly, in embryonic transplantation experiments across species of different developing speeds, the temporal dynamics of the donor tissue are usually conserved [64–66]. PSC-based models of development can exploit this cell-autonomous nature, allowing researchers to better examine the mechanisms controlling developmental tempo across various species. Nevertheless, extrinsic factors can also influence developmental tempo, as shown by the mild acceleration of human neurogenesis during interspecies co-differentiation with mouse PSCs [67]. Additionally, interactions between the host tissue and small heterochronic grafts have been seen to alter the donor tissue contributions during embryonic axial elongation [68]. Characterising the external factors capable of modulating developmental tempo will be critical for understanding this parameter.

1.7 Metabolism as a driver of developmental tempo

In vitro recapitulation of the human and mouse segmentation clocks has shown that differences in the biochemical reaction rates are responsible for the species-specific developmental rates [57]. Cellular metabolism has emerged as a strong candidate to explain these differences due to its direct connection

to energy production and biochemical kinetics [69,70]. Interestingly, when normalised to unit mass, metabolic parameters like the oxygen consumption rate or the glycolytic rate have been measured to be almost twice in mouse induced PSM compared to that of humans [71]. These differences in metabolic rates could be underlying the changes in developmental tempo. Manipulation of the cellular metabolism further supports this connection. Inhibiting electron transport chain components in human cells slowed down their segmentation clock, not by affecting ATP synthesis, but by reducing the NAD+/NADH ratio. Conversely, artificially increasing the NAD+/NADH ratio by expressing a bacterial NADH oxidase led to a mild acceleration of the oscillatory period. Characterisation of cells treated with electron transport chain inhibitors showed reduced protein translation, suggesting a mechanistic connection between metabolism, protein synthesis and the segmentation clock (**Fig. 2B**) [71]. Changes in the metabolic state have also been linked with alterations in PSM differentiation and segmentation *in vivo* [72–75]. Mouse and chicken PSM show a gradient of glycolytic activity along the anterior-posterior axis [72,75]. Altering this glycolytic activity leads to segmental defects and changes in the segmentation clock period through modulation of Wnt signalling, highlighting the role of metabolism in controlling developmental processes [73,74].

Cortical development provides another example of the link between metabolism and developmental tempo. As mentioned previously, brain development in humans is heterochronically protracted, resulting in increased size and complexity [14]. Similarly, human cortical neurons derived from PSCs show a prolonged maturation timing even when transplanted into mouse brains [62,76,77]. This suggests that a cell-intrinsic mechanism governs their developmental program. Stimulating mitochondrial metabolism can significantly accelerate human neuronal development *in vitro*, allowing cortical neurons to reach maturation milestones ahead of time [78]. Conversely, the reduction of mitochondrial activity in murine PSC-derived neurons led to a slower rate of development. These results suggest that, similar to the segmentation clock, metabolic activity and, more concretely, mitochondrial metabolism can modulate the pace of neurogenesis [79]. In the future, it will be important to address the similarity between the regulatory principles controlling developmental tempo across tissues and animal species. For example, it is remarkable that metabolism can act on two very different timescales, i.e. hours in the case of the segmentation clock and months for corticogenesis. The mechanisms through which metabolism acts, as well as its upstream regulators, remain to be elucidated.

Apart from changes in energy production, metabolism can regulate cellular functions by controlling the concentration of key metabolites, such as those involved in epigenetic modifications (reviewed in [80]). Interestingly, studies using *in vitro* models of cortical neuron maturation have highlighted the role of epigenetics in modulating developmental tempo [81]. During human cortical development, an epigenetic barrier acting in progenitor cells has been shown to hold the progression of neuronal maturation programs. Inhibiting a subset of these regulators can accelerate the maturation rate of human cortical neurons differentiating from PSCs, showing earlier appearance of synaptic markers. These results suggest that the temporal progression of cortical neuron development is modulated by gradually releasing this epigenetic repression [81]. Similar *in vitro* models of cortical development are also being used to screen for small molecules with the ability to modulate developmental tempo [82]. They reported a cocktail of methyltransferase and demethylase inhibitors with the ability to promote earlier human neuronal maturation. How these factors regulate developmental tempo across species still has to be tested.

1.8 Allochrony

Both the segmentation clock and motor neuron differentiation have shown a two to three-fold temporal difference between mice and humans [57,59]. Interestingly, comparing the overall sequence of embryonic development between these species reveals a similar pattern. The process of embryogenesis in humans involves the same series of events as in mice but takes two to three times longer (**Fig. 3**) [83]. During this time, embryos have a similar size, generate the same structures and use conserved molecular pathways. However, human embryogenesis takes 60 days, while mouse embryos finish the whole process in only 20 [84]. These scaled differences in the pace of development among species are known as developmental allochronies [85]. Contrary to heterochrony, during allochrony, all temporal processes are scaled proportionally and thus no morphological changes should be immediately expected. Yet, if overall morphology remains unchanged, why do some species develop faster than others?

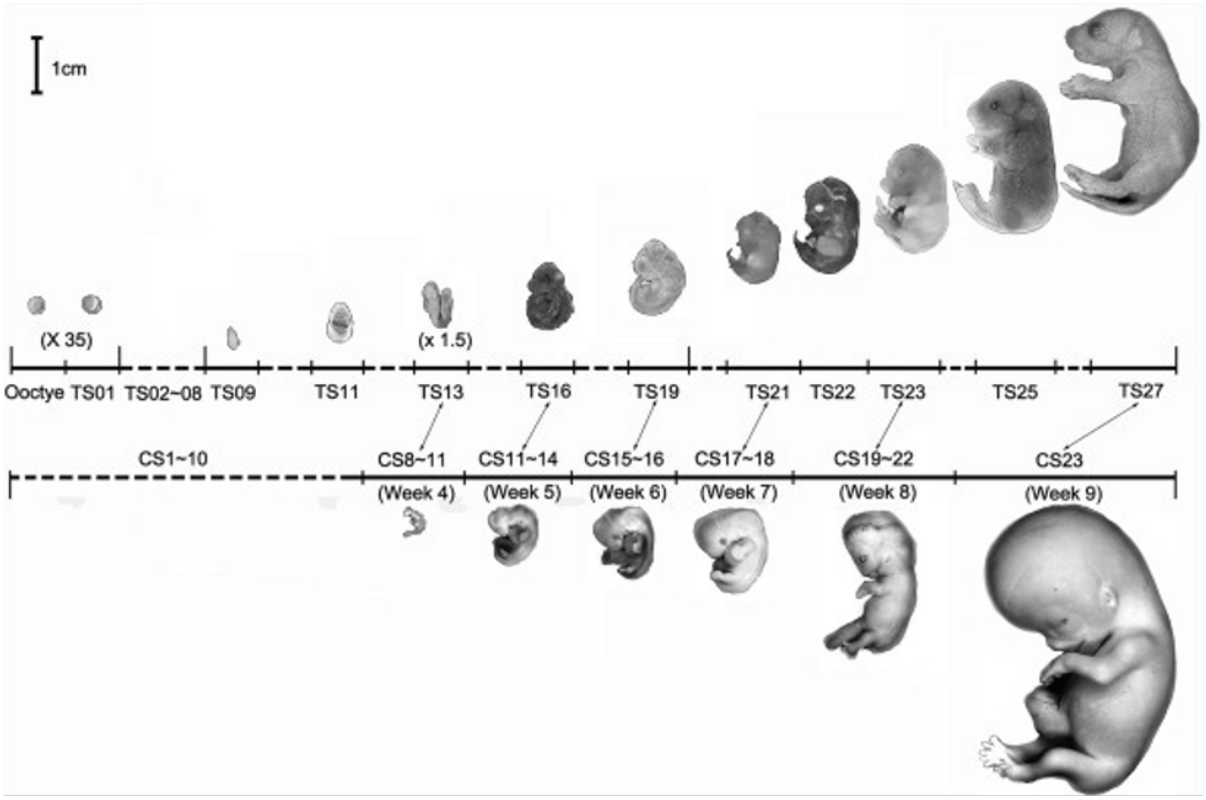

Figure 3: Allochrony between mouse and human embryogenesis.
On the top, mouse embryogenesis based on the Theiler staging system. The last stage is reached at about 20 days post-fertilization. On the bottom are human embryological stages as described by the Carnegie Institution of Washington. It takes approximately 60 days (week 9) to reach the end of human embryogenesis. There is a 2 to 3-fold temporal scaling between mouse and human embryogenesis. The double-headed arrows point to embryos at similar stages of organogenesis. Adapted from Xue et al. [83].

Comparisons of developmental length across animal species have suggested a correlation with adult body size [86,87]. In general, small species develop faster and have shorter gestation periods than bigger species. These temporal differences have been generally related to the life histories of each animal.

Smaller species normally follow the r-strategy, accelerating their development, sexual maturity and senesce to adapt to rapidly changing environments [88]. Big species, on the other hand, tend to live in more stable ecosystems and can follow the K-strategy, which is characterised by slow development, fewer offspring, and longer lifespan [88]. Therefore, tuning their developmental tempo allows animal species to maximise their fitness and survival rate. The pace of early development has also been linked with phenotypic differences during the postnatal and adult stages. For example, the period of somitogenesis is correlated with the duration of brain development and the adult brain size [87]. The synchronisation of developmental timing across tissue types and stages suggests the existence of a common regulator of tempo. This master clock could potentially orchestrate evolutionary changes affecting most tissues in the organism, such as alterations in the body size. Investigating the mechanism behind developmental allochronies could help better understand the evolution of phenotypes like body size or ageing, directly related to the life history strategy of each species.

1.9 Scaling with size

Characterisation of metabolic rates in mouse and human-induced PSM cells, as well as cortical neurons, led to a consistent conclusion. Mouse cells have a higher mass-specific metabolic rate compared to their human counterparts. This is in line with one of the most universal scaling rules found in nature, the Kleiber law [89]. This law postulates that an organism's basal metabolic rate increases to the ¾ power of its total body mass. Therefore, when normalised to their mass, small animals will display higher metabolic rates compared to bigger species. This relationship has been extended across a wide range of organisms and phylogenetic groups, from unicellular organisms to the biggest mammals or plants [90]. Interestingly, a number of different biological parameters show correlations with body weight, also known as allometric relationships [91]. Lifespan, heart rate or gestation period all obey allometric quarter-power scaling laws (reviewed in [92]). Moreover, the recent quantification of species-specific developmental rates would also suggest a connection with body weight [57,59,71,78]. The origin of these universal laws has been a longstanding question in biology.

Metabolism controls the production of energy and building blocks in an organism (reviewed in [93]). Therefore, the rate of metabolism constitutes a limiting step for scaling many biological processes. Cells in an organism cannot grow faster without a sufficient supply of energy and materials. Understanding how metabolic rate scales across organisms is essential for explaining the varying pace of biological processes. Mammalian metabolism is fueled by a hierarchical vascular transport network whose structure can constrain substrate delivery and, thus, metabolic rate. The properties of fractal-like biological networks have been proposed to underly the scaling of metabolism across all levels of organization [90,94]. In favour of this hypothesis, the metabolic rate of mammalian cells measured *in vivo* scales with the body weight of the organism. However, cells cultured *in vitro*, effectively free from the vascular network constraints, show a cellular metabolic rate that converges to a unique value in all mammals irrespective of size [90,95]. This suggests that cellular metabolism is not a cell-intrinsic parameter. Interestingly, in humans and mice, the metabolic rate of PSC-derived PSM cells and neurons scales with both the body size and the species-specific developmental tempo [71,78]. Given that these cells are not constrained by the vascular transport network, if metabolism were to set the pace of development according to the organism's size, how can the size-specific metabolic rate be maintained in the first place? This problem becomes more evident when considering that early developmental processes such as the segmentation clock occur when vasculature is not fully formed and embryonic

size is similar across species [96]. Unravelling the relationship between organism size, metabolic rate, and developmental pace will require analysing these parameters in a larger number of species.

1.10 A zoo of possibilities

Most studies of developmental tempo involving stem cell models have focused on comparing mice and humans. The large phenotypic differences and number of available resources for cell culture make these species convenient choices. However, expanding this research to include additional animals is crucial. This broader approach would help us assess the generality of our findings and determine what constitutes a universal principle of development or a species-specific behaviour. In recent years, the reprogramming of adult somatic cells into induced pluripotent stem cells (iPSCs) has increased our capacity to perform interspecies comparisons (reviewed in [43]). These iPSCs can be generated by expressing the four transcription factors *OCT4*, *SOX2*, *MYC* and *KLF4*, also known as "Yamanaka factors", in somatic cells such as fibroblasts [97,98]. Similar to ESCs, iPSCs can proliferate indefinitely and differentiate into derivatives of the three germ layers. However, by contrast, iPSCs are not derived from embryonic tissue, constituting a more practical PSC source for many animal species. Human iPSCs are already being used for disease modelling, drug screenings and stem cell-based regenerative therapies (reviewed in [99]). Moreover, iPSC lines have been derived from a plethora of wild and farm animals, generating a true zoo of stem cells across the world [100]. Some of these species include bats, opossums, rhinoceros, as well as several primates [43]. Using these PSCs enables the investigation of developmental programs across multiple animal species, shedding light on the evolution of cell- and tissue-autonomous regulatory mechanisms. Nevertheless, it is important to point out that most of the currently available PSCs have a mammalian origin. A better understanding of the mechanisms required for PSCs maintenance is needed to derive high-quality stem cells from other vertebrate species, including fishes, birds and reptiles [101,102]. Only then will stem cell technologies facilitate a holistic understanding of Developmental Biology across the animal kingdom.

Comparisons across PSC-derived brain organoids of various primates are already revealing interspecies differences in their developmental progression [103–105]. Similar to what is observed *in vivo*, human brain organoids were found to be larger than those of gorilla or chimpanzee [103]. A delay in the transition from highly proliferative neuroepithelial cells to neurogenic radial glial cells was found to be responsible for the increased number of neuronal cells in human organoids. This transition was linked to a change in cell shape driven by an epithelial-to-mesenchymal transition regulator. Early overexpression of this transcription factor in human brain organoids produced an ape-like morphology, highlighting the importance of the transition's timing for human brain expansion [103]. Moreover, transcriptomic characterisation of human, chimpanzee and macaque brain organoids has shown human-specific gene expression patterns that could help explain human brain evolution [104–106]. PSCs from these different species can also be fused to generate hybrid tetraploid organoids, providing a controlled system to dissect *cis*- and *trans*-acting regulatory mechanisms [107]. Altogether, the possibility of generating species-specific tissues using iPSCs allows researchers to tackle unprecedented evolutionary and developmental biology questions.

2. Aims of the study

Embryos from different mammalian species, despite using almost indistinguishable molecular toolkits, develop at different speeds. These controlled changes in developmental tempo are known to drive evolutionary variation by altering the morphology and size of the organism. *In vitro* modelling of developmental processes using PSCs has revealed that species-specific rates of biochemical reactions and cellular metabolism are responsible for the differences in developmental tempo observed between mice and humans. Still, whether this mechanism constitutes a general principle of mammalian development, as well as the underlying cause behind these interspecies differences in biochemical kinetics, remains unknown. This thesis aims to expand the interspecies comparisons of developmental tempo to a larger number of animals and examine general scaling relationships between the speed of development and other cellular parameters. To this end, I recapitulated the segmentation clock of various mammalian species *in vitro* using PSCs, establishing a "stem cell zoo" that allows the quantitative study of species-specific developmental rates.

To generate such a general experimental platform, the first aim of this study was to gather PSCs from diverse mammalian species and differentiate them into PSM cells under similar experimental conditions. I then visualised the segmentation clock using a reporter for *HES7* expression and compared the period of oscillations across species. These quantifications allowed me to correlate the speed of development to other organismal properties, such as body size or gestation length.

With the stem cell zoo in hand, the second aim was to characterise the relationship between developmental tempo and different cellular parameters. To this end, I quantified the speed of biochemical reactions, the metabolic rate and the PSM transcriptional signature across species. My goal was to describe cellular properties that scale with developmental tempo and analyse how they potentially influence its rate.

Finally, the third aim was to study the genetic control of developmental tempo. By combining fluorescent reporters of biochemical rates, flow cytometry and single colony segmentation clock measurements, I identified different genetic perturbations that can accelerate the developmental tempo of a given species.

The insights gained from this study have enhanced our understanding of how developmental speed is established across species. By characterising the mechanisms behind developmental tempo, we can start to unravel how temporal differences are encoded in the genome and utilised during evolution to produce morphological changes.

3. Results

3.1 Part I: A stem cell zoo platform to study interspecies differences in the segmentation clock

Comparisons between mouse and human developmental processes have suggested that changes in the speed of biochemical reactions are responsible for the interspecies differences in developmental tempo. However, it remains to be determined whether this represents a universal mechanism for temporal control and how it relates to the organisms' characteristics. Using the segmentation clock as a model, I sought to expand previous results by establishing a general platform to study differences in developmental tempo across several mammalian species. For this, I first needed to collect PSCs from various mammalian species and then develop protocols that allow the differentiation to PSM under similar experimental conditions (**Fig. 4**). Previously analysed parameters in mice and humans have suggested a scaling with body size. Bigger species develop slower and have lower metabolic rates compared to small animals. Therefore, to test the generality of these observations, I expanded the range of body sizes by analysing the developmental properties of species bigger than humans. The aim of studying animals with varying phenotypes is to increase our understanding of how developmental tempo is established across species.

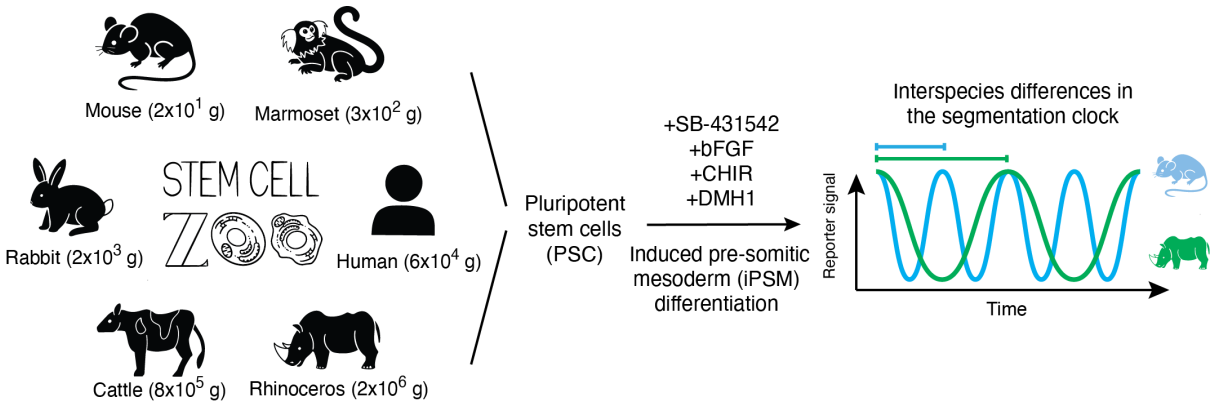

Figure 4: The stem cell zoo.
Schematic illustration of the workflow used for the stem cell zoo. PSM-like cells differentiated under similar culture conditions show species-specific segmentation clock periods. The average adult body weight of each species is displayed.

3.1.1 Assembling the stem cell zoo

To expand our stem cell collection, I gathered PSCs from diverse mammalian species, including common marmoset (*Callithrix jacchus*), rabbit (*Oryctolagus cuniculus*), cattle (*Bos taurus*) and southern white rhinoceros (*Ceratotherium simum*). Together with mouse and human PSCs, these species exhibit adult body weights ranging from 50 grams to 2 tonnes and gestation lengths spanning from 20 days to 17 months. Given the five orders of magnitude difference in body weight, I expected significant variation in the developmental tempo of these animals. Additionally, these species represent three distinct phylogenetic clades: Primates (marmoset and human), Glires (mouse and rabbit), and Ungulates

(cattle and rhinoceros). This selection constitutes a diverse sampling of mammals that is typically uncommon for developmental studies. I used mouse epiblast stem cells (EpiSC) [108], rabbit ESCs [109], cattle ESCs [110], rhinoceros ESCs [111], human iPSCs [98] and marmoset iPSCs [112] to induce PSM-like cells from these species.

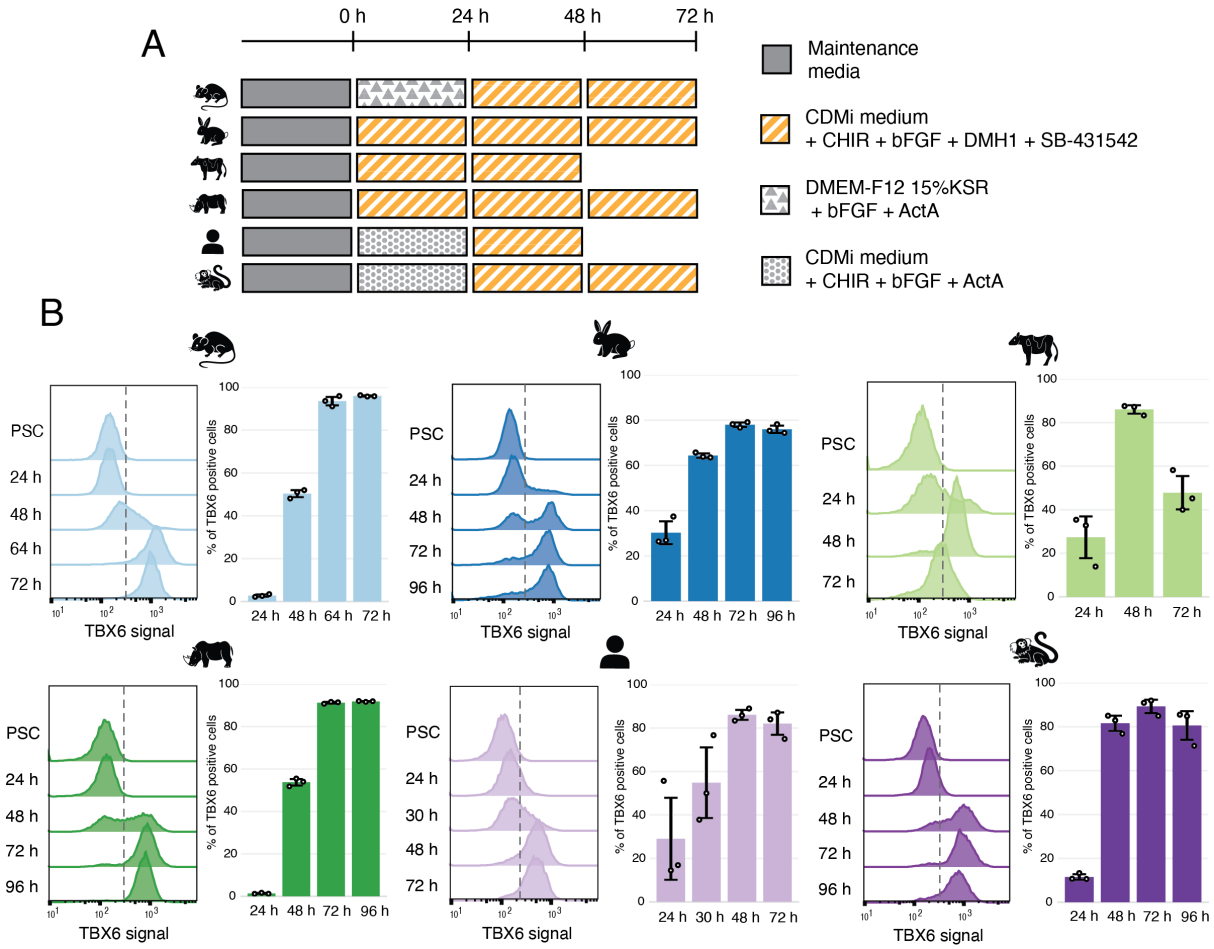

Figure 5: Characterization of the PSM differentiation protocols.
(A) Schematic representation of the protocols used to induce PSM-like cells (iPSM) from PSCs of different mammalian species. PSCs were cultured in the maintenance media optimized for individual species, and the media were changed to the differentiation media at time zero. (B) Left: representative histogram of flow cytometry analysis during iPSM induction for the six species. The staining signal of the PSM marker *TBX6* on each day of differentiation is displayed. The dashed line corresponds to the threshold used to determine positive cells compared to the stem cell control. Right: iPSM induction efficiency throughout differentiation for six species. The percentage of cells expressing *TBX6* was quantified based on the threshold shown on the left (dashed line). Error bars indicate means ± SD (n= 3).

The PSCs were obtained from collaborators, and their culture conditions were optimized in the lab. The culture protocols for mouse and human cells were previously developed by Mitsuhiro Matsuda [30,57]. Maria Costanzo and Marina Sanaki-Matsumiya optimized the culture for cattle ESCs, while I worked on improving rhinoceros, rabbit, and marmoset culture. Optimization consisted in establishing stable feeder-free pluripotent stem cell lines by trying combinations of PSC-formulated media and growth factors (data not shown). The result was six mammalian cell lines with PSC-like morphology, stable

growth rate, and no signs of differentiation. To induce PSM-like cells from all species, I adapted the differentiation protocols already described for mouse EpiSCs and human iPSCs (**Fig. 5A**) [30,57]. These protocols recreate *in vitro* the signalling events necessary for the emergence of PSM. In brief, cells were induced by culturing them in media containing Chiron (CHIR, WNT signalling activator), bFGF, DMH1 (BMP signalling inhibitor), and SB-431542 (TGF-β signalling inhibitor) (see Methods for more details). Before this induction step, human, marmoset and mouse PSCs had to be pre-treated with different factors to accommodate their varying degrees of pluripotency. *In vitro* induction of PSM requires following the correct developmental progression seen during ontogeny. Cells with a high degree of pluripotency cannot be directly differentiated into PSM and should instead follow a stepwise induction that more closely resembles their developmental trajectory. In this case, human and marmoset PSCs were first differentiated into primitive streak by culturing them with Activin A, bFGF and Chiron. Similarly, mouse cells were maintained as EpiSC instead of ESCs to allow a more direct PSM induction. Despite these species-specific initial differences in the protocol, identical media was used for all species when measuring the induced PSM cells, minimizing the effect of external factors in the quantifications (**Fig. 5A**).

The differentiation efficiency was measured using *TBX6* expression, a well-established marker for PSM fate [113]. Over the induction period, *TBX6*-positive cells progressively accumulated within the cultures, ultimately reaching a final yield of 80-90% in all species (**Fig. 5B**). All subsequent measurements were done on the most efficient day of differentiation for each species and using the culture in bulk. The goal of the induction protocols was to bring cells to a similar final condition in which they can be analysed and compared. Interestingly, the time of maximal induction differed across species. This variation in the timing of PSM differentiation could be interpreted as an interspecies difference in developmental tempo. However, the induction trajectories cannot be easily compared with each other, as naïve PSCs could take longer to differentiate than those in a more primed state.

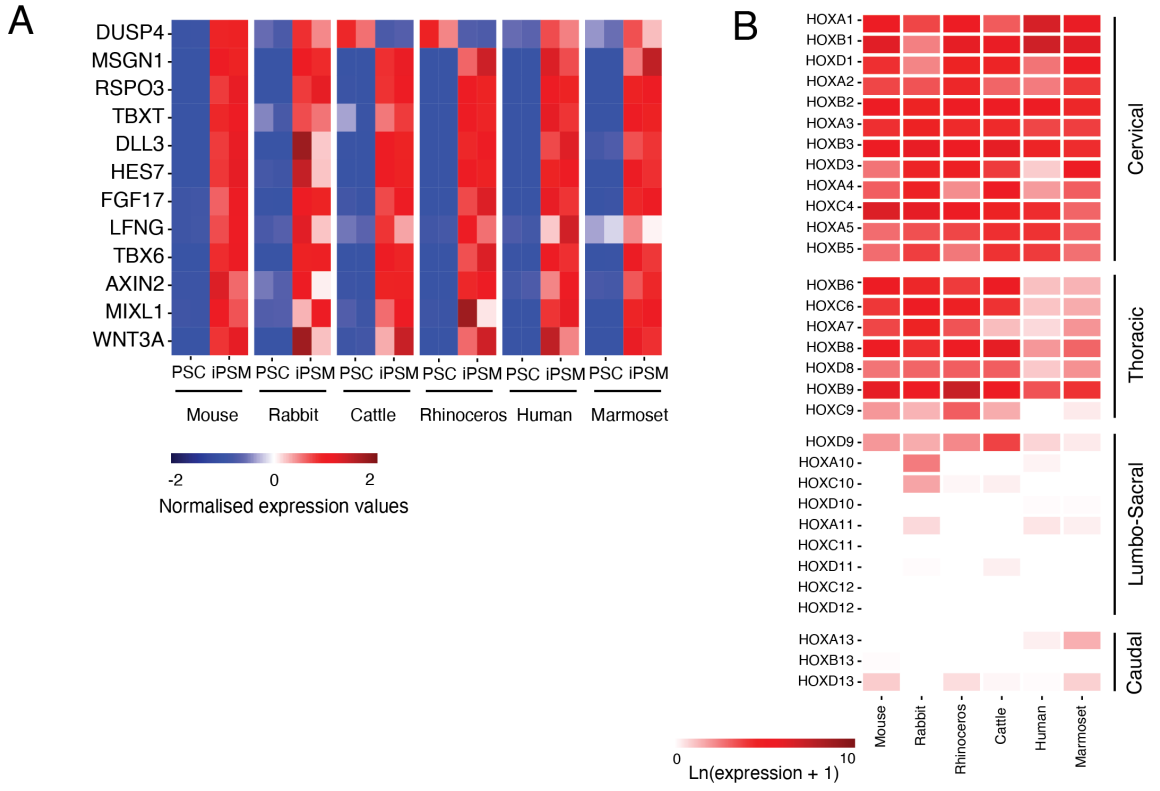

Figure 6: Transcriptomic characterization of the induced PSM cells.
(A) Heatmap of PSM differentiation from the RNA-seq data. Values for each gene were normalized to the mean between PSC and iPSM samples for each species. (B) *HOX* gene expression heatmap in iPSM cells. Rows represent individual *HOX* genes ordered by anterior-posterior position. Missing *HOX* genes did not have one-to-one orthology across all species. The anatomical anterior-posterior identity of each *HOX* group is indicated on the right.

To better characterize the identity of the induced PSM-like cells from the four new mammalian species and compare them to the established mouse and human models, I used bulk RNA-sequencing (RNA-seq) analysis. Induced cells showed a general expression of PSM markers such as *TBX6*, *MSGN1*, *HES7* and *LFNG* in all species (**Fig. 6A**). Moreover, *HOX* gene expression revealed a similar thoracic-lumbar fate across the induced PSM cells (**Fig. 6B**). This is particularly important considering the anterior-posterior slowdown in the timing of somite formation observed *in vivo* [114]. With a common fate and axial identity, the *in vitro*-derived PSM-like cells constitute a reliable platform for comparing the temporal dynamics of the segmentation clock across different species. The induced PSM-like cells are hereafter referred to as iPSM cells.

Overall, I expanded the previous human and mouse developmental models by inducing PSM cells from four novel mammalian species (**Fig. 7**). These cells can be differentiated with high efficiency and compared under the same experimental conditions, constituting an ideal system for studying interspecies differences in development.

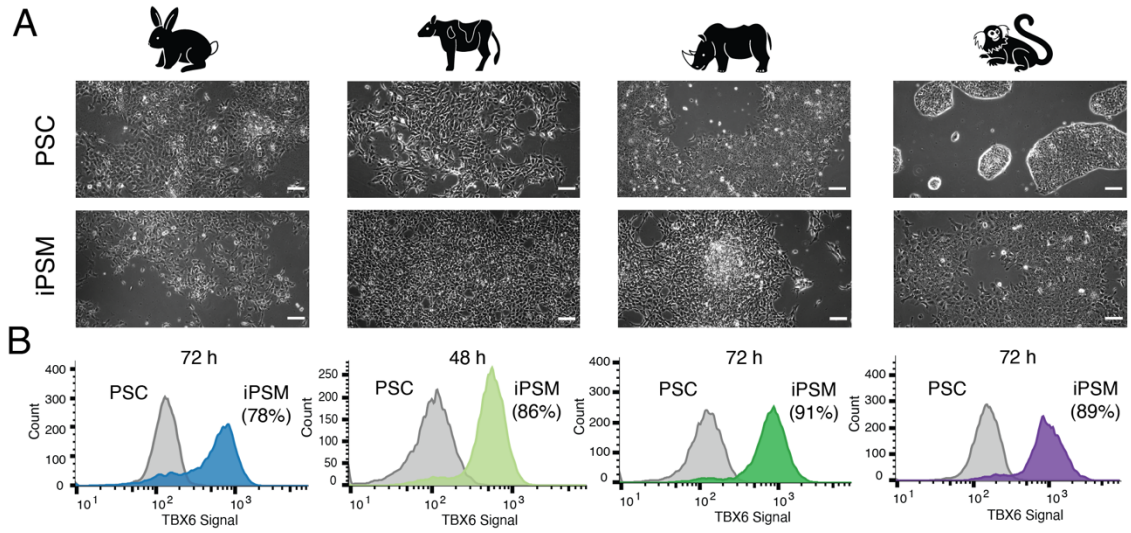

Figure 7: PSM induction in four new mammalian species.
(A) Bright-field microscopy images of PSCs and iPSM cells from each species. Scale bars represent 100 microns. (B) Flow cytometry analysis of the PSM marker *TBX6*. Histograms show *TBX6* expression in PSCs (grey) and iPSM cells (coloured) for each species at the most efficient day of induction. The average percentage of TBX6-positive cells compared to the PSC control and the time of sample collection are indicated.

3.1.2 Quantification of the segmentation clock across species

To visualize the oscillations of the segmentation clock, I utilized an exogenous luciferase protein under the control of the *HES7* promoter. This reporter allows for the quantification of the endogenous *HES7* oscillatory activity [54]. In mammals, *HES7* constitutes one of the core oscillatory genes of the segmentation clock [32,115]. Comparing the *HES7* gene across the six species revealed a high degree of conservation of its protein and mRNA (**Fig. 8** and **Supp. Table 1**). Previous studies have demonstrated that mouse embryos containing the human *HES7* locus maintain their original segmentation clock period [57]. The similarity tree of the *HES7* mRNA, even with introns, closely matched the evolutionary history of these species (**Fig. 8B**). Moreover, the percentage identity between the mouse and human *HES7* promoter sequences is not higher than any other pairwise comparison within the six species (**Supp. Table 1**). For these reasons, in this study, I decided to use a *HES7* reporter based on the human sequences for all species. Utilising the same reporter also reduces the number of variables and helps in focusing on the intracellular differences across species.

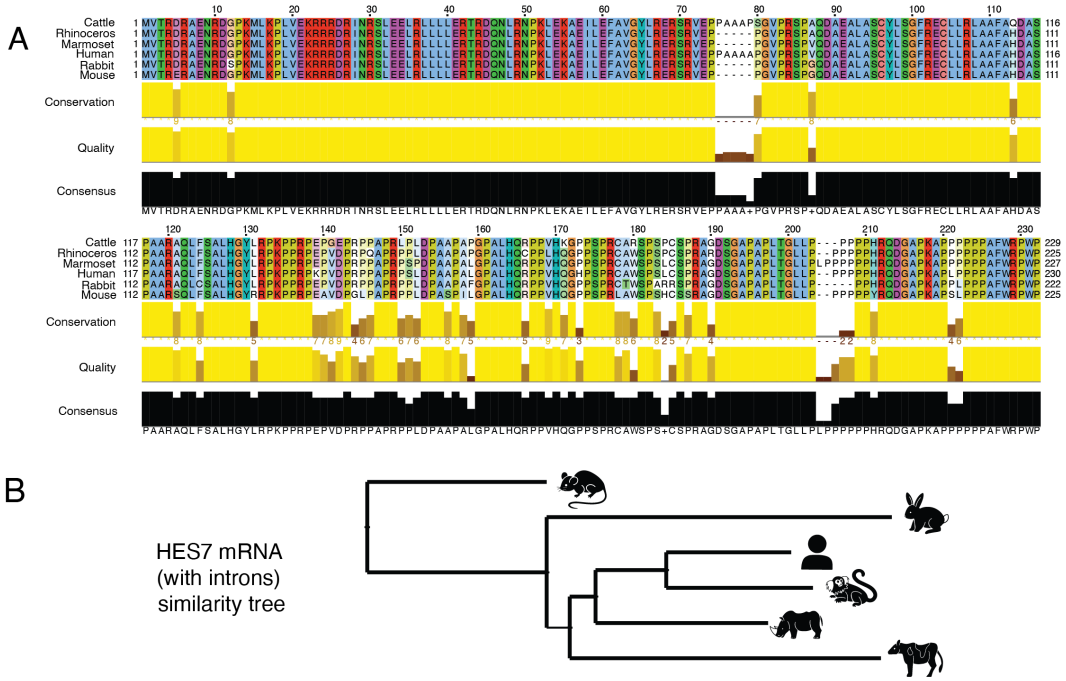

Figure 8: Conservation of the *HES7* gene across mammals.
(A) HES7 protein alignment. The amino acid sequence of HES7 was compared across the six species. Coloured letters indicate sites with similar amino acids between species. The degree of conservation, quality, and consensus of the amino acids among the six species are represented by the yellow and black shading. (B) Neighbour-joining tree based on the matrices of distance calculated for the *HES7* mRNA sequences, including their introns.

To characterise the *HES7* oscillations, luminescence live measurements were performed on iPSM cells containing the *HES7* reporter. Rabbit iPSM oscillated with a period of 153 ± 2 min (mean ± SD), followed by cattle iPSM with a period of 238 ± 5 min, rhinoceros iPSM with a period of 236 ± 3 min, and finally, marmoset iPSM exhibited the longest period of 388 ± 3 min (**Fig. 9A to C**). Measurements were taken from the whole dish, highlighting the synchrony of these oscillations throughout the culture. To validate these results, the measured segmentation clock periods were compared to the available *in*

vivo data. For all the species except the rhinoceros, which lacks embryological information, the *in vivo* somite formation frequency was approximated by using studies describing the number of somites in staged embryos (**Table 1**). Obtaining and accurately staging embryos from unconventional mammalian species is challenging, resulting in scarce and noisy measurements. However, the ranking order between the *in vitro* period and the *in vivo* somite formation frequency matched. The marmoset, for example, which showed the longest period *in vitro*, is known for its particularly slow pace of early embryonic development [116]. These results demonstrate that the segmentation clock of different mammalian species can be recapitulated *in vitro*, with each species oscillating at a specific period. Combined with the previous data on mouse and human periods (122 ± 2 min and 322 ± 6 min, respectively) [57], the segmentation clocks of *in vitro* differentiated PSM cells exhibited a 3.2-fold difference between the fastest and the slowest species (**Fig. 9D**). Therefore, the stem cell zoo provides an ideal platform to investigate the causes behind the interspecies differences in developmental tempo and their connection to the organism characteristics.

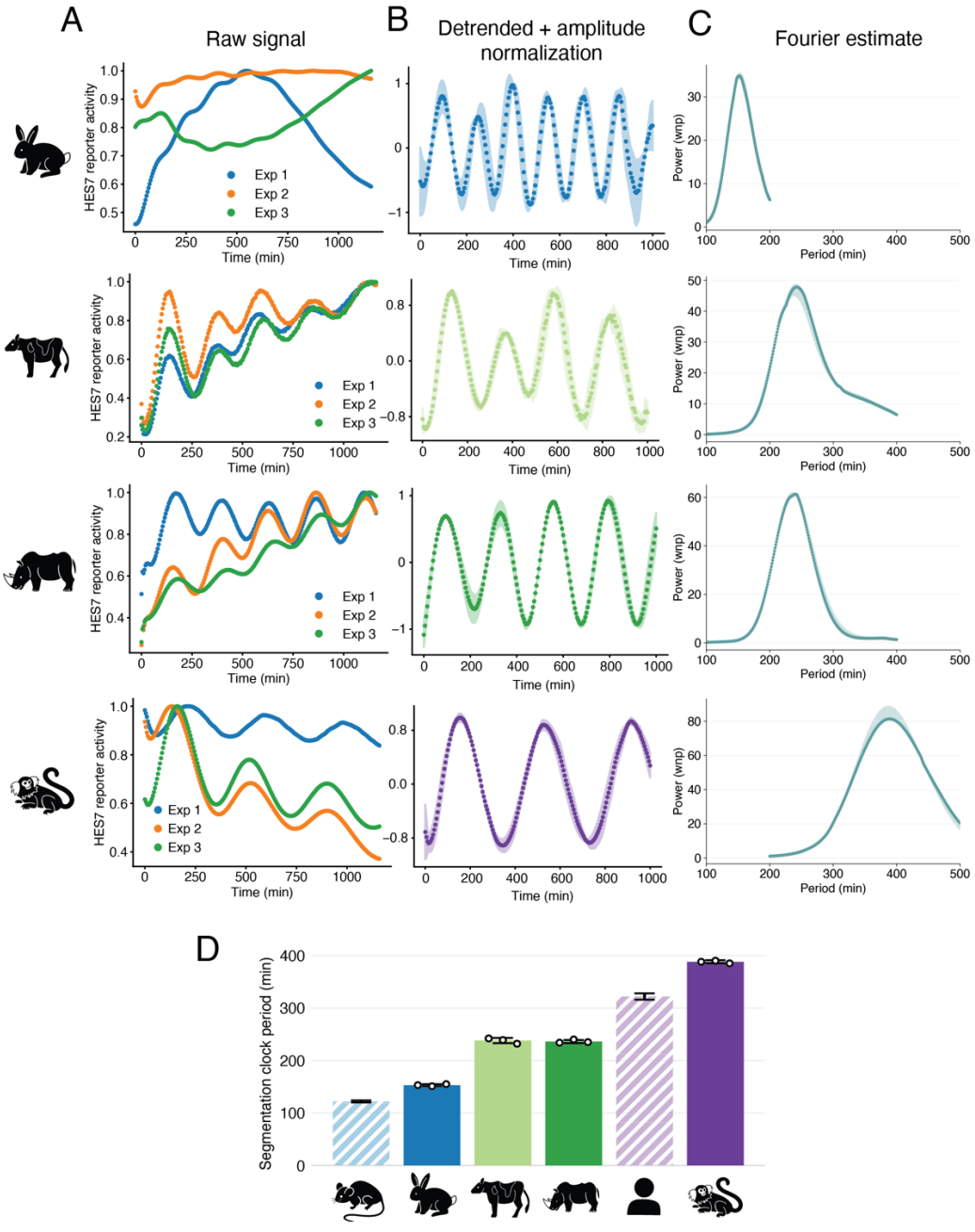

Figure 9: Quantification of the *HES7* oscillations.
(A) *HES7* reporter activity measured over time. Traces represent the collective luminescent activity from a 35-mm dish. Time courses were normalized to the maximum intensity. Data from three independent experiments is shown (B) Oscillatory *HES7* reporter activity after detrending and amplitude normalisation. Shading indicates means ± SD (n = 3) (C) Fourier estimate of the processed oscillatory signals after wavelet spectral analysis. The period with the maximum power for each of the signals was used for (D). Shading indicates median ± the interquartile range (n = 3). (D) Oscillatory periods in each species. Error bars indicate means ± SD (n = 3). Human and mouse data (striped bars) are from Matsuda et al. [57].

Rabbit			Cattle			Marmoset		
Embryonic day	nº somites	nº embryos	Embryonic day	nº somites	nº embryos	Embryonic day	nº somites	nº embryos
10	26,5	40	23	16-22	Not disclosed	50	8	3
11	37,4	61	24	23-27		60	26,5	2
12	46,6	57	25	28-32				
			26	33-36				
			27	37-40				
			28	41-44				
Estimated period of *in vivo* somite formation (min)	Reference		Estimated period of *in vivo* somite formation (min)	Reference		Estimated period of *in vivo* somite formation (min)	Reference	
143	Naya et al. [117]		310	Haldiman [118]		778	Chambers et al. [119]	

Table 1: Approximate *in vivo* somite formation time.
The *in vivo* somite formation period was roughly approximated based on the number of somites observed in embryos at different developmental stages. The period was calculated by linear regression between the number of somites and the embryonic days.

3.1.3 Scaling with the organismal parameters

Previous comparisons of the segmentation clock period between mice and humans have suggested a connection to body weight [57,71]. As introduced in section 1.9, a number of bodily parameters are known to scale with body weight, with larger species usually showing slower biological rates. I thus hypothesized that the differences in the segmentation clock period observed across the six mammalian species could be related to their body weight. However, the average adult body weight of each species did not correlate with their segmentation clock period (**Fig. 10A** and **Supp. Table 2**). Rhinoceros, the biggest species, showed a faster period than humans, whereas the small marmoset monkey was the slowest of them all. This suggests that the timing of the segmentation clock does not have an allometric dependency. Similarly, no correlation could be found between the gestation length and the segmentation clock period (**Fig. 10B**). The timing of birth can be quite variable across species, with some animals being more altricial or precocial in order to maximise their survival [120]. This variability makes the length of gestation a poor benchmark for comparing developmental rates. Instead, I decided to correlate the segmentation clock period with general hallmarks of early development. Interestingly, the length of embryogenesis, defined as the time from fertilization to the end of organogenesis, showed a strong

correlation with the segmentation clock period (**Fig. 10C**). The final step of organogenesis occurs when embryos reach the last Carnegie stage, characterized by the fusion of the secondary palate [84]. This result suggests that the pace and length of early development are tightly connected. Animals adjust the segmentation clock rate depending on their overall developmental speed, exemplifying true allochronic scaling. The high correlation between the measured period and the *in vivo* hallmarks also confirms that *in vitro* recapitulation of the segmentation clock can serve as a good proxy for quantifying embryonic developmental tempo. Additionally, the three phylogenetic clades of the stem cell zoo, Primates, Glires and Ungulates, corresponded to slow, fast, and intermediate segmentation clocks, respectively. This suggests that developmental tempo can be roughly classified according to phylogeny (**Fig. 10D**). However, to fully understand the evolutionary history of developmental tempo across mammals, more species covering a wider range of phylogenies would need to be incorporated into the study.

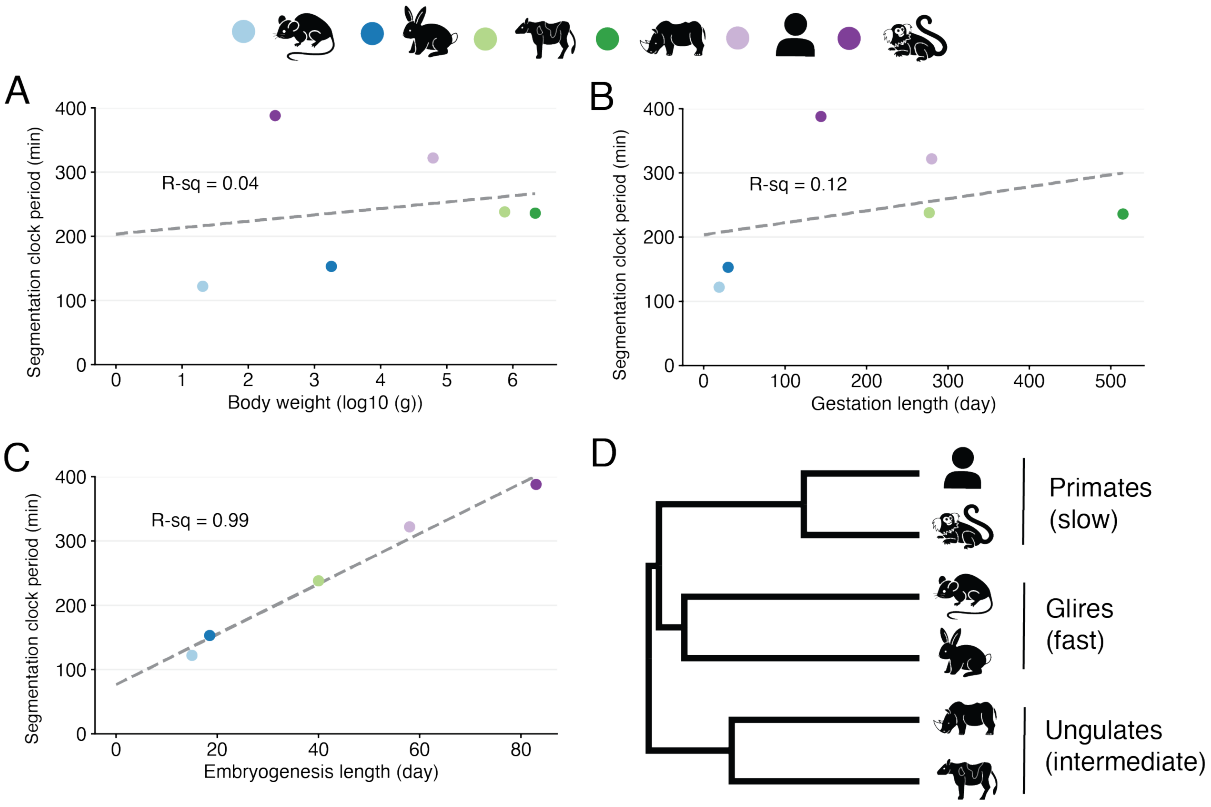

Figure 10: Correlations between the segmentation clock period and the organismal characteristics.
(A) Scatterplot illustrating the relationship between the log10 average adult body weight and the segmentation clock period. (B) Scatterplot illustrating the relationship between the gestation length and the segmentation clock period. (C) Scatterplot illustrating the relationship between the embryogenesis length and the segmentation clock period. The rhinoceros is omitted due to a lack of embryological data. (A-C) The colour scheme representing species is shown at the top of the figure. Dashed lines represent the linear fitting, R-squared values are provided. The values for body weight, gestation length, and embryogenesis length for all the species can be found in Supplementary Table 2. (D) Phylogenetic tree of the six species used in this study, representing a subset of the complete mammalian tree (see Methods). Names of the common clades and the speed of development are shown.

3.2 Part II: Exploring the relationship between developmental tempo and other cellular parameters

The segmentation clock period varies across species, but how is it so precisely established in the first place? Previous studies in mice and humans have highlighted the role of biochemical kinetics and metabolic rates in controlling developmental tempo [57,59,71]. The stem cell zoo now offers the opportunity to extend these observations to a larger number of species, testing the universality of these mechanisms. Moreover, using consistent experimental conditions allows for the investigation of other species-specific cellular properties that could unravel how these cell-intrinsic phenotypes are regulated.

3.2.1 The speed of biochemical reactions scales with the segmentation clock period

The speed of biochemical reactions has been shown to scale with developmental tempo across cell types [57,59]. In the case of the segmentation clock, changes in the molecular kinetics affecting the delayed negative feedback loop of *HES7* can modulate its oscillatory period [34]. Mouse iPSM shows faster degradation of *HES7* mRNA and protein as well as shorter delays in *HES7* gene expression compared to human iPSM [57]. To explore the generality of this observation, I quantified the degradation rates and delays governing the *HES7* negative feedback loop in the four additional mammalian species. Amongst all processes, I focused on the HES7 protein degradation rate and the delay caused by *HES7* introns in transcript processing (**Fig. 11**). These parameters have been previously identified, both experimentally and mathematically, as having the most significant impact on the segmentation clock period [34,57]. Additionally, modifying the HES7 protein degradation and intron delay can affect the segmentation clock temporal dynamics *in vivo* [35,36].

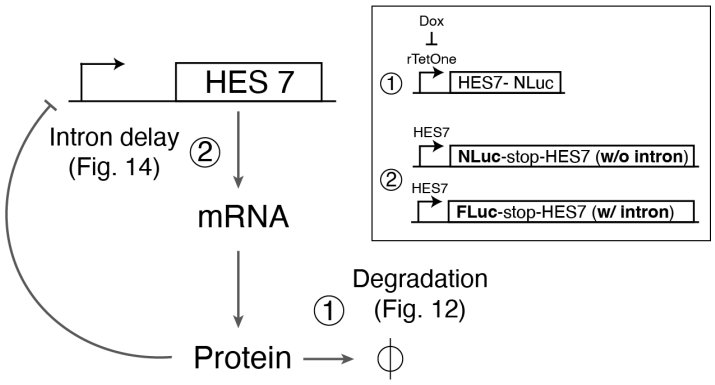

Figure 11: The *HES7* delayed negative feedback loop.
Schematic representation of the *HES7* negative feedback loop. Protein degradation and intron delay were measured in the indicated figures. The reporters used for each assay are shown. NLuc: NanoLuc Luciferase, FLuc: Firefly Luciferase.

To measure the HES7 protein degradation rate, the human HES7 protein fused to a luciferase reporter was overexpressed in the iPSM cells. This reporter protein was completely functional and could rescue oscillations in *HES7* KO mutant cells (data not shown). Protein decay was quantified by halting the

expression of the HES7-Luciferase fusion protein using doxycycline (**Fig. 12A and B**). HES7 protein half-life was then calculated in iPSM cells from different species using the slope of the most linear region in the decay curve. The observed half-lives were 24 ± 0.8 min, 33 ± 2 min, 32 ± 2 min, and 46 ± 3 min in rabbit, cattle, rhinoceros and marmoset iPSM, respectively. Together with the previously reported values in mouse and human iPSM [57], there was a strong correlation between the HES7 protein degradation rate and the segmentation clock period (**Fig. 12C**). Species with slower developmental rates exhibited longer HES7 protein half-lives.

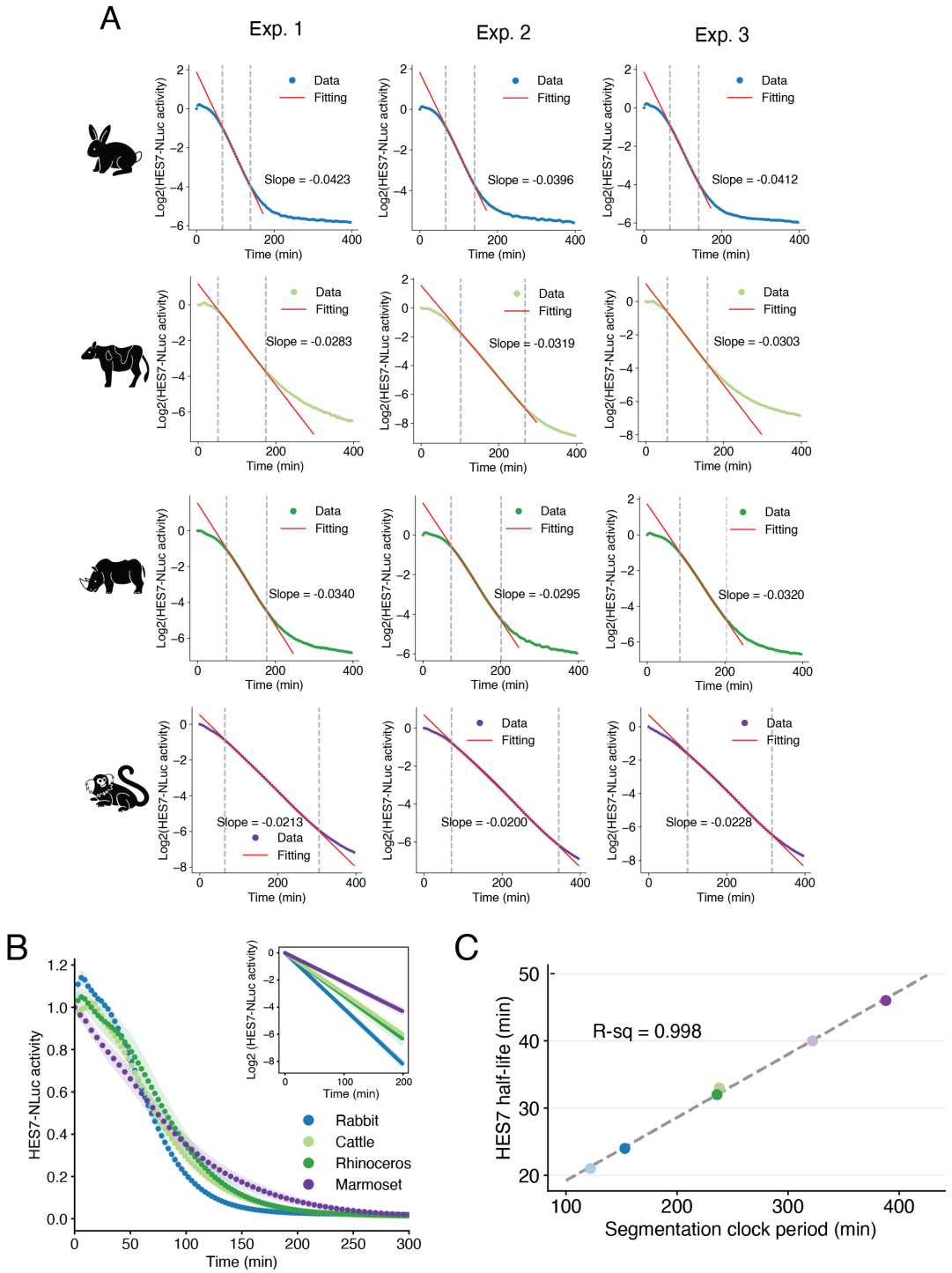

Figure 12: Quantification of HES7 protein degradation rates.
(A) HES7 protein degradation assay. The transcription of a HES7 protein fused with NLuc was stopped by adding doxycycline at time zero. The decay of the NLuc signal was monitored. Dashed lines indicate the most linear region considered by the RANSAC algorithm for the fitting. The slope of the fitted line is displayed and converted to half-life using the equation: Half-life = -1/Slope. (B) Summary of the HES7 protein degradation assay. The inset shows the slopes of the fitted lines used to calculate protein half-life. Shading indicates means ± SD (n = 3). (C) Scatterplot showing the relationship between the segmentation clock period and the HES7 protein half-life for all species. The colour scheme for each species is the same as in Fig. 10. Dashed lines represent linear fitting. R-squared values are shown. Human and mouse data (light purple and light blue) are from Matsuda et al. [57].

To investigate the generality of this behaviour, the degradation rate of two additional proteins was measured. TBX6 protein half-life was much longer than that of HES7 and still showed a high correlation with the segmentation clock period across species (**Fig. 13A and C**). Moreover, the degradation rate of the highly unstable Ubiquitin(G76V)-Luciferase protein moderately correlated with the period of the clock (**Fig. 13B and C**). This exogenous reporter was generated by fusing an uncleavable Ubiquitin to a luciferase protein and can be used as a proxy for proteasomal activity [121]. The luciferase gets directly targeted to the proteasome, whose activity can be quantified based on the luminescent decay. Overall, the general rates of protein degradation scaled with developmental tempo. This is further supported by a recent study that systematically measured protein degradation rates in mouse and human iPSM using SILAC, revealing a general trend of slower protein degradation in human cells [122].

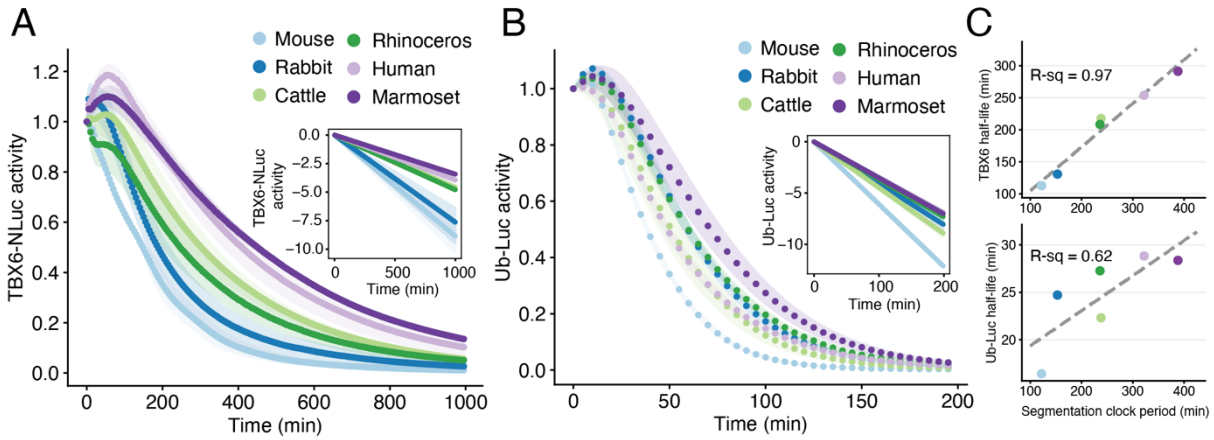

Figure 13: Quantification of TBX6 and Ub-Luc protein degradation rates.
(A and B) TBX6 (A) and Ubiquitin(G76V)-Luciferase (Ub-Luc) (B) protein degradation assays. In both cases, the protein production was stopped by adding doxycycline at time zero. The decay of the respective luminescence signal (NLuc for TBX6 and Luciferase for Ub-Luc) was monitored over time. The insets represent the slope of the fitted lines used to quantify the protein half-life. The shading indicates means ± SD (n = 3). (F) Scatterplots showing the relationship between the segmentation clock period and the measured protein degradation rates (top: TBX6 protein half-life, bottom: Ub-Luc protein half-life). The colour scheme for each species is the same as in Fig. 10. Dashed lines represent linear fitting. R-squared values are shown.

The delay caused by *HES7* introns was measured using *HES7*-promoter luciferase reporters containing or lacking the human *HES7* intron sequences. Both reporters are carried by the same cells and respond to the endogenous *HES7* oscillatory signal. However, the reporter containing introns experiences a delay due to the additional processing steps of intron transcription and splicing. By quantifying the phase

difference between the oscillations of both reporters, the HES7 intron delay could be estimated (**Fig. 14A**). Using this system, the intron delays were found to be 24 ± 3 min, 37 ± 2 min, 36 ± 3 min, and 54 ± 0 min in rabbit, cattle, rhinoceros and marmoset iPSM, respectively (**Fig. 14B**). Similar to the protein degradation rate, the delay caused by *HES7* introns exhibited a strong correlation with the segmentation clock period (**Fig. 14C**). Interestingly, the protein degradation and intron delay, despite being two completely different biological processes, scaled proportionally with one another (**Fig. 15A**). To generate sustained oscillations, the different parameters of the HES7 negative feedback loop need to be somewhat coupled [34]. However, it is important to clarify that they do not necessarily need to change proportionally. For instance, to decelerate the oscillatory period, one could primarily increase the delay without proportionally slowing down protein degradation [34]. The quantifications shown here revealed a proportional scaling between both parameters, suggesting that the species-specific protein degradation and intron delay might share a common regulator (**Fig. 15A**). Simulations of the *HES7* negative feedback loop also confirmed that a linear and proportional scaling of all degradation- and delay-related parameters could largely account for the interspecies differences in the period (**Fig. 15B**). Taken together, these results demonstrate that the speeds of biochemical reactions correlate with the segmentation clock period, potentially serving as a general mechanism to control developmental tempo. Moreover, the use of identical reporter constructs across species highlights that kinetic differences must emerge from changes in the intracellular environment. This raises the question of how these precise environments are established in the cells of each animal.

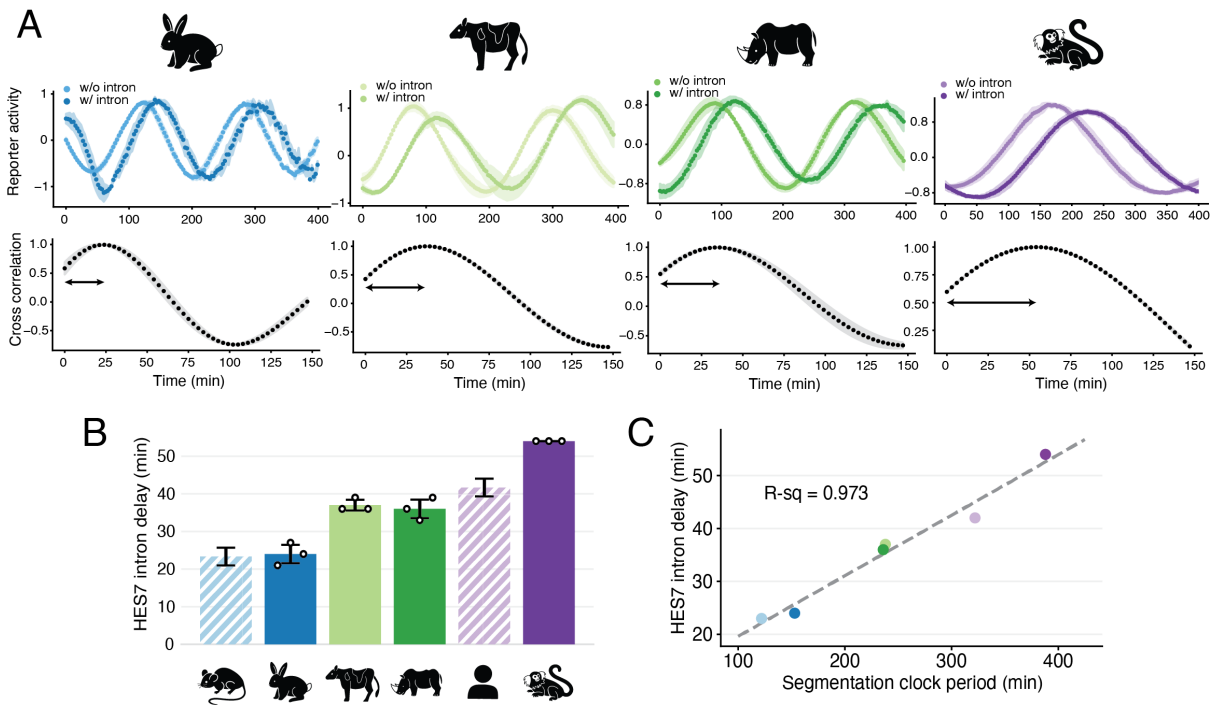

Figure 14: Quantification of the *HES7* intron delay.
(A) *HES7* intron delay assay. Reporter constructs without (w/o) and with (w/) *HES7* introns were measured simultaneously (top). The cross-correlation of the two reporters was calculated (bottom). Shading indicates means ± SD (n = 3). (B) *HES7* intron delays estimated from (A). Error bars indicate means ± SD. Human and mouse data (striped bars) are from Matsuda et al [57]. (C) Scatterplot showing the relationship between the segmentation clock period and the measured *HES7* intron delay. The colour scheme for each species is the same as in Fig. 10. Dashed lines represent linear fitting. R-squared values are shown. Human and mouse data (light purple and light blue) are from Matsuda et al. [57].

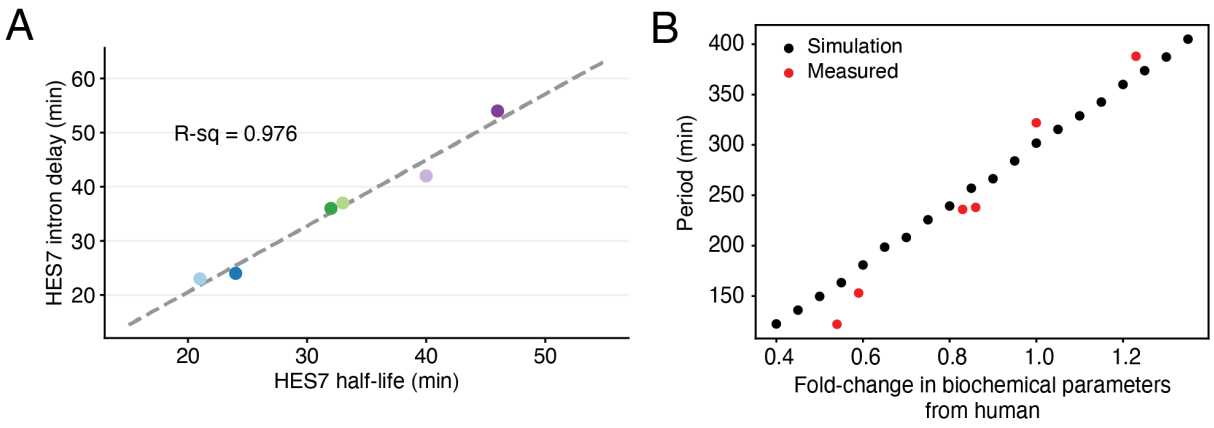

Figure 15: Scaling between the HES7 protein degradation and intron delay.
(A) Scatterplot showing the relationship between the HES7 half-life and *HES7* intron delay across species. The colour scheme representing species is the same as in Fig. 10. Dashed lines represent linear fitting. The R-squared value is shown. (B) Simulations of the *HES7* oscillations. Black: the period of the simulated *HES7* oscillations after linearly scaling all the human degradation and delay parameters. The human biochemical parameters necessary to simulate the *HES7* oscillatory period are extracted from Matsuda et al. [57]. Red: measured oscillatory periods compared to the actual fold-change between the human biochemical parameters and the parameters quantified in other species.

3.2.2 Metabolic rates do not scale with the segmentation clock period

As discussed in section 1.7, changes in the metabolic rates have been proposed as a potential mechanism underlying the interspecies differences in biochemical kinetics. A recent study found that mouse iPSM cells have a higher mass-specific metabolic rate compared to human iPSM cells [71]. This is in line with the Kleiber law, which describes a general scaling relation between basal metabolic rate and body weight [89]. The stem cell zoo offers an unprecedented opportunity to test the relationship between metabolism, body weight, and developmental tempo. For instance, the marmoset, with its small size, showed the slowest period while the rhinoceros, being the largest species, displayed a faster period than the human. The lack of clear scaling between developmental tempo and body weight raises the question of how do metabolic rates change across species.

Human and mouse iPSM cells show large differences in mass and volume, with human cells containing double the amount of biological material [71]. Normalisation of the metabolic rates by mass is, therefore, necessary to correct for differences in cellular size. Measuring cellular mass is challenging and requires very specialised equipment. On the other hand, measurements of cellular volume can be achieved with standard flow cytometry equipment. Given that the density of both mouse and human iPSM was found to be close to one [71], the cell volume was used here to normalise the metabolic rates across species. Measurements of cellular volume by electric conductance revealed differences across species (**Fig. 16A**). Human iPSM cells showed the largest volume, while mouse iPSM cells were the smallest among the species (**Fig. 16B**). The scaling of the segmentation clock with cell volume was weaker compared to that with biochemical kinetics (**Fig. 16C**). Despite the overall positive correlation, marmoset cells, with the slowest period, were smaller than rhinoceros cells. Similarly, cattle and rhinoceros cells, which have similar segmentation clock periods, exhibited differences in volume.

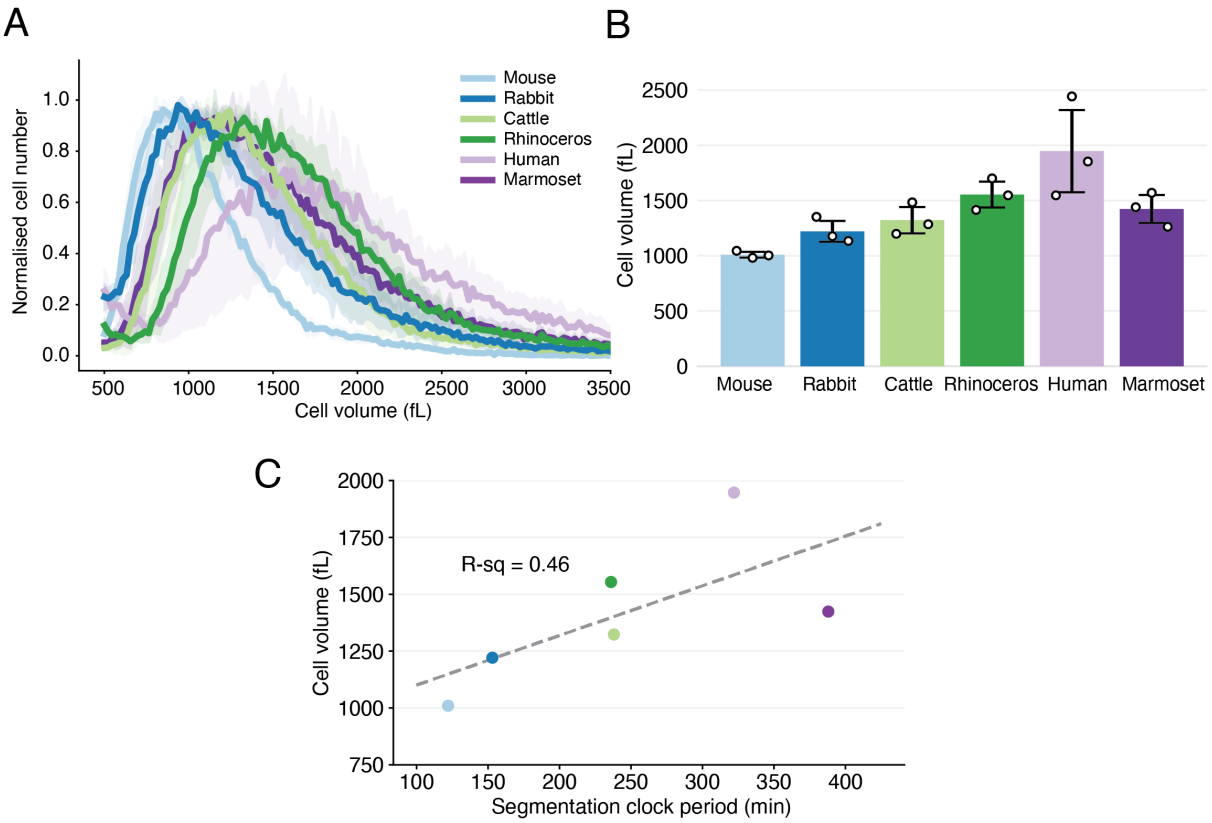

Figure 16: Cellular volume measurements.
(A) Histogram showing the size distribution of iPSM cells. The total cell number was normalized. The shading indicates means ± SD (n = 3). (B) Median cell sizes estimated from (A). Error bars indicate medians ± SD (n = 3). (C) Scatterplot showing the relationship between the median cell volume and the segmentation clock period across species. The colour scheme representing the species is the same as in Fig. 10. Dashed lines represent linear fitting. R-squared value is shown.

To quantify the metabolic rates in iPSM cells of different species, the basal oxygen consumption rate (OCR) was measured using the Seahorse analyser (**Fig. 17A and B**). The OCR is a good indicator of mitochondrial respiration and can be assessed by quantifying changes in the oxygen concentration of the medium [123]. Before cell volume normalisation, the OCR values showed differences across species, with cattle and rhinoceros presenting the highest rates (**Fig. 17B**). The differences in the OCR spanned more than 2-fold across species. Cell volume-specific OCR revealed a slightly different trend (**Fig. 17C**), with mouse iPSM having a higher metabolic rate than human iPSM as previously reported [71]. Nevertheless, no correlation was found between the OCR and the segmentation clock period across species (**Fig. 17D**). Differences in the glycolytic and mitochondrial contributions of iPSM cells were then assessed using the real-time ATP rate assay. In this assay, measurements of the extracellular acidification rate are used to calculate the glycolytic activity of cells, known as GlycoATP or GlycoPER. The total ATP levels, despite being different across species, did not follow any particular trend (**Fig. 18A and D**). Interestingly, the source of these ATPs varied greatly across species (**Fig. 18G**). Mouse iPSM cells relied more on glycolysis, showing the highest cell volume-specific glycolytic rate. In contrast, cattle and rhinoceros iPSM cells displayed a more oxidative metabolic profile (**Fig. 18B, C, E and F**). There was no clear link between the segmentation clock period and the rates of glycolysis or ATP production (**Fig. 18H**). Taken together, these results suggest that while metabolic rates vary across

species, they do not directly scale with the species-specific segmentation clock period. This observation challenges the notion of a simple link between metabolic activity and developmental tempo.

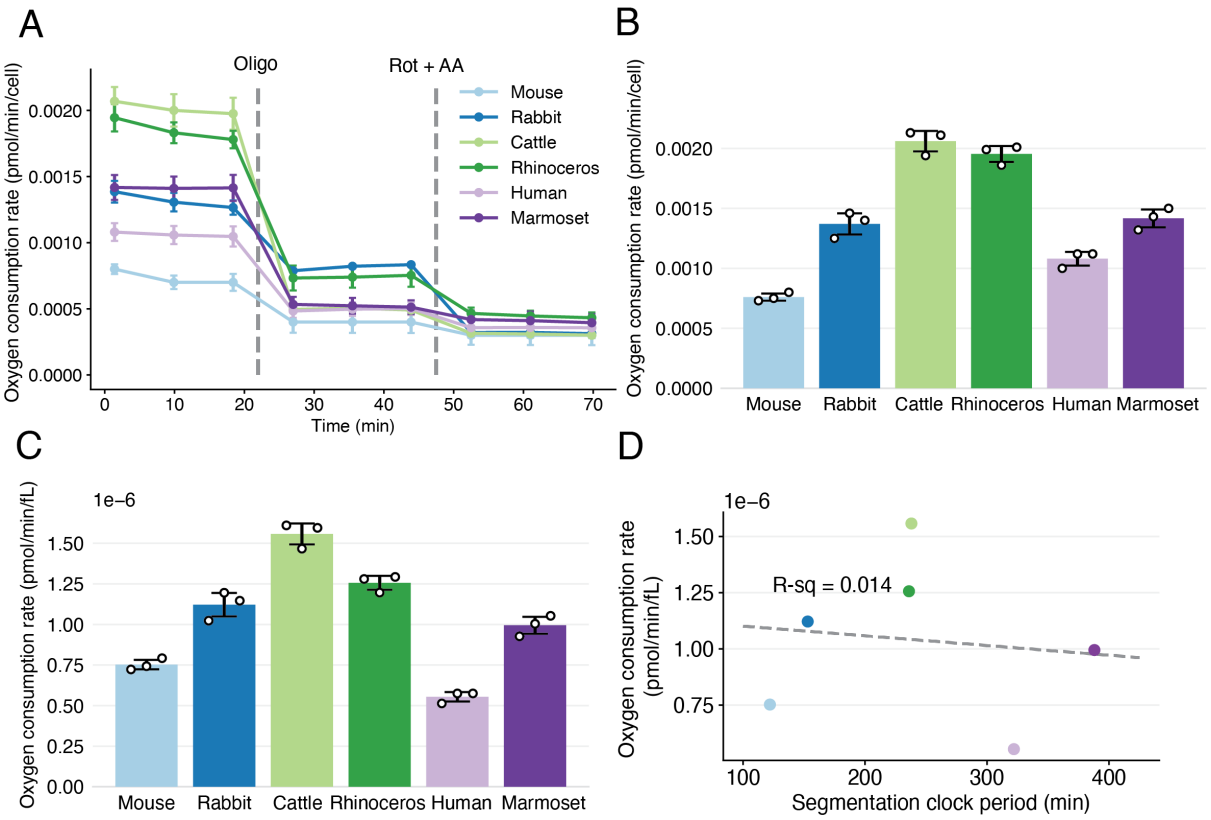

Figure 17: OCR measurements across the stem cell zoo.
(A) Oxygen consumption rate measured throughout the Seahorse real-time ATP rate assay in iPSM cells. Oligomycin (Oligo) and Rotenone + Antimycin A (Rot + AA) were added at the marked time points. (B) Oxygen consumption rate per cell. (C) Volume-specific oxygen consumption rate. (B and C) Error bars indicate means ± SD (n = 3). Data are the same but normalized by cell number (B) or cell volume (C). (D) Scatterplot showing the relationship between the segmentation clock period and the volume-specific oxygen consumption rate. The colour scheme representing the species is the same as in Fig. 10. The dashed lines represent linear fitting. R-squared value is shown.

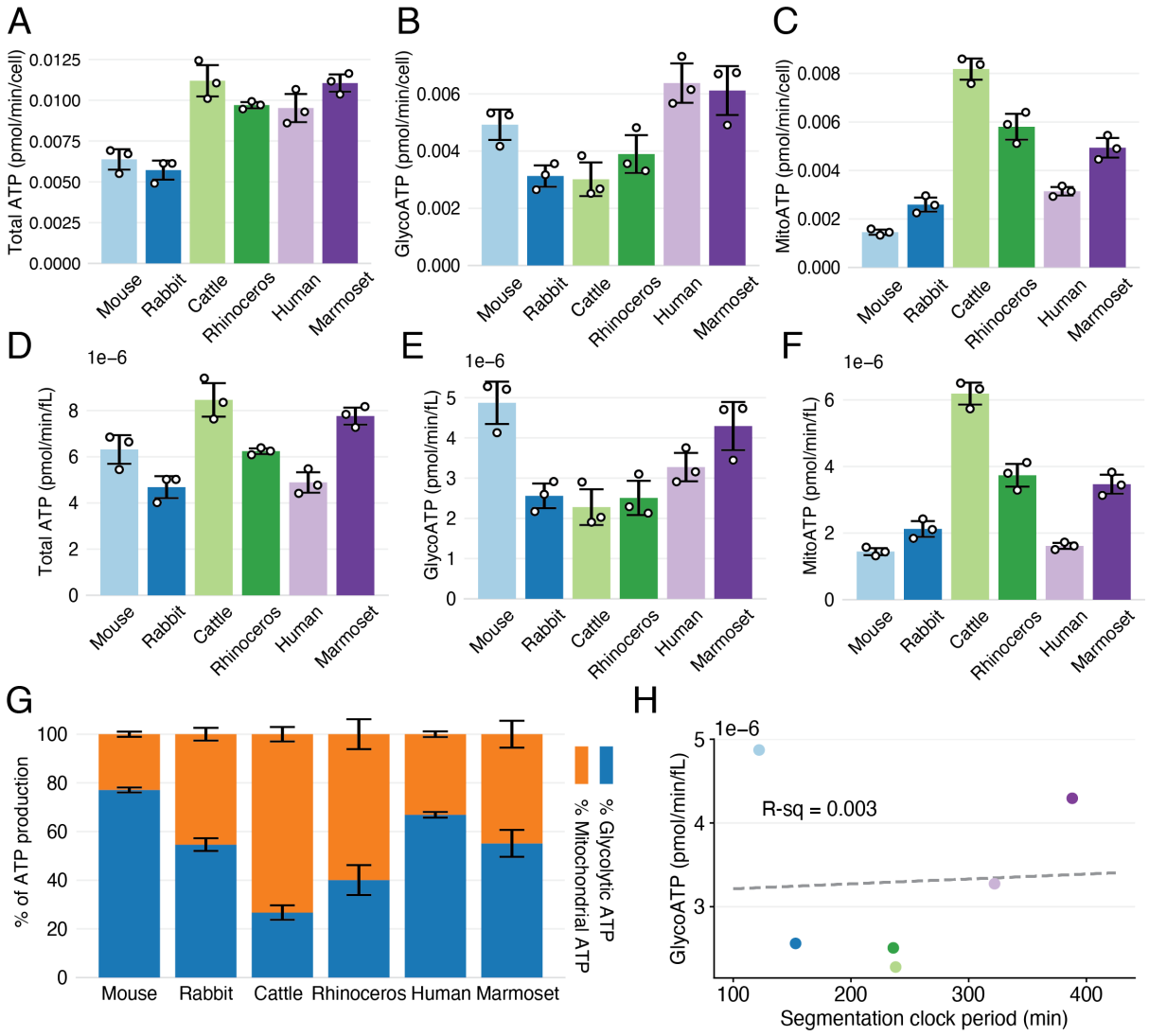

Figure 18: Measuring ATP production rates.
(A) ATP production rate per cell. (B) Glycolytic rate of ATP production per cell. This measurement is equivalent to the glycolic proton efflux rate (GlycoPER) as per the stoichiometry of the glycolysis reaction. (C) Mitochondrial rate of ATP production per cell. (D) Volume-specific ATP production rate. (E) Volume-specific glycolytic rate of ATP production. (F) Volume-specific mitochondrial rate of ATP production. (G) Ratio of glycolytic ATP production to mitochondrial ATP. (A-G) Error bars indicate means ± SD (n = 3). (A-F) Data are the same but normalized by cell number (A-C) or cell volume (D-F). (H) Scatterplot showing the relationship between the segmentation clock period and the volume-specific glycolytic rate of ATP production. The colour scheme representing the species is the same as in Fig. 10. The dashed lines represent linear fitting. R-squared value is shown.

To further explore the effect of cellular metabolism on the segmentation clock dynamics, the metabolic activity of iPSM cells was perturbed using sodium azide. Known for its ability to inhibit the electron transport chain, sodium azide has been shown to slow down the segmentation clock period in human iPSM cells [71]. Consistent with this previous study, a dose-dependent elongation of the segmentation clock period was observed in mouse, rhinoceros, human and marmoset iPSM cells following the addition of sodium azide (**Fig. 19A and B**). However, inhibitor treatment also resulted in dampened oscillatory activity, characterized by a steep decline in the reporter signal. The rhinoceros cells, in line with their higher oxidative activity, exhibited the largest change in the segmentation clock period (**Fig.**

19C). Nonetheless, the 1.7-fold change in the period of rhinoceros cells upon treatment was much smaller than the large interspecies differences observed across the stem cell zoo. This differential response to metabolic inhibitors further highlights the varying contributions of oxidative and glycolytic pathways across iPSM cells from different species. The reason why cells of various species adopt different metabolic strategies remains to be investigated.

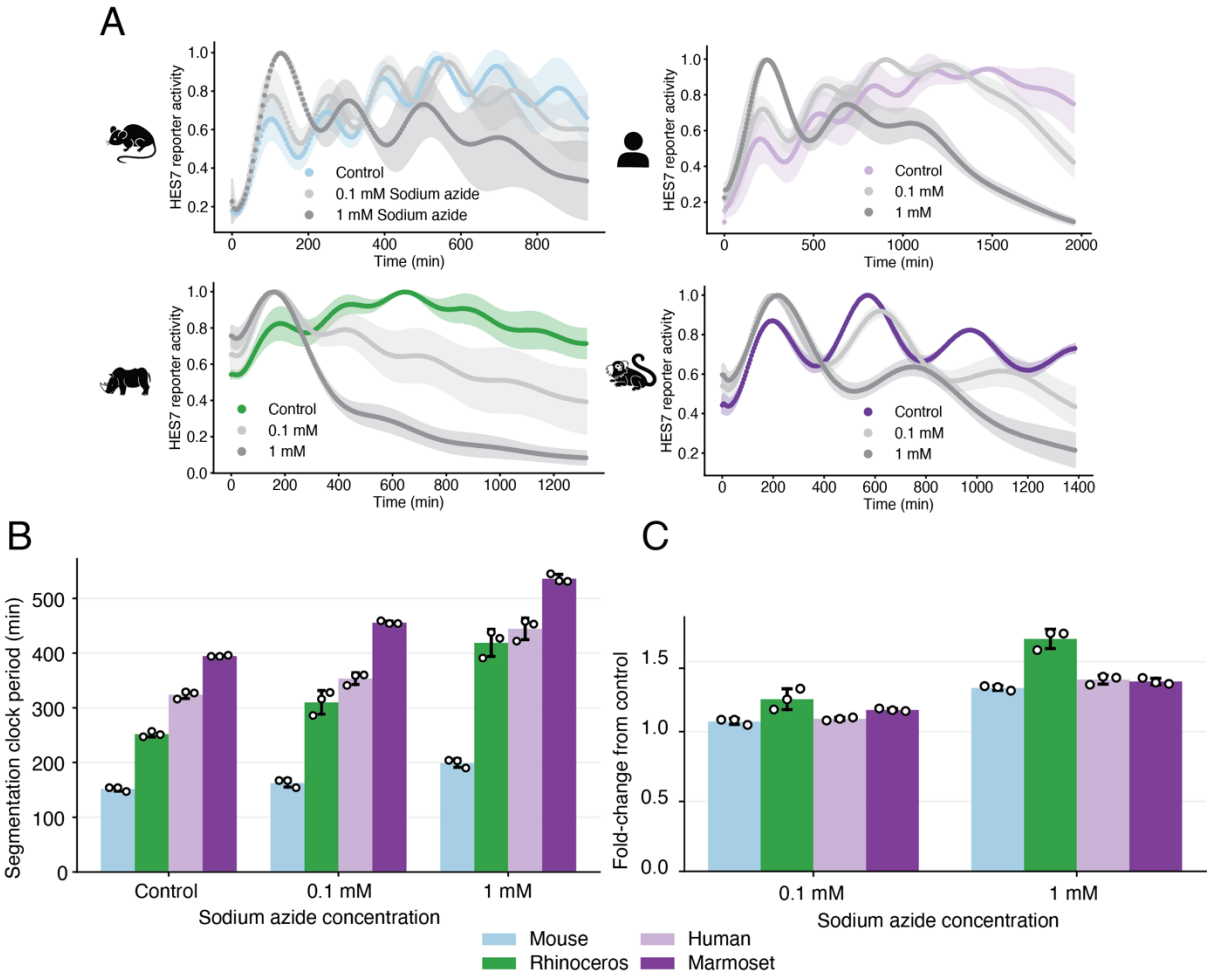

Figure 19: The effect of metabolic inhibitors on the segmentation clock.
(A) Oscillatory HES7 reporter activity of iPSM cells treated with different concentrations of sodium azide. Time course signals were normalized by the maximum intensity. The shading indicates means ± SD (n = 3). (B) Oscillatory periods are estimated from (A). (C) Fold-change in the period of iPSM cells treated with different concentrations of sodium azide compared to the control, calculated from (B). (B and C) Error bars indicate means ± SD (n= 3).

3.2.3 The transcriptional profile of the segmentation clock tempo

After observing the apparent disconnection between metabolism and the segmentation clock period, I hypothesized that the rate of development could be controlled at the gene expression level. To identify a potential transcriptomic signature associated with developmental tempo across species, further

analysis was conducted on the RNA-seq dataset. The relative expression levels of more than 10000 protein-coding orthologous genes were compared across iPSM and PSC samples of the six species. Principal component analysis (PCA) revealed that samples clustered primarily by species rather than tissue type (**Fig. 20A and B**). Similarly, hierarchical clustering of the RNA-seq dataset grouped samples by species, with both cell types from the same species showing high correlation (**Fig. 20C**). These results are in contrast with some observations made in adult tissues reporting that the cell types cluster before species [124]. However, considering the embryonic nature of the PSM tissue and the short differentiation protocols used in this study, iPSM cells likely remain transcriptionally close to PSCs. The fifth PCA axis was able to nicely separate PSCs and iPSM cells, highlighting the transcriptomic signature of the PSM fate (**Fig. 20A**). Interestingly, the first PCA axis revealed a clustering of species based on their segmentation clock period (**Fig. 20A**). Fast (rabbit and mouse), intermediate (cattle and rhinoceros) and slow (marmoset and human) species were grouped together in ascending order. The clustering could be observed in both the PSCs and iPSM cells. This result suggests a potential link between the species-specific gene expression profile and the segmentation clock period.

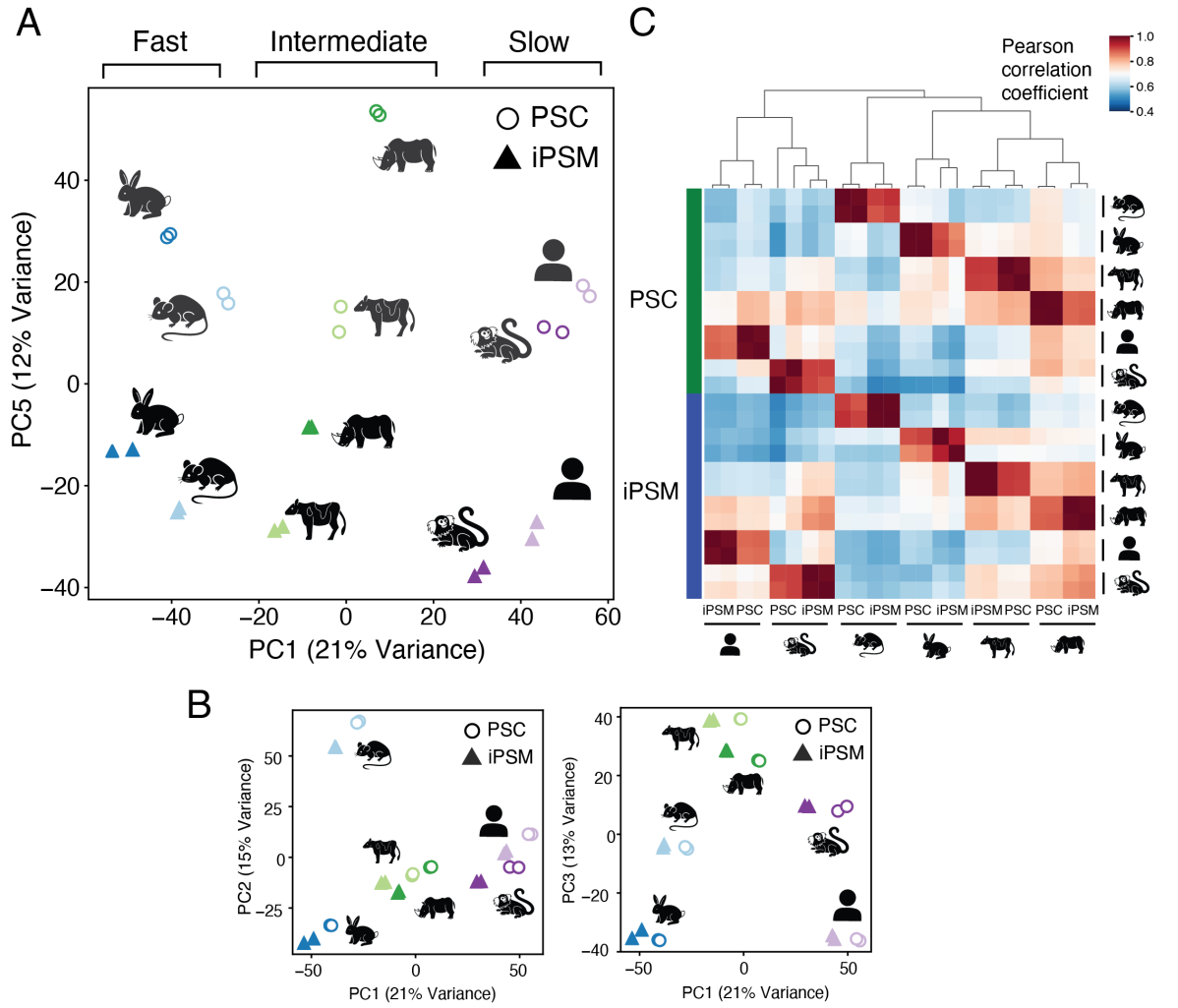

Figure 20: Exploring the transcriptomic signature of iPSM cells.
(A) Principal component analysis (PCA) from bulk RNA-seq. Components 1 and 5 are shown. (B) PCA from bulk RNA-seq. Left: components 1 and 2 are shown. Right: components 1 and 3 are shown (A and B). Two biological replicates of PSCs (circles) and iPSM cells (triangles) of six species were used. The variance explained by each component is indicated. (C) Hierarchical clustering of all RNA-seq samples. The colour code corresponds to the Pearson correlation coefficient across samples.

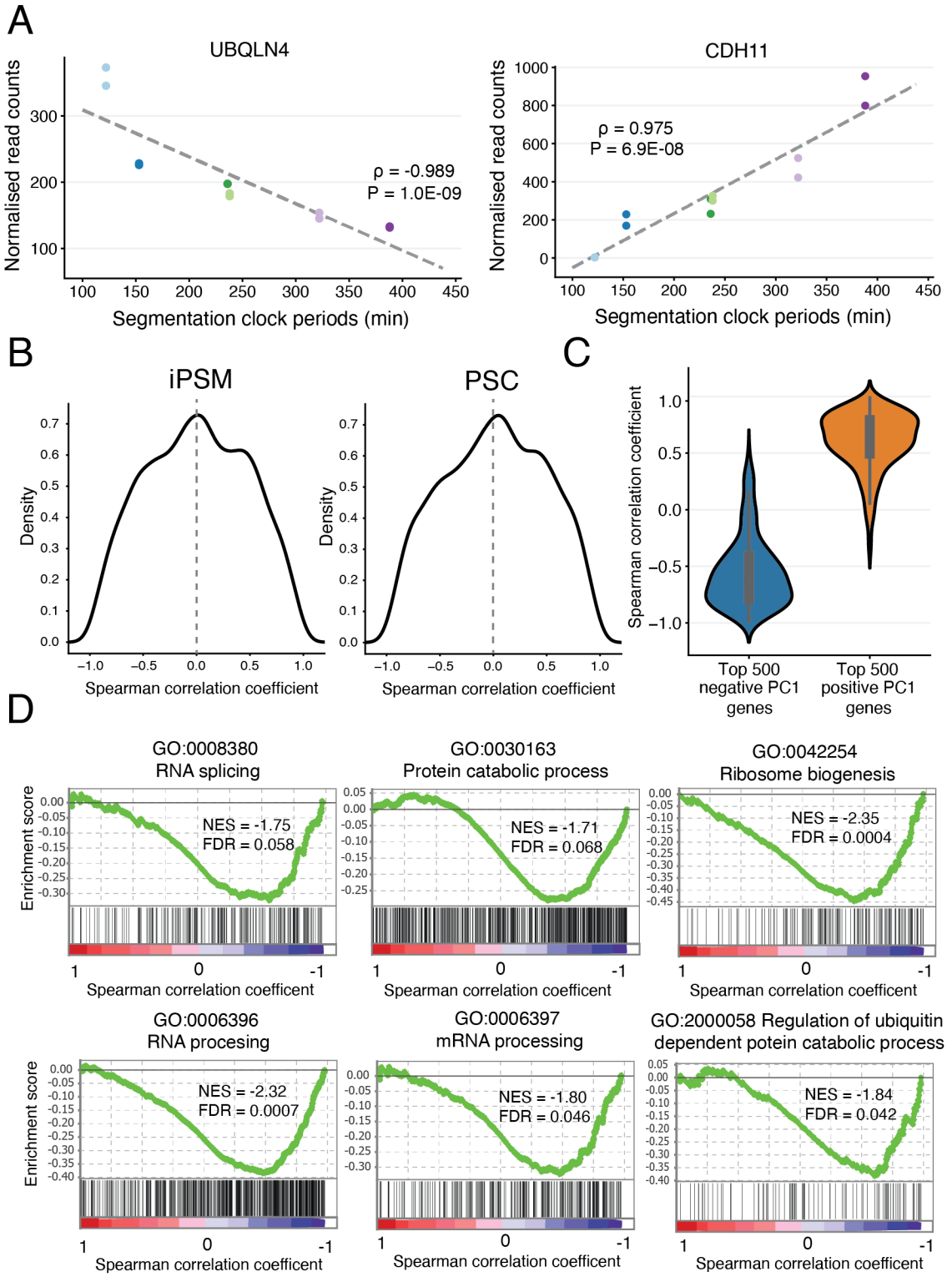

Figure 21: Correlating gene expression and the segmentation clock period.
(A) Scatterplots depicting the relationship between the normalized gene expression levels in iPSM cells and the segmentation clock period across all species. The colour scheme representing species is the same as in Fig. 10. Spearman correlation coefficients (ρ) and their corresponding p-values are displayed within each plot. The two highlighted genes are representative examples of genes with high negative/positive ρ values. (B) Density plots showing the distribution of Spearman correlation coefficients between the gene expression levels and the segmentation clock periods across species. All genes were considered. Results from iPSM samples (left) and PSC samples (right). (C) Violin plots representing the distribution of Spearman correlation coefficients between the

gene expression levels in iPSM samples and the segmentation clock periods across species. The top 500 genes contributing to the negative (left) and positive (right) sides of the PC1 axis were considered. (D) GSEA results for different GO terms related to RNA processing and Protein catabolism/biogenesis. These terms are enriched in genes showing a negatively correlated expression pattern with the segmentation clock period in iPSM samples. Normalised Enrichment Score (NES) and False Discovery Rate (FDR) are displayed.

To better understand this transcriptomic signature, the Spearman correlation coefficient was calculated between the gene expression levels in the iPSM and the segmentation clock period across all genes in the six species (**Fig. 21A and B**). For example, UBQLN4 was expressed at higher levels in fast species compared to slow species and, therefore, showed a negative correlation with the segmentation clock period. Conversely, CDH11 showed a positive correlation, with higher expression in slow species (**Fig. 21A**). The Spearman coefficient reflects the monotonic relationship between the period and the expression values, prioritising the ranking order over strict linear correlations. The distribution of the coefficients across all genes was centred around zero both in PSCs and iPSM samples (**Fig. 21B**). This confirmed that, as expected, the expression levels of most genes did not correlate with the segmentation clock period. Interestingly, the top 500 genes contributing to the negative side of the first PCA axis, where fast species are positioned, correlated negatively with the segmentation clock. By contrast, the genes on the positive side showed a positive correlation (**Fig. 21C**). This further supports the idea that the first PCA axis, which explained the highest amount of variance in gene expression levels, may be linked to the segmentation clock period. Gene set enrichment analysis (GSEA) was then performed on all genes after ranking them by the Spearman correlation coefficient between their expression levels and the segmentation clock period. Genes showing negative correlations, meaning higher expression in faster species, were enriched for gene ontology (GO) terms associated with protein catabolism and RNA processing, among others. (**Fig. 21D**). Combined with previous observations of accelerated HES7 protein degradation and intron delay in fast-developing species, the enrichment of genes associated with these processes suggests a potential role for transcriptional regulation in modulating the speed of biochemical reactions during embryonic development.

Visualisation of the enriched GO terms map revealed a high degree of interconnection, suggesting a coordinated regulation of the biological processes correlated with the segmentation clock (**Fig. 22**). In Figure 22, each dot represents an enriched GO biological process term. Two terms are connected if they share a certain number of genes, causing related functional terms to cluster together. Genes associated with further essential biochemical processes, such as RNA splicing, transcription elongation and nuclear transport, were also enriched among the negatively correlated genes in the iPSM cells (**Fig. 22A**, blue circles). In contrast, terms enriched in the positively correlated genes formed a much smaller cluster (**Fig. 22A**, red circles). Interestingly, a similar pattern could be obtained when performing the same analysis using the gene expression levels in PSCs (**Fig. 22B**). The PSCs do not display evident developmental tempo variations and are cultured on different media across species. However, these results suggest the existence of a core species-specific transcriptional profile present in both cell types. The basic gene regulatory network controlling the speed of biochemical reactions could be wired in all cells of a given species, manifesting as species-specific differences in developmental tempo within relevant cell types.

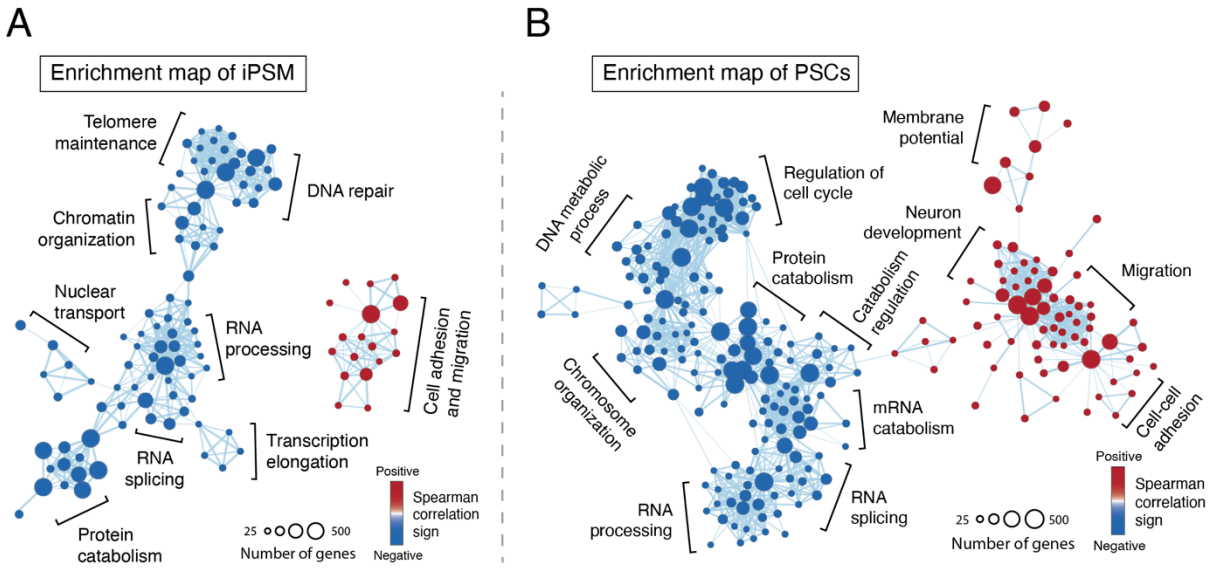

Figure 22: Gene enrichment maps.
(A) Enrichment map network of genes that showed correlated expression with the segmentation clock period in iPSM samples. (B) Enrichment map network of genes that showed correlated expression patterns with the segmentation clock period in PSC samples. (A and B) Circle size represents the number of genes in that process. Blue and red colours represent processes with genes correlating negatively and positively with the segmentation clock period, respectively.

To explore the generality of these findings, the gene expression profiles of mouse and human motor neuron progenitors were compared. As explained in section 1.6, mouse motor neuron progenitors, despite developing using a conserved genetic program, show a faster pace of differentiation compared to human progenitors [59]. These differences in developmental tempo are also associated with changes in protein degradation rates. Interestingly, genes with a negative correlation to the segmentation clock period showed an overall higher expression in mouse motor neuron progenitors compared to those of humans (**Fig. 23**). This suggests that the gene expression profile associated with the segmentation clock period is conserved across cell types, indicating that transcriptional control of developmental rates could be a widespread mechanism. Unravelling how cells from different species establish and maintain these distinct transcriptional profiles will be crucial to better understanding the evolution of developmental tempo.

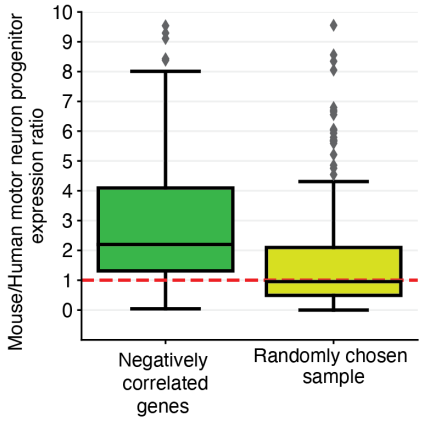

Figure 23: Gene expression pattern in neuronal motor neuron progenitors.
(A) Quantification of the mouse/human motor neuron progenitor gene expression ratio for genes showing a high negative correlation with the segmentation clock period or a random set of genes. Both groups contain the same number of genes. Due to the gene expression normalisation method, the mean of a random sample is expected to be close to one (red dashed line). Boxplots show the median, the first/third quartiles, and the 1.5x the inter-quartile range. Dots represent outliers.

Expanding the classic human and mouse models has revealed a general scaling relationship between the segmentation clock period and the speed of biochemical reactions. The genes related to these biochemical processes show an expression pattern that correlates negatively with the period. It is possible that faster species control their accelerated kinetics through the increased expression of genes involved in biochemical reactions (**Fig. 24**). Overall, these results provide evidence of the potential transcriptional regulation of developmental tempo and its allochronic scaling.

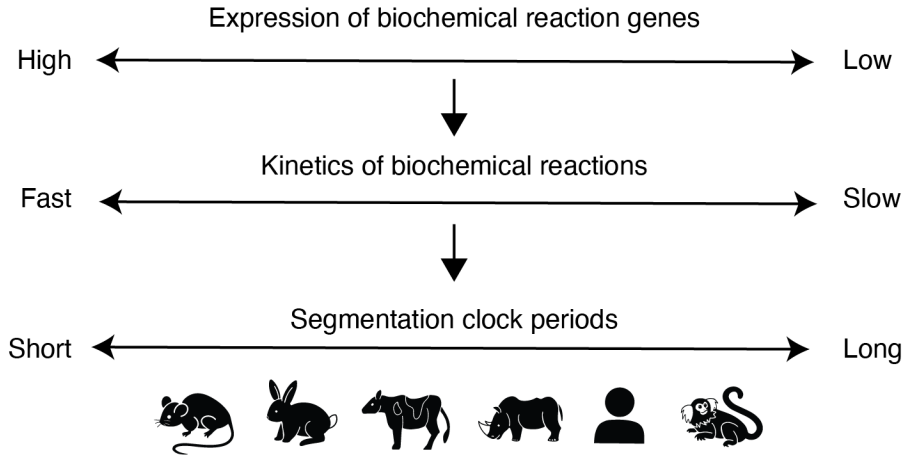

Figure 24: The proposed regulatory cascade of developmental tempo.
Proposed scheme for the regulation of the segmentation clock period across species.

3.3 Part III: Investigating the genetic control of developmental tempo

The analysis of the RNA-seq dataset revealed a transcriptional profile that scales with the segmentation clock period. This suggests that interspecies differences in the period may arise from species-specific gene expression profiles regulating fundamental biological processes. Modifying these profiles could potentially alter the segmentation clock speed, changing the overall developmental tempo of a species. Gain-of-function screens could be used as a powerful tool to identify the genes directly regulating the segmentation clock period, helping establish a causal link between gene expression and the rate of embryonic development. However, the complexity of the segmentation clock phenotype makes characterising changes in the oscillatory dynamics of PSM cells quite challenging. Quantifying the segmentation clock period requires gene expression measurements over several hours, followed by mathematical analysis of the oscillatory traces. Such procedures make direct period quantifications unsuitable for high-throughput screening and sorting of cells. Moreover, measuring the segmentation clock period in single cells is challenging and noisy [57]. Therefore, reporters that allow for precise and rapid quantification of developmental rates are required to effectively screen for genetic alterations affecting the segmentation clock timing. The strong correlation between the speed of biochemical reactions and the segmentation clock period suggests that changes in these kinetic parameters could serve as a good proxy for inferring variations in developmental tempo. In the next section, I will describe how I generated a reporter capable of measuring changes in gene expression delay, a so-called delay reporter. I will then show how I used this reporter to screen for genetic perturbations impacting the segmentation clock period.

3.3.1 The delay reporter

The expression delay encompasses the time taken from gene activation to protein production. In line with the differences in the segmentation clock period, this delay is twice as long in human iPSM cells compared to mouse [57]. Several biochemical processes contribute to the expression delay, including transcription, splicing, mRNA transport, and protein translation. Therefore, genetic perturbations impacting any of these processes could change the overall delay and affect the pace of the segmentation clock. To generate a reporter that can measure changes in the gene expression delay, methods to control the precise timing of gene activation are already available, such as the doxycycline-dependent TetOne systems [125]. However, reliable systems to follow the temporal unfolding of gene expression in a concentration-independent manner remain challenging to establish. For example, with the controlled induction of fluorescent proteins, the amount of fluorescence could be correlated with the gene expression delay. Faster cells with shorter delays would accumulate higher amounts of fluorescence earlier than those with longer delays. This could allow for the separation of fast and slow cells based on fluorescent intensities. A potential issue with regular fluorescent proteins is the high cell-to-cell noise in fluorescent intensity, which would blur the differences in expression delay. Additionally, with such a setting, the perturbations influencing the gene expression levels could not be separated from those really affecting the induction speed. The use of tandem fluorescent timer proteins (tFTs) could overcome some of these issues. These timers are generated by fusing a pair of single-colour fluorescent proteins with well-separated emission spectra. After translation, each protein becomes fluorescent with characteristic maturation kinetics (**Fig. 25A**) [126]. A pair of fused fluorescent proteins can function as a timer when

the two fluorophores mature at different rates. In this case, the ratio of their fluorescent intensity serves as a concentration-independent indicator of the age of the protein pool [126].

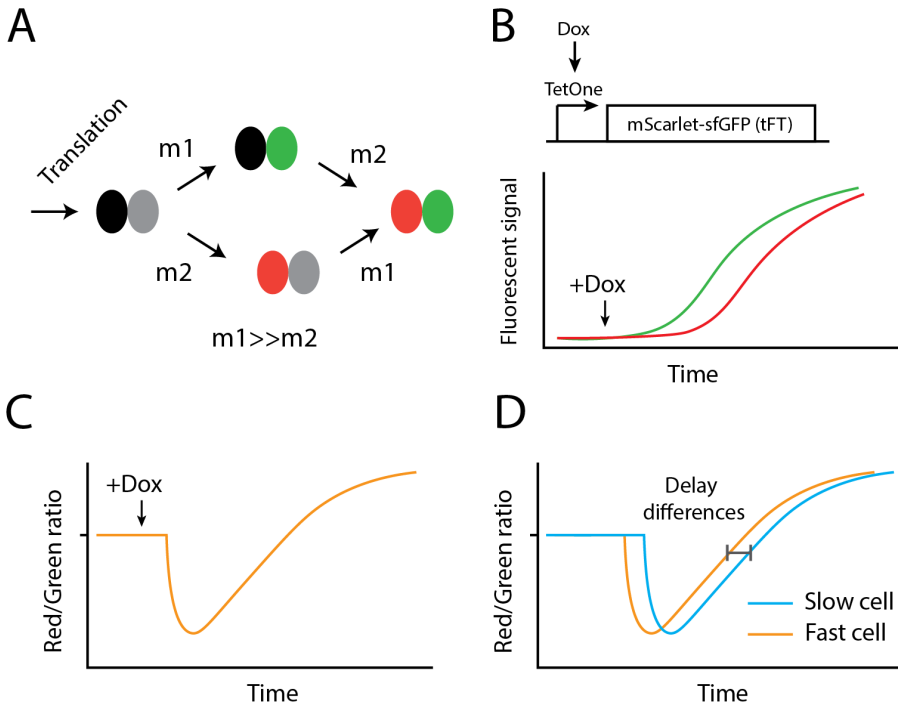

Figure 25: Tandem fluorescent timers.
(A) Schematic representation of the maturation behaviour of a tandem fluorescent protein by fusion of mScarlet (red, black) and sfGFP (grey, green). The maturation constant rate m1 and m2 are represented. Modified from Khmelinskii et al., 2012 [126]. (B) Top: genetic reporter where the expression of the tandem fluorescent timer (tFT) is driven by doxycycline (Dox) using a TetOne promoter. Bottom: Ideal intensity levels of mScarlet (red) and sfGFP (green) upon addition of Dox. (C) Idealized dynamics of the tFT red/green fluorescent ratio upon induction with doxycycline. The final ratio represents the same amount of red and green mature protein. (D) Red/green ideal ratio dynamics of fast and slow-expressing cells. Fast-expressing cells have shorter delays, reaching the steady state earlier. Differences in early dynamics are caused by changes in the expression delay.

I generated a tFT by combining a red mScarlet fluorescent protein, with a maturation half-time of approximately 3 hours, and a super folder green fluorescent protein (sfGFP), which becomes fluorescent within minutes of synthesis. The fused protein was placed under a doxycycline-inducible TetOne promoter to control its expression (**Fig. 25B**, Top). Shortly after production, the pool of mScarlet-sfGFP molecules should be predominantly green-fluorescent, gradually acquiring red fluorescence over time (**Fig. 25B**, Bottom). Thus, the ratio of red to green (R/G) fluorescence should change as a function of the age of the protein pool. Initially, this ratio should decrease due to the fast maturation of the green fluorescent protein; then it would begin to increase until reaching a steady state where the protein production and degradation are balanced (**Fig. 25C**). During the first hours of induction, when degradation of stable fluorescent proteins is negligible, the ratio dynamics are primarily influenced by the expression delay and the maturation rates of both fluorescent proteins. Assuming that the maturation rates of the fluorochromes are constant, the tFT could help report changes in the expression delay across cells. Cells that express the protein quickly would exhibit the decrease and stabilisation of the R/G ratio earlier than slow-expressing cells (**Fig. 25D**). Ultimately, both fast and slow-expressing cells would

converge to the same final value, as the steady-state ratio is determined by the maturation and degradation rates. The advantage of using a ratio between two fluorescent colours of the same protein is that the changes are concentration-independent and solely affected by the system's dynamics. By choosing the appropriate measuring time, differences in the tFT fluorescent ratio could represent variations in the expression delay (**Fig. 25D**).

Following the theoretical predictions, induction of the tFT reporter in human iPSCs using doxycycline revealed distinct dynamics for green and red fluorescence intensities (**Fig. 26**). The sfGFP showed faster maturation and an earlier increase in intensity compared to mScarlet (**Fig. 26A and B**). As expected, considering that both fluorescent proteins are fused, the expression pattern across cells was identical in both the green and red channels (**Fig. 26A**). The R/G ratio also showed the predicted behaviour, with an initial decrease followed by a gradual increase and eventual stabilisation 24 hours post-induction (**Fig. 26C**). Moreover, fitting the intensity curves to a standard gene expression model highlighted the delay as the only difference between the green and red intensity traces (**Fig. 26D**). The mScarlet fluorescence follows the same dynamics as sfGFP but with a delay five times longer. Overall, these results confirmed the behaviour of the tFT in my system and established a time window for its analysis in human iPSCs.

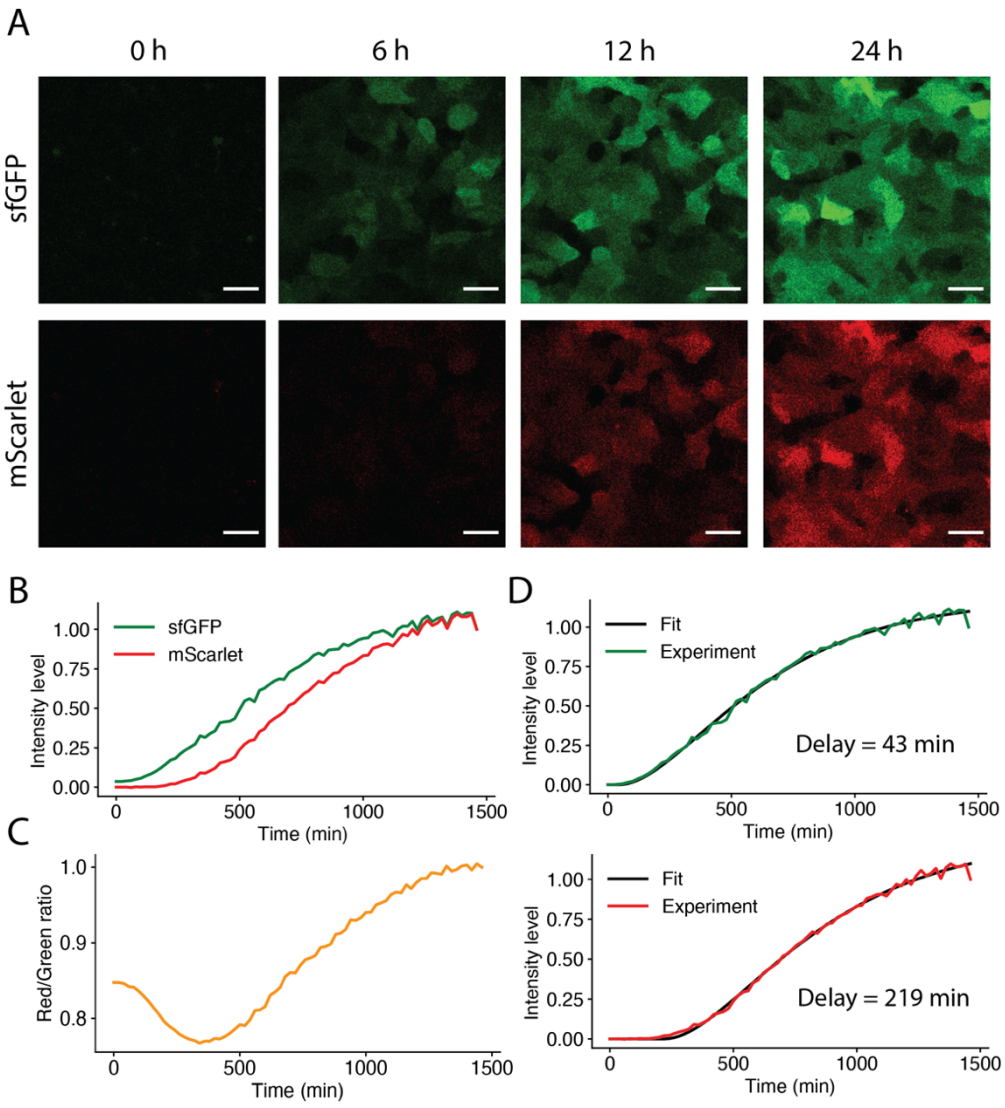

Figure 26: The behaviour of tFTs in human iPSCs.
(A) Imaging of the mScarlet-sfGFP tFT induction dynamics upon addition of Dox. Snapshots at different times after induction are shown. Scale bars are 25 microns. (B) Intensity levels of mScarlet and sfGFP upon addition of Dox. Quantifications correspond to the imaging in (A). The traces are normalised to the maximal intensity and background subtracted. n=1. (C) Red/Green ratio calculated from (B). (D) Fitting of the intensity traces shown in (B) using a gene expression model. Top: sfGFP. Bottom: mScarlet. The fitting line is shown in black. Delay (tau) is highlighted.

To generate the delay reporter, the mScarlet-sfGFP tFT was combined with the genomic sequence of *HES7*, including introns (**Fig. 27A**). This longer transcript would predictably be subject to further expression delay caused by transcription and splicing. As a control, the same construct without the introns was generated. The intron-less version of the reporter should be expressed faster, leading to different R/G ratio dynamics compared to the version with introns. Placing a stop codon before the *HES7* introns could impact transcript stability due to nonsense-mediated mRNA decay [127]. However, to avoid high expression of *HES7*, which could induce cell differentiation, its sequence was positioned after the tFT. Additionally, the *HES7* coding sequence, even without introns, was shown to greatly destabilise mRNA transcripts compared to regular polyA terminations or the *HES7* 3' UTR alone (**Supp. Fig. 1**). This observation is in line with the expected instability of the *HES7* mRNA necessary for sustaining its oscillatory dynamics [34]. The expression dynamics of these reporters were analysed using flow cytometry. A time-course analysis of the R/G ratio at 4, 6, 8, 12 and 72 hours after induction with doxycycline was performed using human iPSCs (**Fig. 27**). In this experiment, bulk populations of cells with the reporter integrated at various genomic sites were compared. The random integration of the reporter is due to the use of a transposon system to generate the transgenic lines. The comparison of expression dynamics between clonal cell lines would ideally require inserting the reporter at the same locus.

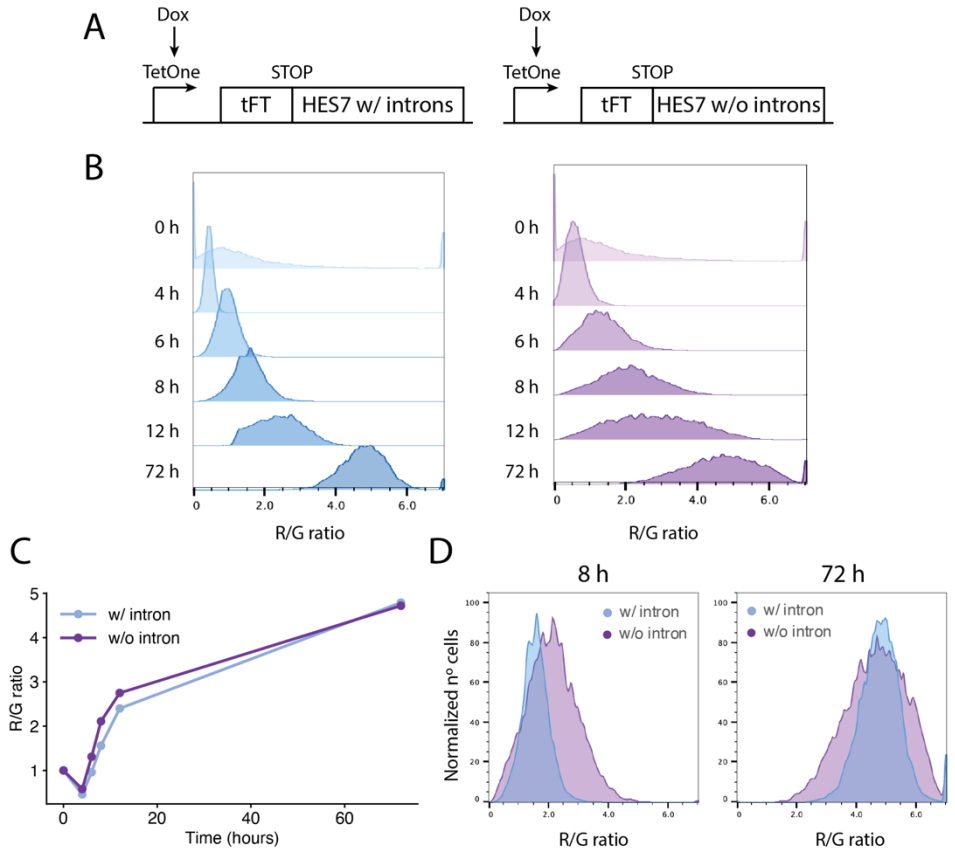

Figure 27: A delay reporter based on tFTs.
(A) Schematic of the inducible delay reporters generated. The only difference is the presence (left) or absence (right) of the *HES7* introns. (B) Histogram of the R/G ratio measured by flow cytometry at different time points upon induction of the reporter with doxycycline. Left: reporter containing introns. Right: reporter without introns. In each time point, 10.000 cells were measured. (C) Mean R/G ratio quantified from (B) and plotted against time. n = 1. (D) R/G ratio histogram of the delay reporter with and without introns at 8h and 72h after induction with doxycycline. The data is the same as in (B).

Upon induction of the delay reporter, the R/G ratio initially decreased and then steadily increased, consistent with the predicted tFT behaviour (**Fig. 27B and C**). The version of the reporter without introns displayed faster dynamics, with its ratio increasing earlier compared to the reporter containing introns (**Fig. 27C**). Importantly, the final R/G ratio was similar for both reporters, indicating that despite the differences in early dynamics, the final steady state was the same (**Fig. 27C and D**). The early behaviour of the R/G ratio is influenced by the expression delay, while the final equilibrium is mostly determined by the protein degradation rates [126]. Therefore, these results suggest that the delay reporter can quantitatively indicate changes in the expression delay generated by the presence or absence of introns. The highest difference was found at 8 hours after induction (**Fig. 27D**). It is important to note that the reporter version without introns shows higher variability, likely due to a higher number of random genome integrations given its smaller size compared to the intron-containing version. In the next section, clonal cell lines were used to reduce this variability and enable the study of perturbations within the same genetic background.

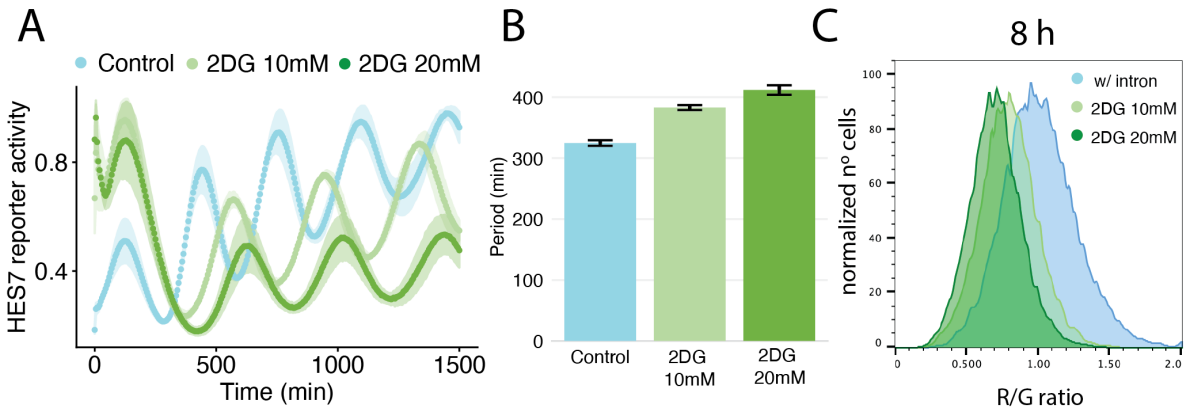

Figure 28: The delay reporter upon glycolytic inhibition.
(A) Oscillatory *HES7* reporter activity of human iPSM cells treated with different concentrations of 2-Deoxy-D-Glucose (2DG). Time course signals were normalised to the maximum intensity. The shading indicates mean ± SD (n=3). Experiment performed by Mitsuhiro Matsuda. (B) Oscillatory periods estimated from (A). Error bars indicate means ± SD (n= 3). (C) R/G ratio histogram of the delay reporter containing introns in PSCs at 8 h after induction with doxycycline. Cells were treated with different concentrations of 2DG.

To further test the delay reporter, changes in the R/G ratio were assessed using perturbations known to affect the segmentation clock period. The addition of 2-Deoxy-D-glucose (2DG), a glycolytic inhibitor, slowed down human PSM cells and increased their period in a dose-dependent manner (**Fig. 28A and B**). Moreover, a recent study demonstrated that 2DG elongates the *HES7* production delay in mouse and human iPSM cells [128]. Human iPSCs treated with 2DG showed a decreased R/G ratio at 8 hours after induction, consistent with a slowdown of the cells and larger expression delays (**Fig. 28C**). Overall,

the delay reporter is capable of responding to both acceleration and slowdown of the expression delay. This reporter can be used in a flow cytometry setting and would allow for the separation of potentially fast and slow cells after genetic perturbation.

3.3.2 Genetic screening of developmental tempo regulators: a directed evolution approach

The ultimate mechanism by which some species display slower or faster biochemical reactions remains unknown. However, in the previous chapter, I identified a list of genes involved in biochemical reactions that correlate with the segmentation clock periods. To gain insight into the role of these genes in regulating the tempo of the segmentation clock, I conducted a gain-of-function screen using human iPSCs. Animal species with faster segmentation clock periods present higher expression of genes related to biochemical reactions. This suggests that altering the gene expression profile of one species could modify its developmental speed. Like many other loss-off function experiments, the slowdown of developmental tempo can be confounded by potential overall cell damage, which would ultimately decelerate many cellular processes. Instead, the acceleration of developmental time offers a clearer readout of tempo modification. To accelerate the segmentation clock period, genes correlating with developmental tempo could be overexpressed in human iPSM cells, aiming to mimic the expression pattern of faster species.

A cDNA library containing 200 genes highly correlated with the segmentation clock and their regulators was generated. This library was constructed by recombining individual clones of the ORFeome collection with a PiggyBac destination vector equipped with a constitutive promoter and a V5 protein tag [129]. The library can be introduced into human cells via electroporation to modify their gene expression profile. FACS-sorting can then be used to isolate potentially faster-expressing cells based on the activity of the delay reporter. The ultimate goal is to identify iPSM cells with accelerated segmentation clock oscillations. However, the limited proliferation capacity of iPSM cells does not allow for their direct perturbation and sorting. Instead, this screening aims to generate accelerated human iPSCs that exhibit a faster segmentation clock period upon differentiation.

Over the years, the segmentation clock has demonstrated robustness to various perturbations [130]. This, combined with the complexity of a phenotype dependent on basic biochemical reaction rates, makes accelerating the segmentation clock a challenging task. Preliminary data showed that individually inducing various genes fails to significantly modify the period of the segmentation clock (**Supp. Fig. 2**). This suggests that the tested genes may not impact developmental tempo or that multiple genes acting together are required to modify the segmentation clock period. It is probably very difficult to alter the developmental tempo of a given species by overexpressing a single gene. To improve the chances of finding combinatorial perturbations that can influence the speed of development, a directed evolution approach was taken. By iteratively perturbing and selecting potentially faster cells, this screening aims to randomly combine multiple changes that could accelerate human iPSCs (**Fig. 29A**). Subsequently, single PSCs from the “accelerated population” can be sorted and differentiated into PSM to evaluate their segmentation clock period.

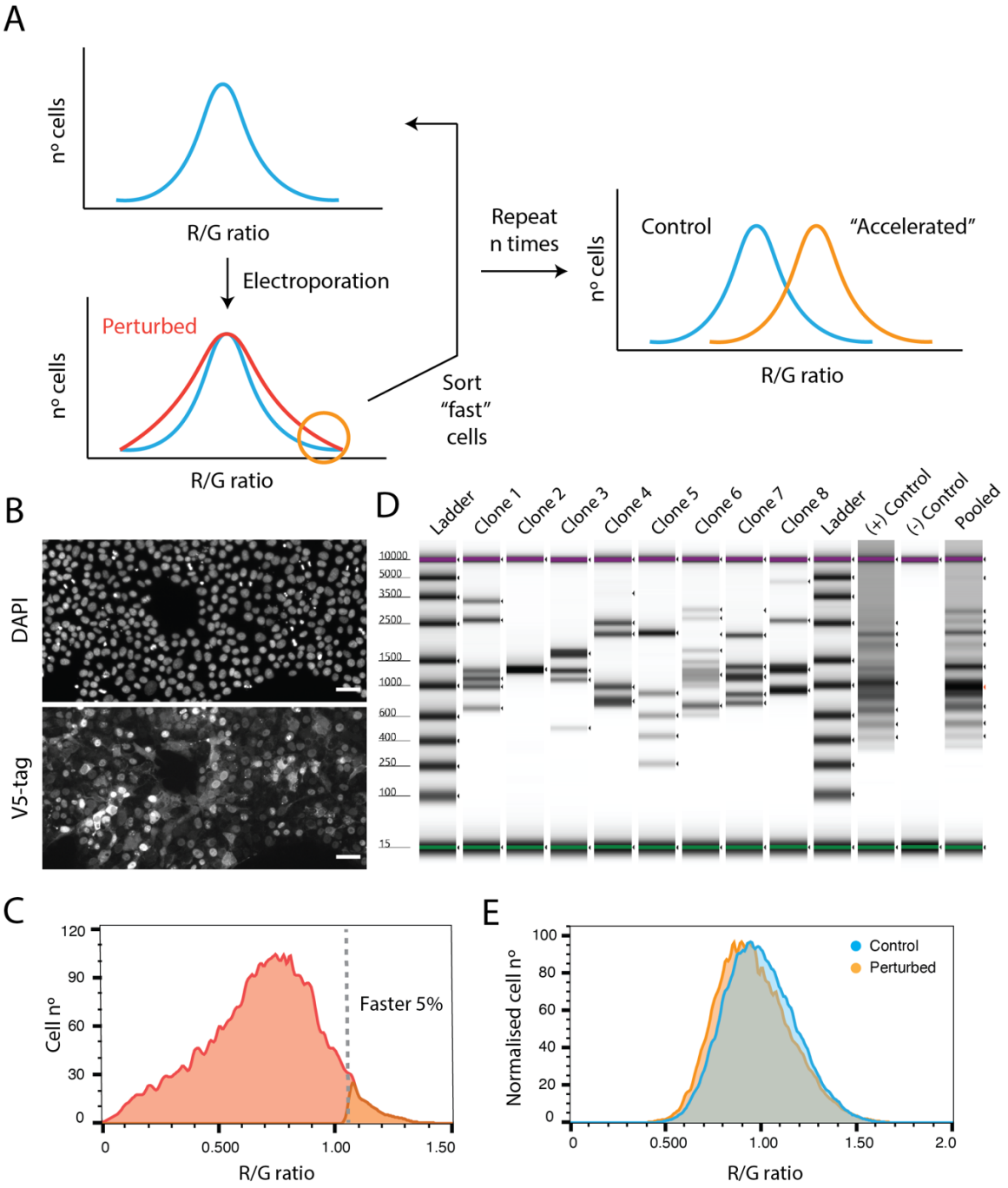

Figure 29: Genetic screening of developmental tempo regulators.
(A) Schematic representation of the directed evolution pipeline. Human iPSCs are perturbed, and the potentially fast cells are sorted based on the ratio of delay reporter. This process is repeated in an iterative way until an accelerated population is generated. (B) Staining for DAPI (top) and anti-V5 tag (bottom) of human iPSCs electroporated with the library. Scale bars are 50 microns. (C) R/G ratio histogram of the delay reporter in electroporated human iPSCs after 8 hours of induction with Dox. The highest 5%, corresponding to the faster cells, is highlighted. (D) DNA electrophoresis of human iPSCs clones after 5 rounds of electroporation and selection. Inserted library genes were amplified from genomic DNA through PCR and analysed using the Agilent D5000 ScreenTape system. The positive control consisted of the purified library mix. The negative control consisted of non-electroporated human genomic DNA. The last sample consisted of the pooled genomic DNA of all electroporated cells. (E) R/G ratio histogram of the delay reporter in control and perturbed human iPSCs after 8 hours of induction with Dox. Perturbed cells were electroporated and selected five times. Skewness: 0.28 and 0.40 in control and perturbed, respectively. Kurtosis: -0.065 and 0.189 in control and perturbed, respectively.

Following electroporation with the cDNA library, the cells exhibited different gene expression patterns, in line with the idea that each cell incorporated a subset of genes from the library (**Fig. 29B**). Since the library primarily consisted of transcription factors, the expression was predominantly localised in the nucleus. Amplification and sequencing of the inserted genes revealed that 87.8% of the library genes were represented in the cell pool after a single electroporation (data not shown). The delay reporter was then induced, and the top 5% faster cells (high R/G ratio) were sorted for another round of electroporation (**Fig. 29C**). The process was repeated five times. Interestingly, 8 hours after reporter induction, the R/G ratio distribution in electroporated cells was skewed to the left, indicating that a significant proportion of the cells experienced a slowdown (**Fig. 29C**). This supports the idea that decelerating biological processes might be less challenging than accelerating them. At the end of the iterative selection process, clones were isolated, and their inserted library genes were amplified through PCR. The clones exhibited a diverse array of bands, indicating a successful combinatorial expression of different library genes (**Fig. 29D**). The variation in patterns across clones confirmed that each cell contained a unique combination of inserted genes. Induction of the delay reporter in these perturbed cells revealed a slightly lower R/G ratio compared to the control cells (**Fig. 29E**). This suggests that the selected cells had an overall slower expression delay, contrary to the initial objective of the screening. Most screened cells were either unaffected or exhibited a slight deceleration in the expression delay. This outcome might have been caused by the small size of the cDNA library, which limits the number of possible perturbations. However, interestingly, the perturbed distribution exhibited higher positive skewness (0.40 vs 0.28) and positive kurtosis (0.189 vs -0.065) compared to the control, indicating an increased proportion of "fast" outliers within the selected cells.

To characterise the segmentation clock period of the perturbed iPSCs, individual human cells were FACS-sorted into 96-well plates, cultured until they formed colonies, and then differentiated to iPSM. The *HES7* oscillatory period was subsequently measured in individual clones, with 170 control and 143 perturbed clones analysed. The distribution of periods revealed that perturbed cells were slightly slower than the control (p-value = 0.0023, K-S test) (**Fig. 30**). This result was consistent with the differences observed in the R/G ratio distribution (**Fig. 29E**), supporting the idea that the delay reporter accurately reflects changes in the segmentation clock period. Interestingly, the periods of perturbed cells showed higher variability compared to the control, suggesting that cells can display more extreme periods after perturbation. The transcriptomes of clones with significantly faster or slower periods were further analysed to identify potential gene expression profiles correlated with these temporal differences.

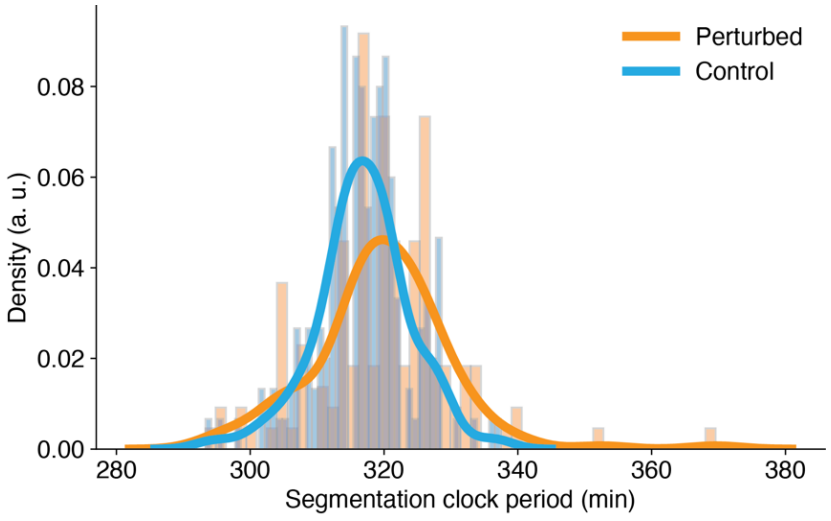

Figure 30: Segmentation clock period analysis of screened cells.
(A) Segmentation clock period distribution of clones isolated from perturbed or control cell populations. Perturbed cells were electroporated with the cDNA library and selected five times for fast expression of the delay reporter. Each period measurement corresponds to one clone grown from a single cell. 170 control clones and 143 perturbed clones were analysed. Histogram of the periods is shown. Distributions are significantly different (p-value = 0.0023, K-S test).

3.3.3 Transcriptomic characterisation of human iPSM clones

The gene expression profile of 12 perturbed and 9 control clones was analysed. For the perturbed clones, only those exhibiting periods at the extremes of the distribution were considered, while the control group encompassed the full range of observed periods. PCA revealed that samples clustered by segmentation clock period, with slower clones grouping together (**Fig. 31A**). Interestingly, both perturbed and control clones were intermixed, indicating that the performed perturbations did not significantly alter the overall transcriptome of the cells (**Fig. 31A and C**). Analysis of the control samples alone also separated the clones by period, forming roughly three groups: “fast,” “intermediate,” and “slow” clones (**Fig. 31B**). The separation observed in control samples indicates that even natural variation in the period can be captured at the transcriptional level. Additionally, plotting the clones in the PCA space generated by the previous transcriptomic dataset across species showed that they clustered close to previous human iPSM samples (**Fig. 31D**). The slight separation of the slowest clones suggests that the transcriptional signature explaining interspecies differences in the segmentation clock period may also be valid for the intraspecies differences observed across human samples.

As in previous analyses, the Spearman correlation coefficient was calculated between gene expression levels and the segmentation clock period across all genes in the 21 clones. GSEA was then performed on the genes ranked by the Spearman correlation coefficient. Visualisation of the enriched GO terms map revealed that genes showing negative correlations, meaning higher expression in faster clones, were enriched for GO terms associated with mRNA transport, DNA replication, chromosome segregation, etc. (**Fig. 32,** blue circles). These terms align with those enriched in species with faster segmentation clock periods, further supporting the idea that the inter- and intraspecies differences in developmental tempo might have a similar transcriptomic signature. Conversely, positively correlated genes were enriched for terms related to proton transport, cytoplasmatic translation, and ribosomal assembly (**Fig. 32**, red circles), suggesting that genes involved in protein translation are affected in slower clones. Overall, these results indicate that the variability in the segmentation clock period observed across human clones can be associated with characteristic changes in gene expression.

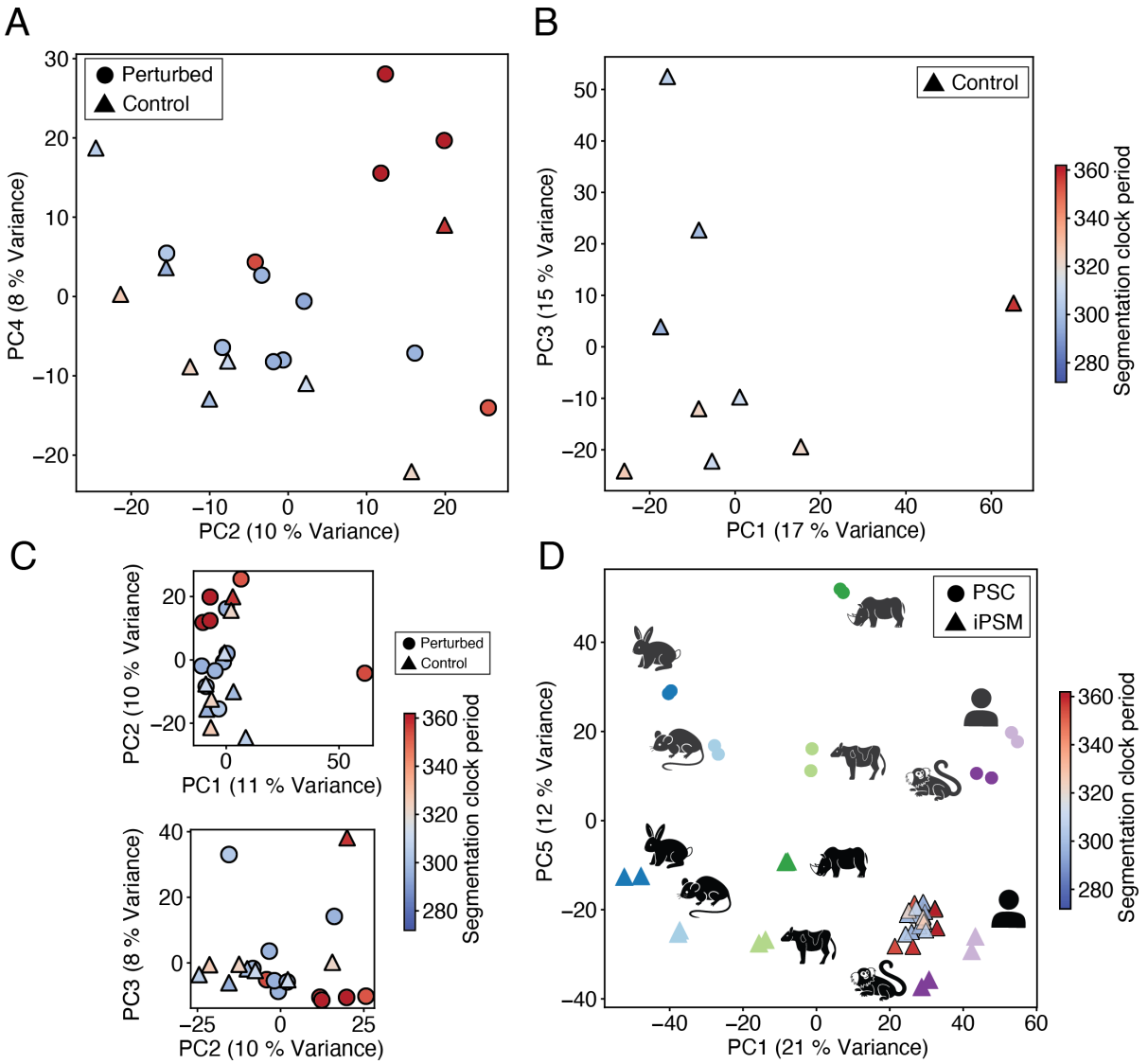

Figure 31: Exploring the transcriptomic signature of iPSM human clones.
(A) Principal component analysis (PCA) from bulk RNA-seq. Components 2 and 4 are shown. The samples are colour-coded by their segmentation clock period. (B) PCA from bulk RNA-seq in the control samples. Components 1 and 3 are shown. Samples are colour-coded by their segmentation clock period. (C) PCA from bulk RNA-seq. Top: components 1 and 2 are shown. Bottom: components 1 and 3 are shown. (A - C) Triangles represent control samples, while circles represent perturbed samples. The variance explained by each component is indicated. (D) iPSM human clones mapped into the PCA space generated by the RNA-seq data across species (data from Fig. 20A). Components 1 and 5 are shown. PSCs (circles) and iPSM cells (triangles) are plotted. Human clones are colour-coded by their segmentation clock period.

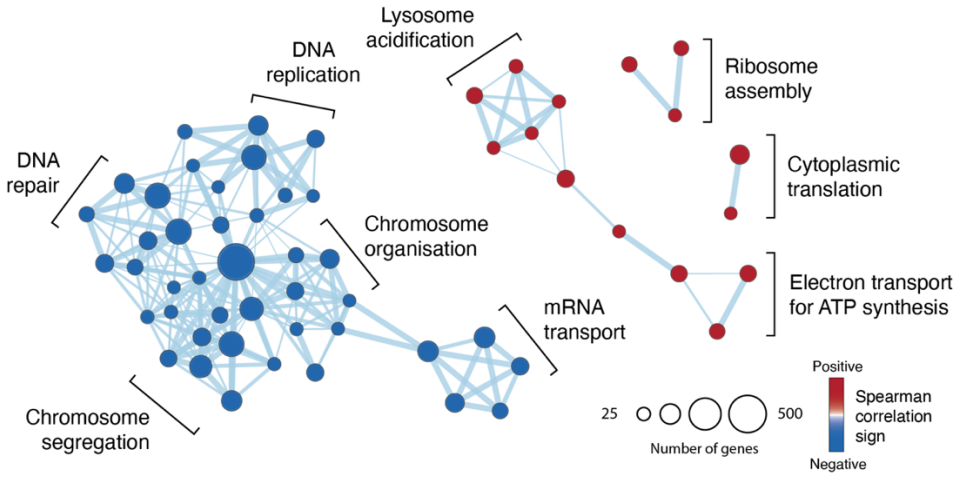

Figure 32: Gene enrichment maps in iPSM human clones.
(A) Enrichment map network of genes that showed correlated expression with the segmentation clock period in human iPSM clones. Circle size represents the number of genes in that process. Blue and red colours represent processes with genes correlating negatively and positively with the segmentation clock period, respectively.

In contrast to the observations across different animal species, the variations in segmentation clock period and gene expression within human iPSM samples were minor. Such small differences can make identifying genes or processes associated with developmental tempo challenging due to noise. To enhance the robustness of these comparisons, human iPSM clones were categorised based on their segmentation clock periods. The focus was placed on the segmentation clock period rather than the perturbations due to the transcriptomic similarity between screened and control samples (**Fig. 31A and C**). Clones with a period lower than 300 minutes were considered "Fast", while clones with periods higher than 350 min were considered "Slow". This final grouping contained 6 slow and 8 fast clones. Differential gene expression analysis between these two groups was performed using a standard DESeq2 workflow [131]. PCA of the samples after fitting the DESeq2 model separated the fast and slow groups (**Fig. 33A**), confirming previous observations. Slow vs Fast comparison revealed that 240 genes were differentially expressed with significant adjusted p-value and high fold change (**Fig. 33B**). Hierarchical clustering based on these genes grouped slow and fast samples (**Fig. 33C**). Interestingly, the heatmap highlighted a certain degree of variability across the gene expression within groups, with some genes being highly expressed in certain clones (**Fig. 33C**). This further supports the idea that grouping samples based on the segmentation clock period could be helpful in generating more robust results. GSEA analysis of all genes ranked by their differential expression parameters revealed strong enrichment of terms related to protein translation, aerobic respiration and ATP synthesis in the slow group (**Fig. 33D**, positive Normalized Enrichment Score, NES). The inhibition of these processes in human iPSM has been associated with a slowdown in the segmentation clock period [71]. Moreover, terms related to centrosome separation and DNA replication, both involved in the control of cell division, were enriched in the fast group, suggesting these clones might have differences in their cell cycle (**Fig. 33D**, negative NES).

Altogether, these results showed that fast and slow human iPSM clones present distinct gene expression signatures. Investigating these differentially expressed genes could help explain the variations in the segmentation clock period observed within a single species. Similar approaches could potentially be employed throughout evolution to modify developmental tempo across species.

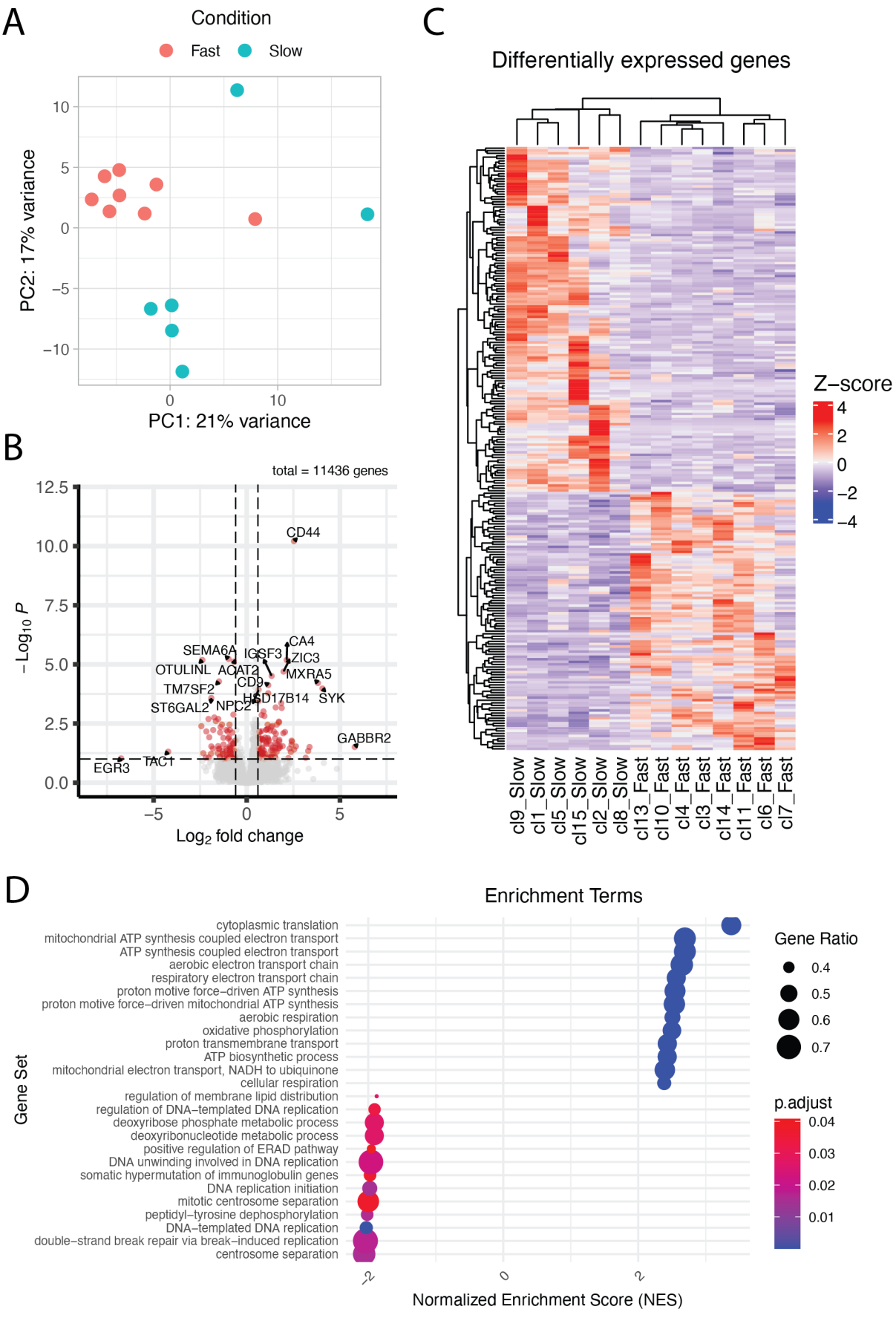
A
Condition
Fast
Slow
PC2: 17% variance
PC1: 21% variance
B
total = 11436 genes
CD44
CA4
ZIC3
MXRA5
SYK
GABBR2
SEMA6A
IGSF3
OTULINL
AQAT2
CD9
TM7SF2
HSD17B14
ST6GAL2
NPC2
EGR3
TAC1
−Log10 P
Log2 fold change
C
Differentially expressed genes
Z−score
cl9_Slow
cl1_Slow
cl5_Slow
cl15_Slow
cl2_Slow
cl8_Slow
cl13_Fast
cl10_Fast
cl4_Fast
cl3_Fast
cl14_Fast
cl11_Fast
cl6_Fast
cl7_Fast
D
Enrichment Terms
Gene Set
cytoplasmic translation
mitochondrial ATP synthesis coupled electron transport
ATP synthesis coupled electron transport
aerobic electron transport chain
respiratory electron transport chain
proton motive force−driven ATP synthesis
proton motive force−driven mitochondrial ATP synthesis
aerobic respiration
oxidative phosphorylation
proton transmembrane transport
ATP biosynthetic process
mitochondrial electron transport, NADH to ubiquinone
cellular respiration
regulation of membrane lipid distribution
regulation of DNA−templated DNA replication
deoxyribose phosphate metabolic process
deoxyribonucleotide metabolic process
positive regulation of ERAD pathway
DNA unwinding involved in DNA replication
somatic hypermutation of immunoglobulin genes
DNA replication initiation
mitotic centrosome separation
peptidyl−tyrosine dephosphorylation
DNA−templated DNA replication
double−strand break repair via break−induced replication
centrosome separation
Normalized Enrichment Score (NES)
Gene Ratio
p.adjust

Figure 33: Differential gene expression analysis between "Slow" and "Fast" clones.
(A) Principal component analysis (PCA) after fitting the DESeq2 model. Components 1 and 2 are shown. The samples are colour-coded by condition. (B) Volcano plot highlighting the most differentially expressed genes between the Slow and Fast groups. The log2 fold change and the -log10 of the adjusted p-value are plotted. The significance thresholds are 0.6 for the fold change and 0.1 for the adjusted p-value. Genes over both thresholds are coloured red. Top differentially expressed genes are labelled. Genes with positive fold change are expressed higher in the "Slow" group. (C) Hierarchical clustering of the samples based on the most differentially expressed genes. The colour code represents the Z-score across samples. Each row represents a gene. (D) Gene sets enriched after ranking all genes based on their differential expression parameters. Gene sets with positive normalised enrichment score (NES) are expressed higher in the "Slow" group, while genes with negative NES are higher in the "Fast" group. Size represents the gene ratio, the percentage of overrepresented genes in that group. The colour code indicates the adjusted p-value. Only those terms with adjusted p-values below 0.05 were considered.

From the 240 differentially expressed genes, only 7 were present in the cDNA library used for the screening. Notably, one of them, *EGR3*, was expressed very highly in the fast group (**Fig. 33B**). Further comparison between the fast and slow clones that have been electroporated with the library (perturbed group) highlighted *EGR3* as one of the more differentially expressed genes from the cDNA library (**Supp. Fig. 3**). This new comparison also revealed *ING2* as a library gene highly expressed in slow clones **(Supp. Fig. 3**). *EGR3* is a growth response transcription factor that regulates muscular development and controls biological rhythms [132,133]. Conversely, *ING2* is an inhibitor of growth that can function as a tumour-suppressive protein by regulating the cell cycle [134]. These genes were individually overexpressed in human iPSM cells to investigate their potential impact on the segmentation clock period (**Fig. 34A**). Notably, overexpressing *EGR3* significantly accelerated the segmentation clock compared to the control (**Fig. 34B and C**, p-value =0.028). The period decreased by approximately 30 min, equivalent to a 10% acceleration. In contrast, overexpressing *ING2* did not significantly alter the segmentation clock (**Fig. 34B and C**). Altogether, the screening strategy used in this study successfully identified genes that can accelerate the speed of the segmentation clock. This approach can be applied in future studies to test additional perturbations and better characterise the genetic regulation of developmental tempo.

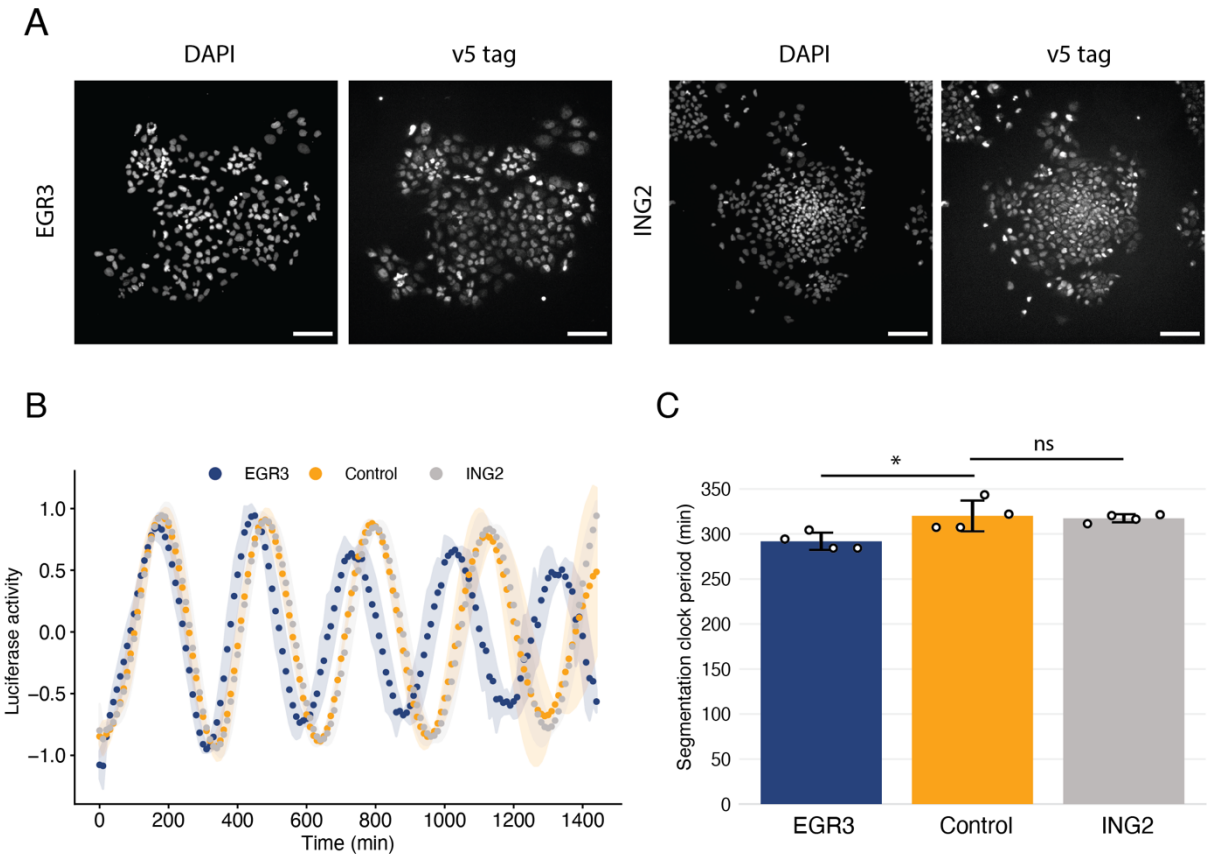

Figure 34: Overexpression of *EGR3* and *ING2* in human iPSM cells.
(A) V5-tag and DAPI staining of human iPSM cells overexpressing a V5-tagged version of *EGR3* and *ING2* individually. Scale bars are 100 microns (B) Oscillatory *HES7* reporter activity after detrending and amplitude normalisation. Shading indicates means ± SD (n = 4). Cells are expressing *EGR3*, *ING2* or none (Control). (C) Oscillatory periods in each condition. Error bars indicate means ± SD (n = 4). Unpaired two-sided t-test: p= 0.028 between EGR3 and control.

4. Discussion

4.1 The stem cell zoo for the study of developmental time

During embryonic development, cells coordinate in space and time to generate complex patterns and morphologies. Controlled differences in the tempo or duration of developmental processes are known to influence animal size and form, being an important mechanism of evolutionary change. However, the mechanisms behind these temporal changes remain elusive due to the difficulties in quantitatively comparing embryos from different animal species. The establishment of stem cell-based *in vitro* models of development now offers an unprecedented opportunity to perform interspecies comparisons [43,85]. Cell- and tissue-autonomous processes can be recapitulated *in vitro* using PSCs and studied under similar experimental conditions. Moreover, the use of stem cells from unconventional species, whose embryos are mostly inaccessible, offers the opportunity to study unique developmental phenotypes. In this thesis, I leveraged the advantages of stem cell systems to investigate how developmental tempo is regulated across species.

I have established a novel experimental platform, the stem cell zoo, that allowed me to investigate the connection between developmental tempo and other cellular parameters or animal characteristics. To this aim, I recapitulated *in vitro* the segmentation clock of four novel mammalian species: rabbit, cattle, rhinoceros and marmoset. Expanding beyond the classic human and mouse developmental models has revealed a general scaling law between developmental tempo and the speed of biochemical reactions. Interestingly, the control of biochemical kinetics was not determined by energy availability, as cellular metabolic rates did not correlate with the segmentation clock period. Instead, the genes related to biochemical reactions showed an expression pattern that scaled with the segmentation clock period, providing evidence for the transcriptional regulation of developmental tempo. Altogether, the analysis of the segmentation clock in six mammalian species has allowed the establishment of robust correlations that would have otherwise remained elusive.

Beyond extending our current investigations to other animals, using PSCs from diverse species could facilitate the study of alternative forms of biological time (**Fig. 35**) [43]. An example is the species-specific heart beating rates. Generally, larger animals have slower heart rates compared to smaller ones [135]. However, the mechanism that establishes these species-specific basal heart rates remains to be determined. The heartbeat is initiated by pacemaker cells in the sinoatrial node, and its frequency can be modulated by various neurotransmitters [136]. While a cell-autonomous mechanism for establishing the basal heart rates in pacemaker cells is a plausible hypothesis, it requires further investigation. Recent advancements have enabled the differentiation of PSCs into cardiac pacemaker cells [137–139]. Studying these cells could shed light on how species establish their characteristic heart rates based on the organism's size.

The stem cell zoo provides a powerful platform for comparing developmental processes across different species. However, while these PSC-based models can recapitulate cell-autonomous behaviours, they fail to fully replicate the complex embryonic environment present during morphogenesis. To better understand how embryos are shaped, it is essential to characterise the extrinsic factors that influence the species-specific developmental phenotypes *in vivo*. Techniques like xenotransplantation [62], species hybridisation [140], or interspecies chimerism [141] offer valuable avenues for these investigations. Ultimately, combining the stem cell zoo with embryology is crucial to avoid artefacts arising from *in vitro* studies and gain a holistic understanding of how developmental tempo varies between species.

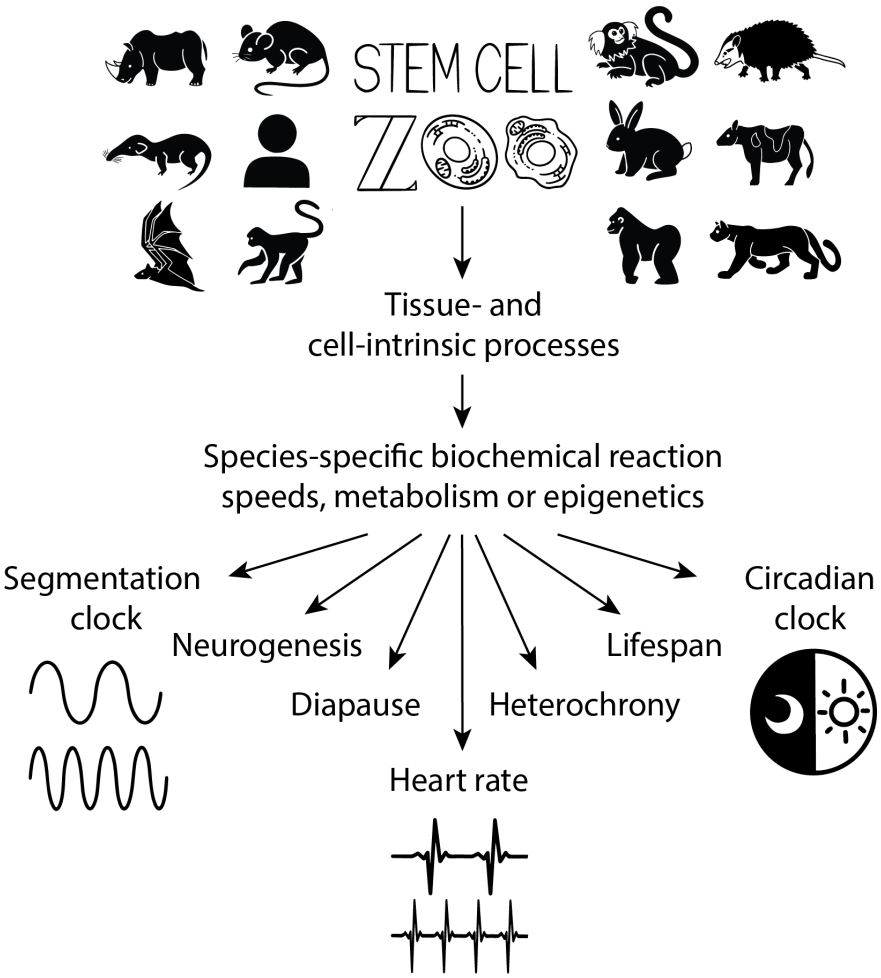

Figure 35: The stem cell zoo for the study of biological time.
PSCs from diverse animal species offer a platform to recreate tissue- and cell-specific biological processes. PSC-derived models can accurately represent species-specific differences in a wide range of biological functions by manipulating factors such as biochemical reaction rates, cellular metabolism, or epigenetics. Figure extracted from Lázaro et al. [43].

4.2 The allochronic scaling of developmental tempo

The size of an organism is a crucial feature with profound implications for its interactions with the surrounding world. Many chemical, physical and biological parameters are known to scale with the animal size [91]. However, the stem cell zoo revealed no correlation between the segmentation clock period and the adult body weight, suggesting that developmental tempo does not follow an allometric dependency. This disconnection becomes clearer when considering the time window of somitogenesis and the segmentation clock, the so-called “phylotypic period”. During this time window of high phenotypic conservation, embryos from different vertebrate species have a similar size and morphology [23]. Therefore, it is reasonable to expect that the rate of developmental processes occurring during the phylotypic period does not correlate with adult body weight. Instead, animal size strongly scales with the gestation period [86], which in many organisms is mostly determined by the length of the foetal phase. This suggests that animal size might begin to be regulated during post-embryonic development. Interestingly, the segmentation clock period showed a strong correlation with the length of

embryogenesis, indicating a close connection between the pace and duration of embryogenesis. By studying the regulation of the segmentation clock period, we can gain a better understanding of how these two parameters are established across different species.

Species with longer segmentation clocks have extended periods of embryogenesis and develop more slowly. While this relationship may seem trivial, it confirms the allochronic scaling of the segmentation clock, with important implications for the evolution of animal morphology. For instance, despite having large differences in their segmentation clock period, mammalian species display a very conserved number of presacral vertebrae [142]. To maintain this number, a proportional acceleration or slowdown of the segmentation clock with other developmental processes must be achieved. This allochronic scaling highlights the tight coupling between the segmentation clock and the embryogenesis rate, suggesting the existence of a common master regulator in mammals. However, the number of segments can be more variable when comparing broadly across vertebrate species [143]. This variation can be achieved through differences in the onset of somitogenesis or by decoupling the segmentation clock from the growth rate. For example, accelerating the segmentation clock with respect to the rate of development in snakes gives rise to their high number of vertebrae, ultimately changing their body plan [24]. These unscaled changes in the timing or rate of developmental processes across taxa are defined as heterochronies [11]. Understanding how temporal uncouplings occur – shifting from allochrony to heterochrony – will be fundamental in unravelling the mechanisms behind the evolution of animal form.

The temporal coupling between developmental processes can also be observed within a single species. As development progresses, the rate of somitogenesis slows down, with posterior somites forming more slowly than anterior ones [114]. An extreme case of this can be seen during marsupial development, where there is a 4-fold change in the somitogenesis rate along the anterior-posterior axis [144]. This heterochronic slowdown is not exclusive to somitogenesis, as the development of the hindlimbs and other posterior structures also shows temporal delays [145,146]. The preferential specification of anterior over posterior structures in non-placental mammals allows them to survive after altricial birth and complete development in the mother's pouch. This coordinated slowdown of the marsupial posterior structures further supports the idea that developmental processes must be temporally coupled to preserve the body plan. Comparing anterior and posterior structures in marsupials could shed light on the mechanisms used by cells to modulate developmental tempo and coordinate it with other processes. Recently, iPSCs have been derived from the marsupial species *Monodelphis domestica*, i.e. the short-grey-tailed opossum [147]. *In vitro* recapitulation of the opossum's segmentation clock at different anterior-posterior positions could be a useful system to uncover the nature of the potential master regulator of vertebrate axial development.

The work reported in this thesis has revealed the allochronic scaling of the segmentation clock across mammalian species. The period of the segmentation clock changes proportionally with the rate of embryogenesis, indicating a close coupling between these processes. This coupling is likely due to the strong constraints present during the phylotypic period that ensure the conservation of the vertebrate canonical body plan [23]. Several developmental modules are responsible for segmenting and patterning the embryonic anterior-posterior axis. Thus, coordinated scaling during this period must involve changing the fundamental mechanisms used by cells to regulate biological time across tissues. Studying species-specific segmentation clock periods may enhance our understanding of how developmental tempo is regulated throughout the embryo. Similar mechanisms might also be co-opted to uncouple temporal processes, leading to the heterochronies that contribute to morphological diversity.

4.3 The mechanism behind the species-specific segmentation clock periods

In vitro modelling of developmental processes using PSCs suggested that the species-specific rates of biochemical reactions are responsible for the differences in developmental tempo observed between mice and humans [57,59]. By extending beyond the canonical mouse and human models, I have identified a general scaling relationship between the segmentation clock period and the speed of the *HES7* biochemical reactions, suggesting that changes in biochemical kinetics may be a general principle of developmental tempo control. This mechanism is not limited to the *HES7* gene, as faster-developing species generally exhibit faster protein degradation [122,148]. Therefore, the period of the segmentation clock results from the overall kinetic environment inside of the cell. Interestingly, the speed of biochemical reactions is also associated with the species-specific lifespan. Animals with increased longevity tend to have slower biochemical reaction rates, such as protein turnover and transcription elongation speed [149–151]. These findings suggest that biochemical kinetics might have a universal role in regulating biological time. Cells from different species could be tunning the rate at which they go through the central dogma of molecular biology to control species-specific phenotypes. However, the mechanisms behind the emergence of these differences in the intracellular environments, the ultimate regulators of biochemical kinetics, still remain elusive.

Cellular metabolism has been proposed as a likely candidate for controlling the speed of biochemical reactions across species. Changes in metabolic rates have been observed to affect the speed of transcription, translation, degradation and cell proliferation [69,70]. A prevalent theory in the field has suggested that cells from different animal species could modulate the speed of biochemical reactions by tuning their energy production. Supporting this idea, a recent study described higher mass-specific metabolic rates in mouse iPSM cells than human cells [71]. However, after examining additional species, I found no correlation between the segmentation clock period and the cellular metabolic rate, indicating that energy output alone cannot explain species-specific biochemical kinetics. This finding does not imply that metabolism has no role in developmental tempo. For example, perturbations in metabolic pathways in human PSM cells, particularly changes in the NAD+/NADH redox balance, can slow down or accelerate the segmentation clock by altering translation rates [71]. Similarly, altering the NAD+/NADH ratio of mouse PSM explants by culturing them in galactose also modified their segmentation clock period [74]. Instead of relying on ATP production, cells could depend on redox homeostasis to maintain the proper developmental pace. To determine whether this constitutes a general mechanism, measurements of the NAD+/NADH redox balance across species would be necessary. Additionally, different species might have adopted various strategies to control their biochemical kinetics, making the search for a universal regulator very challenging. Further studies will be necessary to unravel the relationship between cellular metabolism and the control of developmental rate.

Another candidate proposed for the regulation of developmental tempo across species has been cellular size. The stem cell zoo revealed a mild correlation between cellular volume and the speed of the segmentation clock. With the exception of the marmoset, larger cells tend to exhibit slower periods. Changes in cell size have been previously shown to influence the rate of transcription, translation and protein degradation [152,153]. Increasing the cellular volume can alter the DNA/cytoplasm ratio, effectively leading to cytoplasmic dilution and affecting cellular kinetics [154]. Moreover, mathematical modelling has suggested that changes in nuclear volume could explain the differences observed in the amphibian segmentation clock periods [155]. Cell size could be upstream of the biological processes regulating developmental tempo. However, precise methods for altering cellular volume are necessary to test these hypotheses and determine how species-specific cell size is established in the first place. A potential experimental strategy would be to increase the ploidy of cells, which has been associated with

increased cell volumes and alterations in metabolic rates [156,157]. Interestingly, despite showing a two-fold difference in their temporal progression, human and mouse motor neuron progenitors have similar cell sizes [71]. This suggests that the potential impact of cellular size on the speed of development might be cell type-specific.

The cell cycle speed has also been described as a potential regulator of developmental rates. The timing and regulation of the cell cycle are crucial for coordinating development [158], and differences in cell cycle dynamics could directly impact the speed of the segmentation clock. Some models of somitogenesis have linked the cell cycle in the PSM with the periodic formation of somites [159]. Additionally, accelerating the cell cycle can enhance protein turnover through passive dilution [160]. However, subsequent studies have shown that complete cell cycle arrest does not alter the segmentation clock period [71,161], indicating that the cell cycle is unlikely to be responsible for the species-specific differences in segmentation clock tempo.

The stem cell zoo has uncovered a general mechanism for controlling developmental tempo, wherein cells from different species regulate the pace of their biochemical reactions. The segmentation clock period varies across species by proportionally scaling all the kinetic parameters affecting the *HES7* feedback loop. This coordination suggests the existence of a common regulator of biochemical reaction rates. However, recent findings show that distinct metabolic inhibitions can selectively impact individual processes of the segmentation clock, implying that there may be multiple modulators [128]. In any case, the exact nature of the regulators of the segmentation clock period still remains elusive. Investigating the mechanisms by which different species tune their intracellular environments will contribute to an evolutionary understanding of developmental tempo and offer novel methods to manipulate it.

4.4 The genetic control of the segmentation clock period

Genes related to basic biochemical reactions show an expression pattern that negatively correlates with the segmentation clock period, providing the first evidence of the potential transcriptional regulation of developmental tempo across multiple species. Cells from different species may regulate their intracellular environment by controlling the expression of certain genes related to biochemical kinetics. However, a mechanistic connection between gene expression and the segmentation clock period is still missing. Exploring the regulation of these species-species transcriptional signatures will be critical for understanding how species-specific temporal phenotypes emerged and evolved at one of the smallest biological scales, the cell.

Genes influencing developmental tempo have already been described in various systems. For example, a heterochronic gene network in the worm *Caenorhabditis elegans* is responsible for controlling the rhythmic execution of moulting cycles between larval stages [162]. Mutations in the *lin-4* and *let-7* genes can affect the number and identity of moults [163], whereas changes in *lin-42a* modify their timing [164]. Another example is the progressive degradation of maternally deposited transcription factors, which controls the timing of the midblastula transition in *Xenopus* [165]. These “hourglass” mechanisms are commonly used by embryos to regulate the timing of events through the accumulation or degradation of specific gene products [166,167]. In the context of somitogenesis, a recent study hybridised two closely related medaka fish species to investigate differences in their developmental rates [140]. Quantitative trait loci mapping in F2 hybridised embryos revealed several genomic loci

associated with the timing of the somitogenesis. Knocking out two of these genes in the parental strain produced a mild acceleration of the segmentation clock period [140]. These examples illustrate how particular genes can impact the developmental tempo of a given process. However, whether these genes or their homologs can act as general regulators of tempo across different tissues or species remains to be tested.

The interspecies differences in the segmentation clock periods arise from species-specific intracellular environments and biochemical kinetics. These differences likely result from fine-tuning the expression of multiple genes, making it challenging to genetically perturb the overall kinetic environment of cells and modify the developmental tempo of a given species. To address this, I developed reporters that enable the sorting of cells based on changes in the speed of their biochemical reactions. These reporters can capture small differences in gene expression delays, which are influenced by processes such as transcription, splicing, mRNA transport and translation. To identify the genes contributing to the biochemical environment of cells, I combined these delay reporters with perturbations of the human gene expression profile. By overexpressing a library of genes that correlate with developmental tempo and selecting potentially accelerated clones in an iterative way, I sought to obtain human iPSM cells with expression patterns similar to those of faster-developing species.

Contrary to the initial objective of the screening, the average selected cells exhibited a slight slowdown in both their expression delay and their segmentation period. However, the increased variability of the perturbed distribution suggested that few clones can achieve more extreme temporal phenotypes. Interestingly, during the selection process, many cells showing slower expression delays were observed after each electroporation with the cDNA library. This raises the question of why it is easier to decelerate rather than accelerate this developmental system. Is there an intrinsic limit to how much acceleration is possible? One possibility is that disrupting individual cellular processes causes the system to collapse, whereas only the simultaneous acceleration of multiple processes can produce faster phenotypes. However, it is also possible that active mechanisms are in place to prevent the acceleration of cells. For example, the increased transcription rates, protein degradation and cell division associated with faster cells are often related to cancerous phenotypes [168,169]. Mammalian cells rely on several tumour suppressor genes, such as *TP53* or *RB1*, to prevent oncogenic processes [170]. These mechanisms may be limiting the capacity to accelerate developmental tempo. Therefore, removing some of these genes could potentially generate more sensitive backgrounds for genetic screenings, helping reveal some of the genes controlling the kinetics of biochemical reactions currently masked by the system's robustness.

Transcriptional characterisation of the human iPSM clones with different segmentation clock periods revealed that intraspecies variation in developmental tempo can also be captured at the gene expression level. Clones with slower periods showed higher expression of genes related to cytoplasmic translation, ribosome assembly and ATP production. Inhibition of these processes has been associated with a slowdown of the segmentation clock period [71]. Interestingly, altering the levels of the ribosome-related proteins highlighted in this analysis influences protein translation in very specific ways. For example, shifts in the total concentration of ribosomes can increase or decrease the translation efficiency of different mRNA pools based on their initiation rates [171]. Similarly, disproportionate changes in the amounts of 60S or 40S ribosomal subunits, which must be kept in similar stoichiometry, lead to specific protein synthesis and degradation patterns [172]. The complex network controlling ribosomal concentration and composition makes it difficult to understand the relationship between the expression of ribosomal protein genes and translation efficiency. A proteomic characterization of human iPSM cells with different periods would help unravel how these transcriptional signatures ultimately change protein composition and affect cellular function. Additionally, it is important to note that the observed gene

expression profile could be a consequence of the slower tempo rather than its cause. Further experiments are necessary to characterize the causal relationship between transcription, actual translation kinetics, and the segmentation clock period.

The faster clones were enriched in terms related to DNA replication, chromosome segregation and mitotic transitions, suggesting these cells have an accelerated cell cycle. As previously discussed, the cell cycle does not seem to directly control the speed of the segmentation clock. However, both processes could be influenced by a common regulator. Cells with accelerated biochemical kinetics could show faster segmentation clock periods and cell cycles. For instance, the controlled degradation of proteins through the ubiquitin-proteasome pathway is essential to maintain the periodicity of the cell cycle (reviewed in [173]), similar to what has been shown for the segmentation clock. This further supports the idea that experimentally dissecting the causal relationships of the system is essential for the understanding of its regulation.

Comparing the gene expression profiles between fast and slow human iPSM clones identified *EGR3* as a gene from the cDNA library that is highly expressed in faster cells. Notably, overexpression of *EGR3* significantly accelerated the segmentation clock period in iPSM cells. *EGR3* is a transcription factor with broad expression during development and diverse functions, including a role in muscle spindle development [174] and T-cell activation [175]. As an immediate growth response gene, *EGR3* can be induced by mitogenic stimulation, such as TFG-β signalling or other growth factors [176]. Additionally, *EGR3* plays an important role in the central nervous system, influencing learning processes and biological rhythms like the circadian clock [133,177]. Interestingly, genes involved in the circadian clock have been shown to interfere with the normal segmentation clock, suggesting a functional connection between these two processes [178]. Further experiments are needed to determine whether *EGR3* directly influences the segmentation clock period or acts through changes in species-specific intracellular kinetics. Additionally, it would be interesting to test the general ability of *EGR3* to influence developmental tempo by modulating its expression in different species and cell types.

In this thesis, I have established a general pipeline for screening perturbations that affect developmental tempo. By integrating fluorescent reporters for gene expression delays, cell sorting, and single-colony segmentation clock measurements, I identified one genetic perturbation capable of accelerating the developmental tempo of human iPSM cells. However, most screened cells were either unaffected or exhibited a slight slowdown in expression delay and segmentation clock periods. This could be due to the small size of the cDNA library used, limiting the number of possible perturbations. More general methods of perturbing gene expression, such as mutagenesis or genome-wide CRISPR screens, could be used to explore further genetic variation and potentially generate larger differences in the segmentation clock period. Additionally, given the challenges in accelerating the clock, studying perturbations that slow down the segmentation clock could provide insights into the genetic control of developmental tempo. Overall, the use of PSCs has enabled the screening of genetic changes that influence the speed of biochemical reactions and, ultimately, the pace of development. Understanding how natural or induced genetic variation modulates developmental tempo is crucial for unravelling the evolutionary mechanisms behind this phenotype.

5. Conclusions and Outlook

In this thesis, I investigated the regulation and scaling of developmental tempo across various mammalian species. Using *in vitro* differentiation of pluripotent stem cells, I recapitulated the segmentation clocks of four novel species: rabbit, cattle, rhinoceros and marmoset. Together with the previously characterized mouse and human, this "stem cell zoo" enabled the study of developmental tempo across six mammals spanning a wide range of body sizes and morphologies.

The segmentation clock period across different species did not scale with the adult body weight, indicating that the timing of somitogenesis lacks allometric dependency. Instead, the strong correlation between the segmentation clock period and the length of embryogenesis revealed an allochronic scaling of developmental tempo. This suggests that a tight coupling between the segmentation clock and the embryogenesis rate might be necessary to maintain the canonical mammalian body plan. Interestingly, the speed of biochemical reactions, such as protein degradation and RNA production delays, clearly scaled with the species-specific segmentation clock period. This finding uncovered a general mechanism for controlling developmental tempo, wherein cells from different species adjust their intracellular environments to regulate the pace of biochemical reactions. Surprisingly, these kinetic differences were not driven by energy availability, as cellular metabolism did not correlate with the segmentation clock period. Instead, genes related to biochemical reactions exhibited expression patterns that scaled with the segmentation clock period, providing evidence of the transcriptional regulation of developmental tempo.

To better characterise the transcriptional signature of developmental tempo, I established a pipeline for screening gene expression differences affecting the segmentation clock period in human cells. To achieve this, I first developed novel fluorescent reporters that enable the sorting of cells based on changes in the speed of their biochemical reactions. Combining these reporters with perturbations of the human gene expression profile allowed me to isolate cells with either accelerated or slowed-down segmentation clock periods. By examining the natural and induced gene expression changes impacting developmental tempo, I identified *EGR3* as a gene with the capacity to accelerate the segmentation clock period in human iPSM cells. Studying this and other modulators of developmental tempo will help unravel how species-specific temporal phenotypes emerged and evolved at the cellular level.

The stem cell zoo can be further expanded to include animal species with unique developmental phenotypes, such as the heterochrony observed in marsupials. Currently, most of the available PSC lines are derived from mammals. Nevertheless, advancements in pluripotent stem cell technologies will eventually enable the use of stem cells from other animal groups, such as birds, fish, reptiles, or amphibians, allowing for a more comprehensive phylogenetic representation in developmental studies. Similarly, the stem cell zoo platform can be used to study other forms of biological time or developmental processes. Pluripotent stem cells from different species could help us understand how species-specific differences emerge in processes like neurogenesis, heart rate, or lifespan. Furthermore, combining the stem cell zoo with organoid protocols could allow the generation of complex 3D tissue-like structures comprising several cell types. These structures could be useful for assessing the influence of extrinsic factors and cell-cell interactions in the control of developmental tempo. By using species-specific organoids, we could begin to explore the mechanisms through which cell-autonomous developmental tempo contributes to tissue-level processes, ultimately shaping the unique morphological features of each animal.

Different species modulate their developmental tempo by adjusting their intracellular kinetic environment. The ultimate mechanism by which some species exhibit faster or slower biochemical reactions remains unknown. However, this study has identified a list of genes correlated with developmental tempo as potential candidates and established a novel experimental pipeline to investigate how changes in gene expression affect the segmentation clock period. Species-specific differences appear to emerge at various scales, from biochemical reactions and cell-autonomous processes to tissue dynamics and embryonic morphologies. The stem cell zoo offers an excellent opportunity to quantitatively investigate how species-specific intracellular environments are established. It would be interesting to explore how different cellular functions and subcellular structures change across species. These studies might reveal important mechanisms that contribute to making animal species unique at the cellular level, with implications across many biological levels.

With the establishment of the stem cell zoo, this study has provided an unprecedented opportunity to compare cellular parameters across previously inaccessible mammalian species, uncovering general scaling relationships that would have otherwise remained elusive. Extending beyond the traditional human and mouse models is critical to assess what constitutes a species-specific behaviour or a universal mechanism of development. This research has offered new insights into the fundamental principles followed by evolution to generate morphological diversity.

6. Contributions

I performed most of the experiments, analysed all the data, generated all the plots and wrote the text.

Mitsuhiro Matsuda performed some experiments with human and mouse PSCs and helped with their culture.

Maria Costanzo and Marina Sanaki-Matsumiya optimised cattle cell culture and performed experiments with cattle ESCs.

Charles Girardot performed gene expression analyses from the raw bulk RNA-seq data and assembled the multi-species gene ortholog table.

Masafumi Hayashi and Katsuhiko Hayashi provided a table of orthologous genes between the human, mouse and rhinoceros.

Sebastian Diecke, Thomas B. Hildebrandt and Giovanna Lazzari provided the rhinoceros ESCs and advice on how to culture them.

Jun Wu provided the cattle ESCs and advice on how to culture them.

Stoyan Petkov and Rüdiger Behr provided the marmoset iPSCs and advice on how to culture them.

Patryk Polinski ran the Salmon pipeline on the human iPSM clone dataset.

Miki Ebisuya supervised the project.

Libraries for RNA-seq analysis were done by the EMBL Genecore facility.

The cDNA library described in this study was done in collaboration with the Protein Technology facility in the CRG.

The experiments not performed by me have been identified in the figure legends.

7. Materials and Methods

Cell lines and culture conditions

The following PSC lines were used in this study:

- Mouse (*Mus musculus*) EpiSCs obtained from RIKEN BRC (AES0204) [108].
- Common marmoset (*Callithrix jacchus*) iPSCs obtained from Petkov, S. et al. [112].
- Rabbit (*Oryctolagus cuniculus*) ESCs obtained from RIKEN BRC (AES0174) [109].
- Human (*Homo sapiens*) iPSCs feederless 201B7 obtained from CiRA & RIKEN BRC (HPS0063) [98].
- Cattle (*Bos taurus*) ESCs obtained from Bogliotti, Y. S. et al. [110].
- Southern white rhinoceros (*Ceratotherium simum*) ESCs obtained from Hildebrandt, T. B. et al. [111].

All cells were cultured on a 5% CO2, 37°C, normoxic and humidified incubator. Media were changed every day in all cases.

Mouse EpiSCs were cultured on fibronectin-coated dishes. The culture medium used was DMEM-F12 supplemented with 15% Knockout Serum Replacement, 2 mM Glutamax, 0.1 mM non-essential amino acids, 0.1 mM β-mercaptoethanol, 20 ng/ml Activin A, 10 ng/ml bFGF, and 2.5 μM IWR-1-endo. Cells were passaged every two days using a 3-minute incubation with accutase (Thermo Fisher Scientific). To promote cell survival, 10 μM of the ROCK inhibitor Y-27632 was added to the media when passaging.

Marmoset iPSCs were cultured on dishes coated with Geltrex (Thermo Fisher Scientific). The culture medium used was StemMACS iPS-Brew (Miltenyi) supplemented with 3 μM IWR-1, 0.3 μM CGP77675, 0.3 μM AZD0530, 0.5 μM CHIR99021, 10 μM Forskolin, 1 ng/mL Activin A, and 1 μM OAC1. Cells were passaged every two days using a 5-minute incubation with Versene (Gibco) followed by subsequent 5-minute incubation with Collagenase IV (1 mg/mL). To promote cell survival, 5 μM Pro-Survival compound was added to the media when passaging.

Rabbit ESCs were cultured on dishes coated with Matrigel (Corning). The culture medium consisted of a 1:1 mixture of mTESR1 (StemCell Technologies) and DMEM-F12 supplemented with 20% Knockout Serum Replacement, 2 mM Glutamax, 0.1 mM non-essential amino acids, 0.055 mM β-mercaptoethanol, and 10 ng/mL bFGF. Cells were passaged every two to three days using a 3-minute incubation with accutase (Thermo Fisher Scientific). 10 μM of the ROCK inhibitor Y-27632 was added to the media when passaging.

Human iPSCs were cultured on dishes coated with Matrigel (Corning). The culture medium used was StemFit (Ajinomoto). Cells were passaged every four days using a 3-minute incubation with accutase (Thermo Fisher Scientific). 10 μM of the ROCK inhibitor Y-27632 was added to the media when passaging.

Cattle ESCs were maintained on Matrigel (Corning)-coated 35 mm dishes. The culture medium used was mTESR1 (StemCell Technologies) or StemFit (Ajinomoto) base medium supplemented with 20 ng/mL bFGF, 20 ng/mL Activin A and 2.5 μM IWR-1-endo. Cells were cultured at high density and passaged every two days using a 1 to 2-minute incubation with TrypLE (Gibco). 10 μM of the ROCK inhibitor Y-27632 was added to the media when passaging.

Rhinoceros ESCs were cultured on dishes coated with Matrigel (Corning). The culture medium consisted of a 1:1 mixture of mTESR1 (StemCell Technologies) and DMEM-F12 supplemented with 20% Knockout Serum Replacement, 2 mM Glutamax, 0.1 mM non-essential amino acids, 0.055 mM β-mercaptoethanol, and 10 ng/mL bFGF. Cells were passaged in small clumps every four to five days after a 3-minute incubation with 0.5 mM EDTA.

The RNA-seq reads of each cell line mapped correctly to the genome of their species, partially serving as authentication. All cell lines tested negative for mycoplasma contamination.

iPSM induction

To induce iPSM cells, species-specific protocols were employed. For mouse, 5 x 10^4 EpiSCs were first seeded on 35 mm Matrigel-coated dishes and cultured in their maintenance medium lacking IWR-1 for one day. Induction occurred by then culturing the cells for two days in SCDF media. This media consisted of CDMi [179] supplemented with 10 μM SB431542, 2 μM DMH1, 10 μM CHIR99021 and 20 ng/ml bFGF.

For rabbit, rhinoceros and cattle iPSM, 5×10^4, 1×10^5 and 2.5×10^5 ESCs were seeded on 35 mm Matrigel-coated dishes. The media was changed to SCDF the next day, and cells were cultured for three (rabbit and rhinoceros) or two (cattle) more days.

For marmoset and human iPSM, 2×10^5 and 2×10^4 iPSCs, respectively, were seeded on 35 mm Matrigel-coated dishes and cultured for two to three days before switching to CDMi medium supplemented with 20 ng/ml bFGF, 10 μM CHIR99021, and 20 ng/ml bFGF Activin A for 24 hours. Cells were further cultured in SCDF media for an additional one day (human) or two days (marmoset).

TBX6 staining for flow cytometry analysis

Cells were detached using Accutase (Thermo Fisher Scientific) for 5 minutes at 37°C, then fixed in 4% paraformaldehyde in PBS for 10 minutes at room temperature (RT). For each staining experiment, 3 x 10^5 cells were used. These cells were incubated overnight with an anti-TBX6 antibody (Abcam, ab38883, diluted 1:250) in Perm/Wash buffer (BD) at 4°C. The next day, the cells were washed twice with Perm/Wash buffer and incubated with a donkey anti-rabbit 647 nm Alexa Fluor secondary antibody (diluted 1:500) at room temperature for 2 hours. After incubation, cells were resuspended in 0.5 ml of Perm/Wash buffer and filtered before data acquisition on an LSRII cytometer (BD). A total of 10,000 events identified as single cells were recorded. The data was then analysed using the FlowJo software. Stained pluripotent stem cells (PSCs) were used as a negative control to set a threshold for TBX6 intensity. PSM cells exhibiting TBX6-staining intensity above this threshold were considered TBX6 positive.

DNA constructs and reporter lines

This study utilised various genetic constructs described in Matsuda et al. [57]:

- **HES7 reporter (Fig. 9):** This construct combined the human HES7 promoter and the FLuc-NLS-PEST-UTR (hHES7) sequence.
- **HES7 protein degradation (Fig. 12):** A tetracycline-inducible promoter (rTetOne) was combined with the hHES7-NLuc (without introns) sequence.
- **HES7 intron delay (Fig. 14):** This construct combined the human HES7 promoter with the NLuc-NLS-PEST-stop-hHES7 (w/o intron) or the FLuc-NLS-PEST-stop-hHES7 (w/intron) sequences. Both constructs were incorporated into the cells simultaneously.
- **TBX6 protein degradation (Fig. 13):** Similar to the HES7 protein degradation construct, the rTetOne promoter was combined with the TBX6-NLuc-UTR (hHES7) sequence.

The following constructs were generated for this study:

- **Ubiquitin(G76V)-Luciferase degradation assay (Fig. 13):** The construct was designed by placing the human HES7 CDS and UTR (without introns) downstream of a mutant ubiquitin-luciferase fusion protein (Ubiquitin(G76V)-Luciferase). A stop codon prevented the expression of HES7.
- **Tandem fluorescent timer (Fig. 26):** A TetOne promoter was combined with a mScarlet-mNeonGreen tandem sequence (kindly provided by the Knop lab).
- **Delay reporter (Fig. 27):** The mScarlet-mNeonGreen sequence was placed before the human HES7 CDS and UTR (with introns). A stop codon prevented the expression of HES7. This construct was further combined with a TetOne promoter. As a control, a version using the HES7 CDS without introns was generated.

To generate these constructs, the promoters or genes were first subcloned into a pDONR vector, creating entry clones. Subsequently, these entry clones were recombined with a *piggyBac* vector (a gift from K. Woltjen) [180] using Multisite Gateway technology (Invitrogen). For a stable introduction into PSCs, the constructs were delivered via electroporation using a 4D Nucleofector (Lonza) or lipofection with Lipofectamine (Invitrogen) in the case of cattle ESCs.

HES7 gene sequence conservation analysis

To analyse HES7 gene conservation across species, protein, mRNA with and without introns, and promoter sequences (6 kb upstream of the start codon) were retrieved from the NCBI database. These sequences were then subjected to multiple sequence alignment using Clustal Omega [181]. Pairwise comparisons, visualisation of conserved protein regions, and similarity tree reconstruction were done using Jalview [182].

Oscillation analyses

To monitor the oscillations of the HES7 reporter after iPSM induction, D-luciferin (200 μM) was added to the culture medium. Bioluminescence was then measured with a Kronos Dio Luminometer (Atto). The luminometer recorded the luminescence signal for the entire plate at each time point. The resulting traces were analysed using pyBOAT 0.9.6 [183], a Python software specifically designed for the time-frequency analysis of biological data. A species-specific threshold was used for Sinc-detrending and amplitude normalisation of the signal (500 min for marmoset, cattle, and rhinoceros; 250 min for rabbit).

Following this initial processing, the signal was analysed using wavelets with periods ranging from 100 to 500 minutes. A Fourier estimate of the wavelet analysis provided a distribution of periods and their corresponding power. The period with the highest power for each signal was considered. For visualisation purposes, the time-series data was normalised to the first peak of the oscillations.

To investigate the influence of various inhibitors on the segmentation clock dynamics, different concentrations of sodium azide or 2-Deoxy-D-glucose (2DG) were added alongside D-luciferin just before the luminescence measurement started in the luminometer.

Oscillation analyses in single human clones

Single human iPSCs harbouring the HES7 reporter were sorted into laminin-coated 96-well plates using a BD Influx cell sorter. ROCK inhibitor was used during the sorting process to reduce cellular death. The cells were cultured for 5-6 days until colonies formed. The colony-forming efficiency was around 40-60%. PSM was induced by changing the media to SCDF for 3 days. To monitor the HES7 oscillations, the media was changed to SCDF containing 1 μM CHIR and 200 μM D-luciferin. Lowering the amount of CHIR helps coordinate the oscillatory activity of cells. Plates were measured with a Kronos HT luminometer (Atto). Measurements of single wells were further analysed with PyBOAT 0.9.12 to determine the oscillatory period of each clone.

Organismal characteristics

The approximate time it takes for somites to form *in vivo* was estimated using existing studies on the number of somites present at different embryonic stages (values and references in Table 1). A linear relationship between the embryonic day and the number of somites was used to calculate the somite formation period. It is important to note that these calculations have high uncertainty due to the challenges associated with obtaining and accurately staging many embryos from non-traditional mammalian models. Data on average adult body weight and gestation length for each species was retrieved from the AnAge database (Build 14, accessed August 2022). The length of the embryonic period for each species was obtained from various embryology manuals (references in Supplementary Table 2).

Phylogenetic tree reconstruction

The evolutionary relationships between the six species were investigated using a subset of the mammalian phylogenetic tree published by Upham et al. [184]. This subset tree was obtained using their online resource (http://vertlife.org/phylosubsets/).

Protein degradation assay

Similar to the method described in Matsuda et al. [57], a reverse tetracycline-inducible system (rTetOne) was used to control the overexpression of a HES7-NLuc fusion protein. After iPSM induction in media

containing Doxycycline (Dox, 100 ng/ml), the Dox was washed out to activate HES7-NLuc expression and the media was changed to CDMi with protected furimazine (Promega; 1 μM). Following an increase in the NLuc signal, Dox was re-added (300 ng/ml) to halt protein production. The NLuc signal decay was then monitored using a Kronos Dio luminometer. Only the decay curve's later time points, exhibiting a single exponential decline, were considered for analysis. This minimises the influence of residual mRNA on the decay curve. The protein half-life of HES7 was estimated by calculating the slope of the log2-transformed most linear decay curve using a RANSAC algorithm (scikit-learn). This same method was used to measure the degradation rate of the TBX6-NLuc fusion protein. It is important to note that the measured half-lives for mouse and human TBX6 differed slightly from those reported in Matsuda et al. [57] due to measurements being performed on a different day of the induction protocol. For Ubiquitin(G76V)-Luciferase protein half-life measurement, D-luciferin was used instead of furimazine. This mutant form of ubiquitin (G76V) is resistant to cleavage by ubiquitin hydrolases, ensuring the luciferase protein is targeted for degradation by the proteasome [121].

HES7 intron delay assay

Similar to the method described in Matsuda et al. [57], the HES7 promoter-NLuc-stop-HES7 (w/o intron) and HES7 promoter-FLuc-stop-HES7 (w/ intron) reporter constructs were introduced into the PSCs. Following iPSM induction, the medium was changed for CDMi containing protected furimazine (1 μM) and D-luciferin (1 mM), and both NLuc and FLuc oscillations were monitored simultaneously using a Kronos Dio luminometer. The intron delay of HES7 was estimated by calculating the phase difference between the oscillatory signal of the “w/o intron” and “w/intron” reporters using cross-correlation analysis (SciPy). Notably, this method differs from the previous report by not accounting for the difference in maturation times between NLuc and FLuc.

tFT imaging

iPSC containing the tFT under the TetOne promoter were plated on matrigel-coated glass-bottom plates and cultured until they formed colonies. Doxycycline (300 ng/ml) was added to the media right before imaging to induce the tFT expression. A SiR-Actin dye (674 nm emission; SpiroChrome; 1:1000) was also included to facilitate locating and focusing cells before the expression of the tFT. Live imaging was acquired using an Olympus FV3000 confocal microscope at 37 ºC and 5% CO_2. The time resolution was set to 20 min. Images were further analysed using Fiji [185].

tFT expression fitting

The intensity traces obtained after imaging the induction of the tFT were fitted to a simple gene expression model. The following model was considered:

$$\frac{dm}{dt} = -\delta_m \mathrm{m} \quad (\mathrm{t} < \tau_{\mathrm{Tx}})$$

$$\frac{dm}{dt} = \beta_T - \delta_m \mathrm{m} \quad (\mathrm{t} \geq \tau_{\mathrm{Tx}})$$

$$\frac{dp}{dt} = \alpha m(t - \tau_{Tl}) - \delta_p \mathrm{p}$$

Where m and p are the concentrations of mRNA and protein, δ_m and δ_p are the degradation rates of mRNA and protein, β_T is the transcription rate of the TetOne promoter, α is the translation rate, and τ_{Tx} and τ_{Tl} are the transcription and translation delays.

The solution of this is

$$\mathrm{p(t)} = 0 \ (\mathrm{t} < \tau)$$

$$\mathrm{p(t)} = \frac{a}{\delta_m - \delta_p}\left(e^{-\delta_m(t-\tau)} - \frac{\delta_m}{\delta_p}e^{-\delta_p(t-\tau)}\right) + \frac{a}{\delta_p} \ (\mathrm{t} \geq \tau) \quad (1)$$

where $\tau = \tau_{Tx} + \tau_{Tl}$, and $a = \alpha\beta_T/\delta_m$.

The production delay τ was estimated by fitting the intensity traces to equation (1) with Python (SciPy)'s basin-hopping algorithm.

Delay reporter analysis by flow cytometry

Human iPSCs containing the delay reporter (with or without introns) were induced at different time points by adding doxycycline to the media. At the end of the time course, cells were detached using Accutase (Thermo Fisher Scientific) for 5 minutes at 37°C, filtered and placed in ice. The R/G ratio of live cells was then quantified using an LSR Fortessa analyser (BD). A total of 10.000 events identified as single cells were recorded. The data was analysed using the FlowJo software.

Simulation of the HES7 oscillations

Delay differential equations were employed to simulate HES7 oscillations. The equations representing the HES7 feedback loop model were described by Matsuda et al. [57]. Human biochemical parameters from the same study served as the starting point. Simulations were then conducted by linearly scaling all biochemical parameters associated with degradation and delays. This scaling factor affected the mRNA degradation rate, protein degradation rate, intron delay, and transcription/translation delay (specific human values used were 0.044 min^{-1}, 0.0175 min^{-1}, 36.7 min, and 29.8 min, respectively). The peak-to-peak distance was calculated to estimate the oscillatory period within each simulation. A Python code was used to perform numerical calculations and period estimations. To compare the scaling behaviour across different species, the real fold-change between the human biochemical parameters and those measured in the other species was calculated. This fold change was determined by averaging the changes observed in the HES7 protein degradation rate and intron delay.

Cell volume quantifications

iPSM cells were dissociated with Accutase (Thermo Fisher Scientific) for 5 min at 37 °C. The cells were then washed in IMDM medium (Sigma) with osmolarity matched to the induction medium (293

mOsm). Within 10-15 minutes of dissociation, cell volume was measured using a Z2 Coulter counter (Beckman) by electrical conductance. The measurement range was set to detect particles between 7 and 21 microns in diameter. Cells were maintained in IMDM media during the measurement. Approximately 6 x 10^4 to 8 x 10^4 cells were measured per experiment. A Python script was then employed to analyse the distribution of cell volumes.

Seahorse metabolic rate analysis

During the most efficient differentiation day, iPSM cells were dissociated using Accutase for 5 minutes at 37°C. The cells were then re-plated on fibronectin-coated Seahorse plates (Agilent) at a density of 7.27 x 10^5 cells per cm^2 using100 µL of Seahorse medium (Seahorse XF DMEM supplemented with 10 mM glucose, 1 mM pyruvate, and 2 mM glutamine, all from Agilent). Following a 15-minute attachment period at room temperature, the plates were transferred to a 37°C incubator without CO_2 for 40 minutes. Subsequently, 400 µL of pre-warmed (37°C) Seahorse medium was carefully added to each well without disturbing the attached cells, bringing the final volume to 500 µL. The cells were further incubated at 37°C without CO_2 for an additional 15 minutes. The Seahorse XF cartridge was hydrated overnight. For the real-time ATP rate assay, oligomycin (1 µM), rotenone (0.5 µM), and antimycin A (0.5 µM) were used to assess cellular respiration. Each condition was analysed in 7-10 replicates using a Seahorse XFe24 Analyzer (Agilent). Three independent biological replicates were performed for each species. The Wave Desktop software, or the manufacturer's online application, was used for data analysis.

cDNA library generation

200 genes highly correlating with the segmentation clock period were isolated from the hORFeome library (Horizon). A version of the library containing genes without endogenous stop codons was used. Entry clones were purified from the library's glycerol stock and recombined with a PiggyBac destination vector equipped with a constitutive promoter and a V5 protein tag using Multisite Gateway technology (Invitrogen). The final constructs were purified using miniprep columns. The library was generated by mixing equimolar amounts of all constructs.

Screening through directed evolution

One million human iPSCs harbouring the delay reporter were electroporated with the cDNA library mix using a 4D Nucleofector (Lonza). Each electroporation used 5 µg of DNA (70% library and 30% piggyBac transposase construct). After recovery, the delay reporter was induced with doxycycline for 8 hours, and the top 5% of cells showing the highest R/G ratio (potentially faster) were sorted using a BD Influx cell sorter. ROCK inhibitor was used during the sorting process to reduce cell death. The cells were cultured for approximately a week to recover from the sorting, and then the entire process was repeated. This procedure was performed a total of five times before further analysis. During the first round, cells were selected with puromycin before induction of the reporter and sorting to ensure that all cells had incorporated genes from the library. This step was unnecessary in subsequent rounds as all cells were already puromycin-resistant.

V5 staining

Cells electroporated with the cDNA library were fixed with 4% paraformaldehyde for 10 minutes at room temperature. After fixation, the cells were washed three times for 5 minutes with PBS and then permeabilised with 0.5% Triton X-100 for 15 minutes at room temperature. Following permeabilisation, the cells were washed thrice for 5 minutes with PBS. To stain the V5 protein tag, the cells were incubated with an anti-V5 antibody (Invitrogen R960-25; 1:1000) in 3% bovine serum albumin (BSA) (Sigma) / PBS overnight at 4°C. The next day, the cells were washed three times for 5 minutes with PBS and then incubated with a donkey anti-mouse Alexa Fluor 488 secondary antibody (1:500 in 3% BSA/PBS) at room temperature for 2 hours. After this incubation, the cells were washed three times with PBS and then incubated in PBS containing DAPI (ThermoFisher; 1:1000). The stained cells were imaged using an Olympus IX73 episcope.

Amplification of inserted genes

The library genes inserted into human iPSCs after electroporation were amplified using nested PCR. Two sets of primers were designed to anneal to the constant region of the construct inserted alongside the specific genes. The reaction was performed using KOD DNA polymerase (Sigma). The protocol involved 25 cycles with the first set of primers and 25 cycles with the second set. The elongation time was extended to ensure the amplification of the larger genes in the library. The amplified bands were visualised using the D5000 ScreenTape kit from Agilent's Tapestation system.

First primer set:

- Forward (5'-3'): TTTTGGCAAAGAATTCGCGG
- Reverse (5'-3'): CGTAGAATCGAGACCGAGGA

Second primer set:

- Forward (5'-3'): GGATCCTGCAGGTTATCACAAG
- Reverse (5'-3'): GGTTAGGGATAGGCTTACCAGT

RNA library preparation

RNA was extracted from cultured cells using the RNeasy Mini Kit (Qiagen), following the manufacturer's protocol. On-column DNase digestion ensured the removal of genomic DNA from all samples. High-quality total RNA (300 ng) was used to prepare barcoded, stranded mRNA-sequencing libraries with the NEBNext Poly(A) mRNA Magnetic Isolation Module and NEBNext Ultra II Directional RNA Library Prep Kit for Illumina (New England Biolabs (NEB), Ipswich, MA, USA). The library preparation process was automated on a Beckman i7 liquid-handling robot. Libraries passing quality control were pooled in equal amounts, and a 2.1 pM solution of this pool was loaded onto the Illumina NextSeq 500 sequencer for single-end sequencing. This generated approximately 150 million reads, each 150 bases long.

The RNA-seq data can be found in ArrayExpress (E-MTAB-12263)

RNA library preparation from single iPSM clones

RNA was extracted from cultured cells using the RNeasy Micro Kit (Qiagen), following the manufacturer's protocol. On-column DNase digestion ensured the removal of genomic DNA from all samples. Samples were processed following the smartseq 2 protocol adapted from Picelli et al. [186]. 1 ng was taken for each sample, and dessicated with the speedvac for 20 minutes at RT. Samples were resuspended in 2.4 uL water, then had oligo dT and dNTPs added, then proceeded with RT and cDNA amplification. cDNA was amplified with 15 PCR cycles and the addition of ISPCR primers. cDNA was diluted to 0.2 ng and tagmented with a 1/300 dilution of loaded Tn5. Libraries were indexed and amplified with 12 PCR cycles. Samples were cleaned up with a 0.7x bead ratio and pooled equimolarly. The pool was loaded Illumina NextSeq 2000 sequencer for single-end sequencing. This generated approximately 400 million reads, each 100 bases long.

Gene expression analysis

Primary processing of the RNA-seq data was performed using the Galaxy [187] platform with the following workflow steps:

1. **Read Cleaning**: *Trim Galore!* (Galaxy Version 0.6.3) was used with automatic adapter detection, trimming low-quality ends with a threshold of 20, requiring an overlap with adapter sequence to trim a sequence of 1, a maximum allowed error rate of 0.1, and discarding reads shorter than 20 bases.

2. **Read Mapping**: STAR [188] (Galaxy Version 2.7.8a) was used with default single-end options to map reads to the hg38 (*H. sapiens*), mm10 (*M. musculus*), bosTau9 (*B. taurus*), calJac4 (*C. jacchus*), OryCun2 (*O. cuniculus*), and CerSim1 (*C. simum simum*) genomes.

3. **Read Filtering**: The Filter SAM or BAM tool (Galaxy Version 1.8) retained only mapped reads with a MAPQ score greater than 19, eliminating multi-mapping reads.

4. **Read Counting**: Strand-specific read counts were summarised at the gene level using featureCounts (Galaxy Version 1.6.3) with the reverse stranded option. GTF files from GENCODE/Ensembl (v39 for human and vM23 for mouse, Bos_taurus.ARS-UCD1.2.106.chr.gtf for cattle, and Oryctolagus_cuniculus.OryCun2.0.106.chr.gtf for rabbit) and RefSeq-based GTF files from UCSC (cerSim1.ncbiRefSeq.gtf for rhinoceros and calJac4.ncbiRefSeq.gtf for marmoset) were used across all analyses.

5. **Quality Assessment**: FastQC (Galaxy Version 0.72) was used to assess sequencing quality and monitor filtering efficiency at different steps. Picard CollectRnaSeqMetrics (Galaxy Version 2.18.2.1) was used to check RNA alignment to various functional classes of loci in the genome. Finally, read trimming and mapping reports were compared across samples for consistency and to detect potential outliers using MultiQC [189] (Galaxy Version 1.9).

Pairwise gene orthology tables between each species and human were exported using Ensembl BioMart. The gene orthology table (mouse-human-rhino) provided by Hayashi et al. [190] was used for the rhinoceros. A stringent multi-species gene orthology table was assembled using human genes as the reference and considering only one-to-one orthology relationships.

Only the genes showing one-to-one orthology across all species were retained for further analysis. Raw counts were normalised using the Gene length corrected trimmed mean of M-values (GeTMM) method for optimal intra- and intersample comparisons [191]. Reads per kilobase (RPK) were calculated for each gene using the gene lengths provided in the GTF file for each species. TMM normalisation was performed in R using the edgeR package [192]. For subsequent PCA and correlation analysis with the segmentation clock period, genes with a GeTMM value below 10 in all samples were discarded. It is important to note that this normalisation method yields relative, not absolute, RNA expression values. Further research is needed to determine whether these species rely on relative or absolute changes in gene expression.

Gene expression analysis of single iPSM human clones was performed following the same protocol.

DESeq2 analysis

RNA-seq reads of single iPSM human clones were mapped into the hg38 (*H. sapiens*) genome using a standard Salmon pipeline [193]. The count matrix was imported into R and annotated using the human GTF v39 file obtained from ENSEMBL. A standard workflow for DESeq2 analysis described by Love et al. [131] was followed. All further plots were generated in R. For GSEA analysis, the package described in Wu et al. [194] was used.

Principal component analysis

Principal component analysis was performed using the Python library scikit-learn. GeTMM values were log-normalised before the analysis.

Gene set enrichment analysis

Gene set enrichment analysis (GSEA) [195] was performed using version 4.2.3 of the GSEA desktop app for iOS. All genes were pre-ranked based on the Spearman correlation coefficients calculated between their expression levels and the segmentation clock period across six species. The analysis utilised the Gene Ontology (GO) biological process v7.5.1 gene set collection from MSigDB [196]. Only gene sets containing between 15 and 800 genes were retained for further analysis. Network visualisation of enriched similar terms was performed using the EnrichmentMap plug-in for Cytoscape software (version 3.9.1) [197,198]. The map displayed only those enriched GO terms with a False Discovery Rate (FDR) below 0.1 and a p-value less than 0.005.

Gene expression analysis of human and mouse motor neuron progenitors

The analysis used the human and mouse motor neuron progenitor bulk RNA-seq dataset published by Rayon et al. [59] (accession number: GSE140749). Mouse samples collected at 1.5 days of differentiation, and human samples collected at 4 days of differentiation were chosen. These time points were selected due to their maximally correlated gene expression, suggesting equivalent differentiation

stages despite the 2.5-fold difference in actual time. The gene expression analysis employed the same workflow described previously for the iPSM and PSC samples. The approximately 300 genes with the strongest anticorrelation (< -0.8 Spearman correlation coefficient) with the segmentation clock period were selected to assess their expression levels in mouse and human motor neuron progenitors. A random selection of genes of the same size was also used for comparison.

8. Supplementary figures and tables

	Promoter	mRNA (with introns)	mRNA (without introns)	Protein
Pairwise comparisons	Percentage identity			
Rabbit - Mouse	53,3	69,24	86,19	90,22
Cattle - Mouse	54,79	71,46	87,27	87,83
Cattle - Rabbit	55,19	73,87	89,93	90,39
Rhinoceros - Mouse	56,63	69,87	74,23	91,11
Rhinoceros - Rabbit	56,4	76,15	89,48	92,89
Rhinoceros- Cattle	59,64	86,64	92,07	93,04
Human - Mouse	55,72	70,14	74,31	90
Human - Rabbit	55,03	77,4	91,01	90,87
Human - Cattle	57,15	82,05	91,82	93,04
Human - Rhinoceros	62,64	85,73	88	93,04
Marmoset - Mouse	55,57	72,24	83,83	91,63
Marmoset- Rabbit	56,27	76,12	90,42	92,95
Marmoset - Cattle	57,24	81,06	89,9	91,81
Marmoset - Rhinoceros	62,47	84,92	89,47	95,15
Marmoset - Human	77,35	92,83	94,4	95,26

Supplementary Table 1: **Pairwise comparison of *HES7* sequences.**
Table summarizing the percentage identity of the different *HES7* sequences across species. Promoter regions consisted of sequences of 6 kb upstream of the *HES7* start codon.

Species	Body weight (g)	Gestation length (day)	Embryogenesis length (day)	References for embryogenesis length
Mouse	20,5	19	15	[84,199]
Rabbit	1800	30	18,5	[84,200]
Cattle	750000	277	40	[201]
Rhinoceros	2175000	515	Not available	
Human	62035	280	58	[84,202]
Marmoset	255	144	83	[116,119]

Supplementary Table 2: **Organismal parameters considered in this study.**
Average adult body weight and gestation length in the different species extracted from the AnAge database. Embryogenesis length extracted from different embryology manuals.

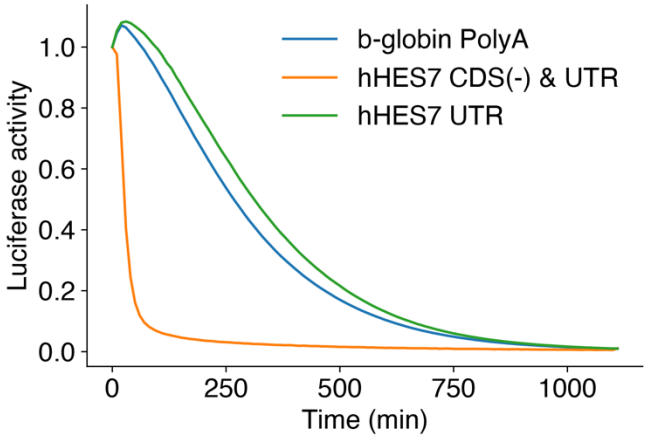

Supplementary Figure 1: Stability of different mRNA terminators.
Ubiquitin(G76V)-Luciferase (Ub-Luc) protein degradation assay with different 3'UTR terminator sequences. Protein production was stopped by adding doxycycline at time zero. The decay of the luminescence signal was monitored over time. The sequence downstream of the Ub-Luc protein was changed to the rabbit b-globin polyA, the human HES7 CDS (without introns) followed by the HES7 3'UTR or the HES7 3'UTR alone. Experiment performed by Mitsuhiro Matsuda. n=1.

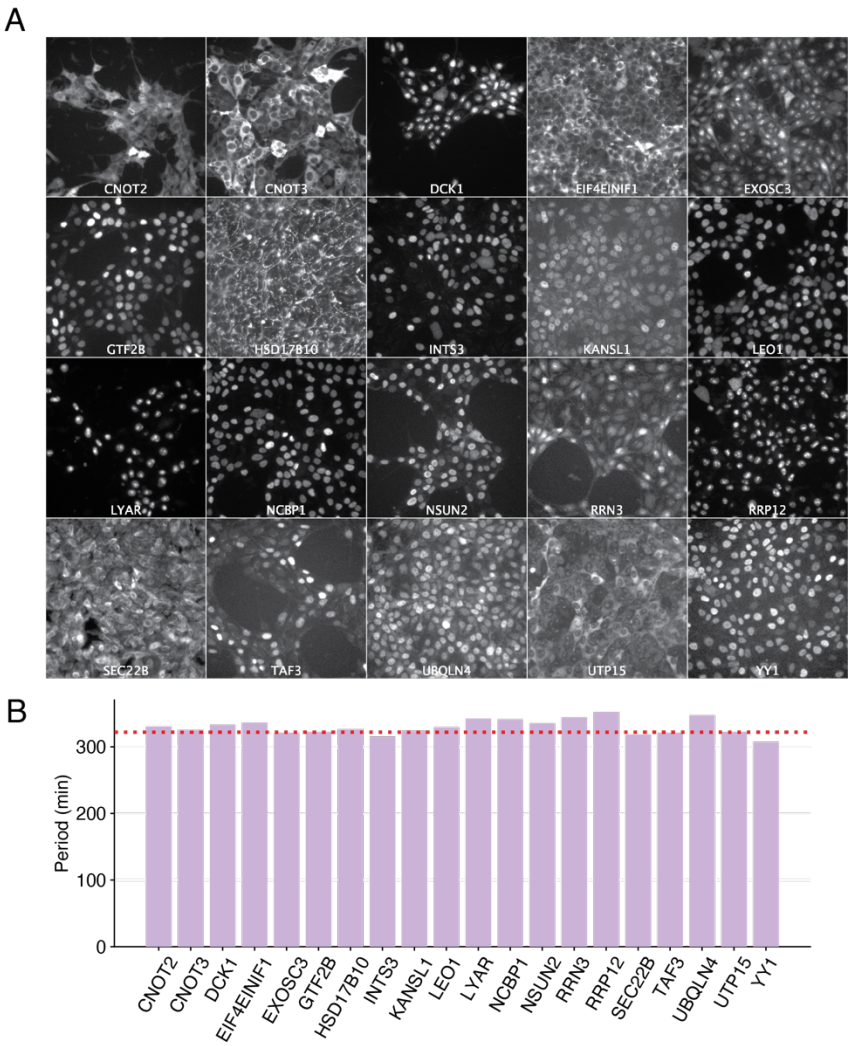

Supplementary Figure 2: Effect of overexpressing single genes correlating with the segmentation clock period.
(A) V5-tag staining of human iPSCs overexpressing a V5-tagged version of genes anti-correlating with the segmentation clock period. (B) Oscillatory periods of human iPSM cells overexpressing candidate genes. After each gene was cloned and introduced into human iPSCs harbouring HES7 reporter, iPSM cells were induced (n = 1). The red dotted line represents the human iPSM wild-type period of 322 min.

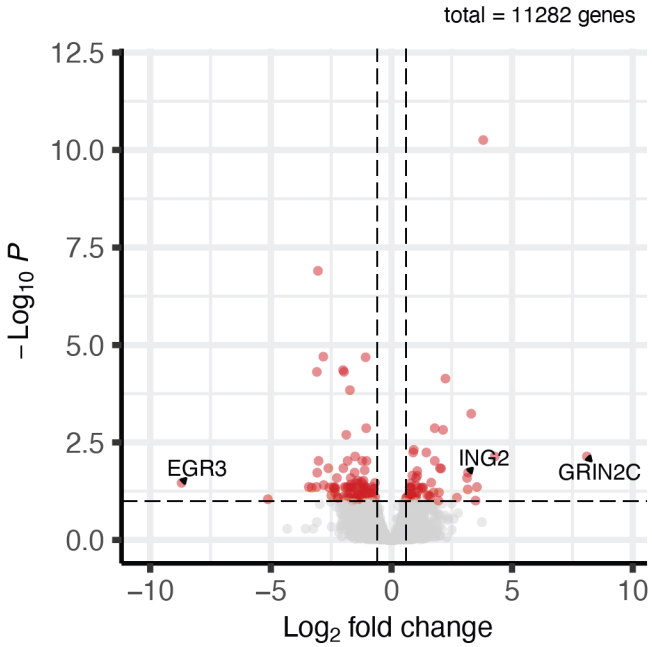

Supplementary Figure 3: Gene expression differences between perturbed fast and slow human iPSM clones.
(A) Volcano plot highlighting the most differentially expressed genes between the Slow and Fast clones of the perturbed group. The log2 fold change and the -log10 of the adjusted p-value are plotted. The significance thresholds are 0.6 for the fold change and 0.1 for the adjusted p-value. Genes over both thresholds are coloured red. Only the top differentially expressed genes, which are also present in the cDNA library, are labelled. Genes with positive fold change are expressed higher in the Slow group.

9. References

1. Garstang W: **The Theory of Recapitulation: A Critical Re-statement of the Biogenetic Law.** *J Linn Soc London, Zool* 1922, **35**:81–101.

2. Ebisuya M, Briscoe J: **What does time mean in development?** *Dev* 2018, **145**:dev164368.

3. Nasiadka A, Dietrich BH, Krause HM: **Anterior-posterior patterning in the Drosophila embryo**. *Adv Dev Biol Biochem* 2002, **12**:155–204.

4. Von Dassow G, Meir E, Munro EM, Odell GM: **The segment polarity network is a robust developmental module**. *Nature* 2000, **406**:188–192.

5. Holland PWH: **Evolution of homeobox genes**. *Wiley Interdiscip Rev Dev Biol* 2013, **2**:31–45.

6. Hubert KA, Wellik DM: **Hox genes in development and beyond**. *Dev* 2023, **150**.

7. Deschamps J, Duboule D: **Embryonic timing, axial stem cells, chromatin dynamics, and the Hox clock**. *Genes Dev* 2017, **31**:1406–1416.

8. Jacob F: **Evolution and tinkering**. *Science* 1977, **196**:1161–1166.

9. Needham J: **On the dissociability of the fundamental processes in ontogenesis**. *Biol Rev* 1933, **8**:180–223.

10. De Beer G: *Embryos and ancestors*. Oxford: Clarendon Press; 1951.

11. Smith KK: **Heterochrony revisited: the evolution of developmental sequences**. *Biol J Linn Soc* 2001, **73**:169–186.

12. Russell ES: *Form and function*. London, J. Murray; 1916.

13. Gould SJ: *Ontogeny and phylogeny*. Harvard University Press; 1977.

14. Libé-Philippot B, Vanderhaeghen P: **Cellular and Molecular Mechanisms Linking Human Cortical Development and Evolution**. *Annu Rev Genet* 2021, **55**:555–581.

15. Hall BK: **Evolutionary Developmental Biology (Evo-Devo): Past, Present, and Future**. *Evol Educ Outreach* 2012, **5**:184–193.

16. Hubaud A, Pourquié O: **Signalling dynamics in vertebrate segmentation**. *Nat Rev Mol Cell Biol* 2014, **15**:709–721.

17. Christ B, Huang R, Scaal M: **Amniote somite derivatives**. *Dev Dyn* 2007, **236**:2382–2396.

18. Palmeirim I, Henrique D, Ish-Horowicz D, Pourquié O: **Avian hairy gene expression identifies a molecular clock linked to vertebrate segmentation and somitogenesis.** *Cell* 1997, **91**:639–48.

19. Oates AC, Morelli LG, Ares S: **Patterning embryos with oscillations: structure, function and dynamics of the vertebrate segmentation clock**. *Development* 2012, **139**:625–639.

20. Duboule D: **Temporal colinearity and the phylotypic progression: a basis for the stability of a vertebrate Bauplan and the evolution of morphologies through heterochrony**. *Development* 1994, **1994**:135–142.

21. Irie N, Kuratani S: **Comparative transcriptome analysis reveals vertebrate phylotypic period during organogenesis**. *Nat Commun 2011 21* 2011, **2**:1–8.

22. Alberch P: **The logic of monsters: Evidence for internal constraint in development and evolution**. *Geobios* 1989, **22**:21–57.

23. Duboule D: **The (unusual) heuristic value of Hox gene clusters; a matter of time?** *Dev Biol* 2022, **484**:75–87.

24. Gomez C, Özbudak EM, Wunderlich J, Baumann D, Lewis J, Pourquié O: **Control of segment number in vertebrate embryos**. *Nature* 2008, **454**:335–339.

25. Moreau C, Caldarelli P, Rocancourt D, Roussel J, Denans N, Pourquie O, Gros J: **Timed Collinear Activation of Hox Genes during Gastrulation Controls the Avian Forelimb Position**. *Curr Biol* 2019, **29**:35-50.e4.

26. Cohn MJ, Tickle C: **Developmental basis of limblessness and axial patterning in snakes**. *Nature* 1999, **399**:474–479.

27. Aulehla A, Johnson RL: **Dynamic expression of lunatic fringe suggests a link between notch signaling and an autonomous cellular oscillator driving somite segmentation**. *Dev Biol* 1999, **207**:49–61.

28. Holley SA, Geisler R, Nüsslein-Volhard C: **Control of her1 expression during zebrafish somitogenesis by a Delta-dependent oscillator and an independent wave-front activity**. *Genes Dev* 2000, **14**:1678.

29. Li Y, Fenger U, Niehrs C, Pollet N: **Cyclic expression of esr9 gene in Xenopus presomitic mesoderm**. *Differentiation* 2003, **71**:83–89.

30. Matsuda M, Yamanaka Y, Uemura M, Osawa M, Saito MK, Nagahashi A, Nishio M, Guo L, Ikegawa S, Sakurai S, et al.: **Recapitulating the human segmentation clock with pluripotent stem cells**. *Nature* 2020, **580**:124–129.

31. Diaz-Cuadros M, Wagner DE, Budjan C, Hubaud A, Tarazona OA, Donelly S, Michaut A, Al Tanoury Z, Yoshioka-Kobayashi K, Niino Y, et al.: **In vitro characterization of the human segmentation clock**. *Nature* 2020, **580**:113–118.

32. Ferjentsik Z, Hayashi S, Dale JK, Bessho Y, Herreman A, De Strooper B, Del Monte G, De La Pompa JL, Maroto M: **Notch Is a Critical Component of the Mouse Somitogenesis Oscillator and Is Essential for the Formation of the Somites**. *PLoS Genet* 2009, **5**:1000662.

33. Bessho Y, Hirata H, Masamizu Y, Kageyama R: **Periodic repression by the bHLH factor Hes7 is an essential mechanism for the somite segmentation clock**. *Genes Dev* 2003, **17**:1451–1456.

34. Lewis J: **Autoinhibition with transcriptional delay: A simple mechanism for the zebrafish somitogenesis oscillator**. *Curr Biol* 2003, **13**:1398–1408.

35. Harima Y, Takashima Y, Ueda Y, Ohtsuka T, Kageyama R: **Accelerating the Tempo of the Segmentation Clock by Reducing the Number of Introns in the Hes7 Gene**. *Cell Rep* 2013, **3**:1–7.

36. Hirata H, Bessho Y, Kokubu H, Masamizu Y, Yamada S, Lewis J, Kageyama R: **Instability of Hes7 protein is crucial for the somite segmentation clock**. *Nat Genet 2004 367* 2004, **36**:750–754.

37. Schröter C, Herrgen L, Cardona A, Brouhard GJ, Feldman B, Oates AC: **Dynamics of zebrafish somitogenesis**. *Dev Dyn* 2008, **237**:545–553.

38. Aulehla A, Wiegraebe W, Baubet V, Wahl MB, Deng C, Taketo M, Lewandoski M, Pourquié O: **A β-catenin gradient links the clock and wavefront systems in mouse embryo segmentation**. *Nat Cell Biol* 2008, **10**:186.

39. Conrad JV, Meyer S, Ramesh PS, Neira JA, Rusteika M, Mamott D, Duffin B, Bautista M, Zhang J, Hiles E, et al.: **Efficient derivation of transgene-free porcine induced pluripotent stem cells enables in vitro modeling of species-specific developmental timing**. *Stem cell reports* 2023, **18**:2328–2343.

40. Giudicelli F, Özbudak EM, Wright GJ, Lewis J: **Setting the Tempo in Development: An Investigation of the Zebrafish Somite Clock Mechanism**. *PLOS Biol* 2007, **5**:e150.

41. Hoyle NP, Ish-Horowicz D: **Transcript processing and export kinetics are rate-limiting steps in expressing vertebrate segmentation clock genes**. *Proc Natl Acad Sci U S A* 2013, **110**:E4316–E4324.

42. Vibe CB: **The temperature response of the medaka segmentation clock and its link to robustness in embryonic patterning**. 2021, doi:10.11588/HEIDOK.00028769.

43. Lázaro J, Sochacki J, Ebisuya M: **The stem cell zoo for comparative studies of developmental tempo**. *Curr Opin Genet Dev* 2024, **84**:102149.

44. Till JE, McCulloch E. A.: **A direct measurement of the radiation sensitivity of normal mouse bone marrow cells**. *Radiat Res* 1961, **14**:213–222.

45. Liu G, David BT, Trawczynski M, Fessler RG: **Advances in Pluripotent Stem Cells: History, Mechanisms, Technologies, and Applications**. *Stem Cell Rev Reports 2019 161* 2019, **16**:3–32.

46. Gouti M, Tsakiridis A, Wymeersch FJ, Huang Y, Kleinjung J, Wilson V, Briscoe J: **In Vitro Generation of Neuromesodermal Progenitors Reveals Distinct Roles for Wnt Signalling in the Specification of Spinal Cord and Paraxial Mesoderm Identity**. *PLOS Biol* 2014, **12**:e1001937.

47. Clevers H: **Modeling Development and Disease with Organoids**. *Cell* 2016, **165**:1586–1597.

48. Takasato M, Er PX, Becroft M, Vanslambrouck JM, Stanley EG, Elefanty AG, Little MH: **Directing human embryonic stem cell differentiation towards a renal lineage generates a self-organizing kidney**. *Nat Cell Biol* 2014, **16**:118–126.

49. Lancaster MA, Renner M, Martin CA, Wenzel D, Bicknell LS, Hurles ME, Homfray T, Penninger JM, Jackson AP, Knoblich JA: **Cerebral organoids model human brain development and microcephaly**. *Nature* 2013, **501**:373–379.

50. Spence JR, Mayhew CN, Rankin SA, Kuhar MF, Vallance JE, Tolle K, Hoskins EE, Kalinichenko V V., Wells SI, Zorn AM, et al.: **Directed differentiation of human pluripotent stem cells into intestinal tissue in vitro**. *Nature* 2011, **470**:105–110.

51. Zhu Z, Huangfu D: **Human pluripotent stem cells: an emerging model in developmental biology**. *Development* 2013, **140**:705.

52. Matsumiya M, Tomita T, Yoshioka-Kobayashi K, Isomura A, Kageyama R: **ES cell-derived presomitic mesoderm-like tissues for analysis of synchronized oscillations in the segmentation clock**. *Development* 2018, **145**:dev156836.

53. Chu LF, Mamott D, Ni Z, Bacher R, Liu C, Swanson S, Kendziorski C, Stewart R, Thomson JA: **An In Vitro Human Segmentation Clock Model Derived from Embryonic Stem Cells**. *Cell Rep* 2019, **28**:2247-2255.e5.

54. Takashima Y, Ohtsuka T, González A, Miyachi H, Kageyama R: **Intronic delay is essential for oscillatory expression in the segmentation clock**. *Proc Natl Acad Sci U S A* 2011, **108**:3300–3305.

55. Tsiairis CD, Aulehla A: **Self-Organization of Embryonic Genetic Oscillators into Spatiotemporal Wave Patterns**. *Cell* 2016, **164**:656–667.

56. Webb AB, Lengyel IM, Jörg DJ, Valentin G, Jülicher F, Morelli LG, Oates AC: **Persistence, period and precision of autonomous cellular oscillators from the zebrafish segmentation clock**. *Elife* 2016, **5**.

57. Matsuda M, Hayashi H, Garcia-Ojalvo J, Yoshioka-Kobayashi K, Kageyama R, Yamanaka Y, Ikeya M, Toguchida J, Alev C, Ebisuya M: **Species-specific segmentation clock periods are due to differential biochemical reaction speeds.** *Science* 2020, **369**:1450–1455.

58. Iwata R, Vanderhaeghen P: **Metabolic mechanisms of species-specific developmental tempo**. *Dev Cell* 2024, **59**:1628–1639.

59. Rayon T, Stamataki D, Perez-Carrasco R, Garcia-Perez L, Barrington C, Melchionda M, Exelby K, Lazaro J, Tybulewicz VLJ, Fisher EMC, et al.: **Species-specific pace of development is associated with differences in protein stability**. *Science* 2020, **369**:eaba7667.

60. Iwata R: **Temporal differences of neurodevelopment processes between species**. *Neurosci Res* 2022, **177**:8–15.

61. Davis-Dusenbery BN, Williams LA, Klim JR, Eggan K: **How to make spinal motor neurons**. *Development* 2014, **141**:491–501.

62. Linaro D, Vermaercke B, Iwata R, Ramaswamy A, Libé-Philippot B, Boubakar L, Davis BA, Wierda K, Davie K, Poovathingal S, et al.: **Xenotransplanted Human Cortical Neurons Reveal Species-Specific Development and Functional Integration into Mouse Visual Circuits**. *Neuron* 2019, **104**:972-986.e6.

63. Barry C, Schmitz MT, Jiang P, Schwartz MP, Duffin BM, Swanson S, Bacher R, Bolin JM, Elwell AL, McIntosh BE, et al.: **Species-specific developmental timing is maintained by pluripotent stem cells ex utero**. *Dev Biol* 2017, **423**:101–110.

64. Fuhrmann JF, Buono L, Adelmann L, Martinez-Morales JR, Centanin L: **Genetic developmental timing revealed by inter-species transplantations in fish**. *Dev* 2020, **147**.

65. Hall J, Jheon AH, Ealba EL, Eames BF, Butcher KD, Mak SS, Ladher R, Alliston T, Schneider RA: **Evolution of a developmental mechanism: species-specific regulation of the cell cycle and the timing of events during craniofacial osteogenesis**. *Dev Biol* 2014, **385**:380.

66. Dady A, Davidson L, Halley PA, Storey KG: **Human spinal cord in vitro differentiation pace is initially maintained in heterologous embryonic environments**. *Elife* 2022, **11**:e67283.

67. Brown J, Barry C, Schmitz MT, Argus C, Bolin JM, Schwartz MP, van Aartsen A, Steill J, Swanson S, Stewart R, et al.: **Interspecies chimeric conditions affect the developmental rate of human pluripotent stem cells**. *PLoS Comput Biol* 2021, **17**:e1008778.

68. Busby L, Nájera GS, Steventon BJ: **Intrinsic and extrinsic cues time somite progenitor contribution to the vertebrate primary body axis**. *Elife* 2024, **13**:e90499.

69. Guantes R, Rastrojo A, Neves R, Lima A, Aguado B, Iborra FJ: **Global variability in gene expression and alternative splicing is modulated by mitochondrial content**. *Genome Res* 2015, **25**:633–644.

70. Johnston IG, Gaal B, das Neves RP, Enver T, Iborra FJ, Jones NS: **Mitochondrial Variability as a Source of Extrinsic Cellular Noise**. *PLOS Comput Biol* 2012, **8**:e1002416.

71. Diaz-Cuadros M, Miettinen TP, Skinner OS, Sheedy D, Díaz-García CM, Gapon S, Hubaud A, Yellen G, Manalis SR, Oldham WM, et al.: **Metabolic regulation of species-specific developmental rates**. *Nature* 2023, **613**:550–557.

72. Bulusu V, Prior N, Snaebjornsson MT, Kuehne A, Sonnen KF, Kress J, Stein F, Schultz C, Sauer U, Aulehla A: **Spatiotemporal Analysis of a Glycolytic Activity Gradient Linked to Mouse Embryo Mesoderm Development**. *Dev Cell* 2017, **40**:331.

73. Miyazawa H, Snaebjornsson MT, Prior N, Kafkia E, Hammarén HM, Tsuchida-Straeten N, Patil KR, Beck M, Aulehla A: **Glycolytic flux-signaling controls mouse embryo mesoderm development**. *Elife* 2022, **11**:e83299.

74. Miyazawa H, Rada J, Gerald P, Sanchez L, Esposito E, Bunina D, Girardot C, Zaugg J, Aulehla A: **Glycolysis-Wnt signaling axis tunes developmental timing of embryo segmentation**. *bioRxiv* 2024, doi:10.1101/2024.01.22.576629.

75. Oginuma M, Moncuquet P, Xiong F, Karoly E, Chal J, Guevorkian K, Pourquié O: **A gradient of glycolytic activity coordinates FGF and Wnt signaling during elongation of the body axis in amniote embryos**. *Dev Cell* 2017, **40**:342.

76. Marchetto MC, Hrvoj-Mihic B, Kerman BE, Yu DX, Vadodaria KC, Linker SB, Narvaiza I, Santos R, Denli AM, Mendes APD, et al.: **Species-specific maturation profiles of human, chimpanzee and bonobo neural cells**. *Elife* 2019, **8**:e37527.

77. Otani T, Marchetto MC, Gage FH, Simons BD, Livesey FJ: **2D and 3D Stem Cell Models of Primate Cortical Development Identify Species-Specific Differences in Progenitor Behavior Contributing to Brain Size**. *Cell Stem Cell* 2016, **18**:467–480.

78. Iwata R, Casimir P, Erkol E, Boubakar L, Planque M, Gallego López IM, Ditkowska M, Gaspariunaite V, Beckers S, Remans D, et al.: **Mitochondria metabolism sets the species-specific tempo of neuronal development**. *Science* 2023, **379**:eabn4705.

79. Casimir P, Iwata R, Vanderhaeghen P: **Linking mitochondria metabolism, developmental timing, and human brain evolution**. *Curr Opin Genet Dev* 2024, **86**:102182.

80. Miyazawa H, Aulehla A: **Revisiting the role of metabolism during development**. *Development* 2018, **145**:dev131110.

81. Ciceri G, Baggiolini A, Cho HS, Kshirsagar M, Benito-Kwiecinski S, Walsh RM, Aromolaran KA, Gonzalez-Hernandez AJ, Munguba H, Koo SY, et al.: **An epigenetic barrier sets the timing of human neuronal maturation**. *Nature* 2024, **626**:881–890.

82. Hergenreder E, Minotti AP, Zorina Y, Oberst P, Zhao Z, Munguba H, Calder EL, Baggiolini A, Walsh RM, Liston C, et al.: **Combined small-molecule treatment accelerates maturation of human pluripotent stem cell-derived neurons**. *Nat Biotechnol 2024* 2024, doi:10.1038/s41587-023-02031-z.

83. Xue L, Cai JY, Ma J, Huang Z, Guo MX, Fu LZ, Shi YB, Li WX: **Global expression profiling reveals genetic programs underlying the developmental divergence between mouse and human embryogenesis**. *BMC Genomics* 2013, **14**:568.

84. Butler H, Juurlink BHJ: *An Atlas for Staging Mammalian and Chick Embryos*. CRC Press, Inc.; 1987.

85. Rayon T, Briscoe J: **Cross-species comparisons and *in vitro* models to study tempo in development and homeostasis**. *Interface Focus* 2021, **11**:rsfs.2020.0069.

86. Martin RD, Genoud M, Hemelrijk CK: **Problems of allometric scaling analysis: Examples from mammalian reproductive biology**. *J Exp Biol* 2005, **208**:1731–1747.

87. Halley AC: **The Tempo of Mammalian Embryogenesis: Variation in the Pace of Brain and Body Development**. *Brain Behav Evol* 2022, **97**:96.

88. Pianka ER: **On r- and K-Selection**. *Am Nat* 1970, **104**:592–597.

89. Kleiber M: **Body size and metabolic rate**. *Physiol Rev* 1947, **27**:511–541.

90. West GB, Woodruff WH, Brown JH: **Allometric scaling of metabolic rate from molecules and mitochondria to cells and mammals**. *Proc Natl Acad Sci U S A* 2002, **99**:2473–2478.

91. Schmidt-Nielsen K: *Scaling, why is animal size so important?* Cambridge University Press; 1984.

92. West GB, Brown JH: **The origin of allometric scaling laws in biology from genomes to ecosystems: towards a quantitative unifying theory of biological structure and organization**. *J Exp Biol* 2005, **208**:1575–1592.

93. Zhu J, Thompson CB: **Metabolic regulation of cell growth and proliferation**. *Nat Rev Mol Cell Biol 2019 207* 2019, **20**:436–450.

94. West GB, Brown JH, Enquist BJ: **A general model for the origin of allometric scaling laws in biology**. *Science* 1997, **276**:122–126.

95. Brown MF, Gratton TP, Stuart JA: **Metabolic rate does not scale with body mass in cultured mammalian cells**. *Am J Physiol Regul Integr Comp Physiol* 2007, **292**:R2115-21.

96. Udan RS, Culver JC, Dickinson ME: **Understanding vascular development**. *Wiley Interdiscip Rev Dev Biol* 2013, **2**:327–46.

97. Takahashi K, Yamanaka S: **Induction of Pluripotent Stem Cells from Mouse Embryonic and Adult Fibroblast Cultures by Defined Factors**. *Cell* 2006, **126**:663–676.

98. Takahashi K, Tanabe K, Ohnuki M, Narita M, Ichisaka T, Tomoda K, Yamanaka S: **Induction of pluripotent stem cells from adult human fibroblasts by defined factors**. *Cell* 2007, **131**:861–872.

99. Shi Y, Inoue H, Wu JC, Yamanaka S: **Induced pluripotent stem cell technology: a decade of progress**. *Nat Rev Drug Discov* 2016, **16**:115–130.

100. Friedrich Ben-Nun I, Montague SC, Houck ML, Tran HT, Garitaonandia I, Leonardo TR, Wang YC, Charter SJ, Laurent LC, Ryder OA, et al.: **Induced pluripotent stem cells from highly endangered species**. *Nat Methods* 2011, **8**:829–831.

101. Rosselló RA, Chen CC, Dai R, Howard JT, Hochgeschwender U, Jarvis ED: **Mammalian genes induce partially reprogrammed pluripotent stem cells in non-mammalian vertebrate and invertebrate species**. *Elife* 2013, **2**:e00036.

102. Lu Y, West FD, Jordan BJ, Mumaw JL, Jordan ET, Gallegos-Cardenas A, Beckstead RB, Stice SL: **Avian-induced pluripotent stem cells derived using human reprogramming factors**. *Stem Cells Dev* 2012, **21**:394–403.

103. Benito-Kwiecinski S, Giandomenico SL, Sutcliffe M, Riis ES, Freire-Pritchett P, Kelava I, Wunderlich S, Martin U, Wray GA, McDole K, et al.: **An early cell shape transition drives evolutionary expansion of the human forebrain**. *Cell* 2021, **184**:2084-2102.e19.

104. Kanton S, Boyle MJ, He Z, Santel M, Weigert A, Sanchís-Calleja F, Guijarro P, Sidow L, Fleck JS, Han D, et al.: **Organoid single-cell genomic atlas uncovers human-specific features of brain development**. *Nature* 2019, **574**:418–422.

105. Pollen AA, Bhaduri A, Andrews MG, Nowakowski TJ, Meyerson OS, Mostajo-Radji MA, Di Lullo E, Alvarado B, Bedolli M, Dougherty ML, et al.: **Establishing Cerebral Organoids as Models of Human-Specific Brain Evolution**. *Cell* 2019, **176**:743-756.e17.

106. Mora-Bermúdez F, Badsha F, Kanton S, Camp JG, Vernot B, Köhler K, Voigt B, Okita K, Maricic T, He Z, et al.: **Differences and similarities between human and chimpanzee neural progenitors during cerebral cortex development**. *Elife* 2016, **5**:e18683.

107. Agoglia RM, Sun D, Birey F, Yoon S-J, Miura Y, Sabatini K, Pașca SP, Fraser HB: **Primate cell fusion disentangles gene regulatory divergence in neurodevelopment**. *Nature* 2021, **592**:421–427.

108. Sugimoto M, Kondo M, Koga Y, Shiura H, Ikeda R, Hirose M, Ogura A, Murakami A, Yoshiki A, De Sousa Lopes SMC, et al.: **A simple and robust method for establishing homogeneous mouse epiblast stem cell lines by wnt inhibition**. *Stem cell reports* 2015, **4**:744–757.

109. Honda A, Hirose M, Hatori M, Matoba S, Miyoshi H, Inoue K, Ogura A: **Generation of induced pluripotent stem cells in rabbits: Potential experimental models for human regenerative medicine**. *J Biol Chem* 2010, **285**:31362–31369.

110. Bogliotti YS, Wu J, Vilarino M, Okamura D, Soto DA, Zhong C, Sakurai M, Sampaio RV, Suzuki K, Izpisua Belmonte JC, et al.: **Efficient derivation of stable primed pluripotent embryonic stem cells from bovine blastocysts**. *Proc Natl Acad Sci U S A* 2018, **115**:2090–2095.

111. Hildebrandt TB, Hermes R, Colleoni S, Diecke S, Holtze S, Renfree MB, Stejskal J, Hayashi K, Drukker M, Loi P, et al.: **Embryos and embryonic stem cells from the white rhinoceros**. *Nat Commun* 2018, **9**:1–9.

112. Petkov S, Dressel R, Rodriguez-Polo I, Behr R: **Controlling the Switch from Neurogenesis to Pluripotency during Marmoset Monkey Somatic Cell Reprogramming with Self-Replicating mRNAs and Small Molecules**. *Cells* 2020, **9**:2422.

113. Hofmann M, Schuster-Gossler K, Watabe-Rudolph M, Aulehla A, Herrmann BG, Gossler A: **WNT signaling, in synergy with T/TBX6, controls Notch signaling by regulating Dll1 expression in the presomitic mesoderm of mouse embryos**. *Genes Dev* 2004, **18**:2712–2717.

114. Tam PPL: **The control of somitogenesis in mouse embryos**. *Development* 1981, **65**:103–128.

115. Bessho Y, Sakata R, Komatsu S, Shiota K, Yamada S, Kageyama R: **Dynamic expression and essential functions of Hes7 in somite segmentation**. *Genes Dev* 2001, **15**:2642–7.

116. Phillips IR: **The embryology of the common marmoset (Callithrix jacchus).** *Adv Anat Embryol Cell Biol* 1976, **52**:3–47.

117. Naya M, Kito Y, Eto K, Deguchi T: **Development of Rabbit Whole Embryo Culture during Organogenesis**. *Congenit Anom (Kyoto)* 1991, **31**:153–156.

118. Haldiman JT: **Bovine Somite Development and Vertebral Anlagen Establishment***. *Anat Histol Embryol* 1981, **10**:289–309.

119. Chambers PL, Hearn JP: **Embryonic, foetal and placental development in the Common marmoset monkey (Callithrix jacchus)**. *J Zool* 1985, **207**:545–561.

120. Derrickson EM: **Comparative Reproductive Strategies of Altricial and Precocial Eutherian Mammals**. *Funct Ecol* 1992, **6**:57.

121. Luker GD, Pica CM, Song J, Luker KE, Piwnica-Worms D: **Imaging 26S proteasome activity and inhibition in living mice**. *Nat Med 2003 97* 2003, **9**:969–973.

122. Matsuda M, Hammaren HM, Lazaro J, Savitski MM, Ebisuya M: **Systematic analysis of protein stability associated with species-specific developmental tempo**. *bioRxiv* 2024, doi:10.1101/2024.06.07.597977.

123. Wu M, Neilson A, Swift AL, Moran R, Tamagnine J, Parslow D, Armistead S, Lemire K, Orrell J, Teich J, et al.: **Multiparameter metabolic analysis reveals a close link between attenuated mitochondrial bioenergetic function and enhanced glycolysis dependency in human tumor cells**. *Am J Physiol - Cell Physiol* 2007, **292**:125–136.

124. Sudmant PH, Alexis MS, Burge CB: **Meta-analysis of RNA-seq expression data across species, tissues and studies**. *Genome Biol* 2015, **16**:1–11.

125. Gossen M, Bujard H: **Tight control of gene expression in mammalian cells by tetracycline-responsive promoters**. *Proc Natl Acad Sci U S A* 1992, **89**:5547–5551.

126. Khmelinskii A, Keller PJ, Bartosik A, Meurer M, Barry JD, Mardin BR, Kaufmann A, Trautmann S, Wachsmuth M, Pereira G, et al.: **Tandem fluorescent protein timers for in vivo analysis of protein dynamics**. *Nat Biotechnol* 2012, **30**:708–714.

127. Hug N, Longman D, Cáceres JF: **Mechanism and regulation of the nonsense-mediated decay pathway**. *Nucleic Acids Res* 2016, **44**:1483.

128. Matsuda M, Lazaro J, Ebisuya M: **Metabolic activities are selective modulators for individual segmentation clock processes**. *bioRxiv* 2024, doi:10.1101/2024.06.04.597451.

129. Yang X, Boehm JS, Yang X, Salehi-Ashtiani K, Hao T, Shen Y, Lubonja R, Thomas SR, Alkan O, Bhimdi T, et al.: **A public genome-scale lentiviral expression library of human ORFs**. *Nat Methods* 2011, **8**:659–661.

130. Ay A, Knierer S, Sperlea A, Holland J, Özbudak EM: **Short-lived her proteins drive robust synchronized oscillations in the Zebrafish segmentation clock**. *Development* 2013, **140**:3244–3253.

131. Love MI, Huber W, Anders S: **Moderated estimation of fold change and dispersion for RNA-seq data with DESeq2**. *Genome Biol* 2014, **15**:1–21.

132. Fernandes MO, Tourtellotte WG: **Egr3-Dependent Muscle Spindle Stretch Receptor Intrafusal Muscle Fiber Differentiation and Fusimotor Innervation Homeostasis**. *J Neurosci* 2015, **35**:5566–78.

133. Morris ME, Viswanathan N, Kuhlman S, Davis FC, Weitz CJ: **A Screen for Genes Induced in the Suprachiasmatic Nucleus by Light**. *Science* 1998, **279**:1544–1547.

134. Larrieu D, Ythier D, Brambilla C, Pedeux R: **ING2 controls the G1 to S-phase transition by regulating p21 expression**. *Cell Cycle* 2010, **9**:3984–3990.

135. Stahl WR: **Scaling of respiratory variables in mammals**. *J Appl Physiol* 1967, **22**:453–460.

136. Kohajda Z, Loewe A, Tóth N, Varró A, Nagy N: **The Cardiac Pacemaker Story—Fundamental Role of the Na+/Ca2+ Exchanger in Spontaneous Automaticity**. *Front Pharmacol* 2020, **11**:516.

137. Wiesinger A, Li J, Fokkert L, Bakker P, Verkerk AO, Christoffels VM, Boink GJJ, Devalla HD: **A single cell transcriptional roadmap of human pacemaker cell differentiation**. *Elife* 2022, **11**:e76781.

138. Protze SI, Liu J, Nussinovitch U, Ohana L, Backx PH, Gepstein L, Keller GM: **Sinoatrial node cardiomyocytes derived from human pluripotent cells function as a biological pacemaker**. *Nat Biotechnol 2016 351* 2016, **35**:56–68.

139. Engel JL, Zhang X, Lu DR, Vila OF, Arias V, Lee J, Hale C, Hsu Y-H, Li C-M, Wu RS, et al.: **Single Cell Multi-Omics of an iPSC Model of Human Sinoatrial Node Development Reveals Genetic Determinants of Heart Rate and Arrhythmia Susceptibility**. *bioRxiv* 2023, doi:10.1101/2023.07.01.547335.

140. Seleit A, Brettell I, Fitzgerald T, Vibe C, Loosli F, Wittbrodt J, Naruse K, Birney E, Aulehla A: **Modular control of time and space during vertebrate axis segmentation**. *bioRxiv* 2023, doi:10.1101/2023.08.30.555457.

141. Wu J, Platero-Luengo A, Sakurai M, Sugawara A, Gil MA, Yamauchi T, Suzuki K, Bogliotti YS, Cuello C, Morales Valencia M, et al.: **Interspecies Chimerism with Mammalian Pluripotent Stem Cells**. *Cell* 2017, **168**:473-486.e15.

142. Williams SA, Spear JK, Petrullo L, Goldstein DM, Lee AB, Peterson AL, Miano DA, Kaczmarek EB, Shattuck MR: **Increased variation in numbers of presacral vertebrae in suspensory mammals**. *Nat Ecol Evol 2019 36* 2019, **3**:949–956.

143. Richardson MK, Allen SP, Wright GM, Raynaud A, Hanken J: **Somite number and vertebrate evolution**. *Development* 1998, **125**:151–160.

144. Keyte A, Smith KK: **Heterochrony in somitogenesis rate in a model marsupial, Monodelphis domestica**. *Evol Dev* 2012, **14**:93–103.

145. Keyte AL, Smith KK: **Developmental origins of precocial forelimbs in marsupial neonates**. *Development* 2010, **137**:4283–4294.

146. Chew KY, Shaw G, Yu H, Pask AJ, Renfree MB: **Heterochrony in the regulation of the developing marsupial limb**. *Dev Dyn* 2014, **243**:324–338.

147. Kumar S, De Leon EM, Granados J, Whitworth DJ, VandeBerg JL: **Monodelphis domestica Induced Pluripotent Stem Cells Reveal Metatherian Pluripotency Architecture**. *Int J Mol Sci* 2022, **23**:12623.

148. Nakanoh S, Stamataki D, Garcia-Perez L, Azzi C, Carr HL, Pokhilko A, Howell S, Yu L, Skehel M, Oxley D, et al.: **Protein degradation shapes developmental tempo in mouse and human neural progenitors**. *bioRxiv* 2024, doi:10.1101/2024.08.01.604391.

149. Swovick K, Firsanov D, Welle KA, Hryhorenko JR, Wise JP, George C, Sformo TL, Seluanov A, Gorbunova V, Ghaemmaghami S: **Interspecies Differences in Proteome Turnover Kinetics Are Correlated With Life Spans and Energetic Demands**. *Mol Cell Proteomics* 2021, **20**:100041.

150. Swovick K, Welle KA, Hryhorenko JR, Seluanov A, Gorbunova V, Ghaemmaghami S: **Cross-species Comparison of Proteome Turnover Kinetics**. *Mol Cell Proteomics* 2018, **17**:580–591.

151. Debès C, Papadakis A, Grönke S, Karalay Ö, Tain LS, Mizi A, Nakamura S, Hahn O, Weigelt C, Josipovic N, et al.: **Ageing-associated changes in transcriptional elongation influence longevity**. *Nature* 2023, **616**:814–821.

152. Basier C, Nurse P: **The cell cycle and cell size influence the rates of global cellular translation and transcription in fission yeast**. *EMBO J* 2023, **42**:e113333.

153. Liu S, Tan C, Melo-Gavin C, Mark KG, Ginzberg MB, Blutrich R, Patel N, Rape M, Kafri R: **Large cells activate global protein degradation to maintain cell size homeostasis**. *bioRxiv* 2021, doi:10.1101/2021.11.09.467936.

154. Neurohr GE, Terry RL, Lengefeld J, Bonney M, Brittingham GP, Moretto F, Miettinen TP, Vaites LP, Soares LM, Paulo JA, et al.: **Excessive Cell Growth Causes Cytoplasm Dilution And Contributes to Senescence**. *Cell* 2019, **176**:1083-1097.e18.

155. Taylor AN, Mueller RL, Prasad A: **Amphibian segmentation clock models suggest mechanisms of slowed development across increasing genome size and nuclear volume**. *bioRxiv* 2023, doi:10.1101/2023.07.16.549220.

156. Yahya G, Menges P, Amponsah PS, Ngandiri DA, Schulz D, Wallek A, Kulak N, Mann M, Cramer P, Savage V, et al.: **Sublinear scaling of the cellular proteome with ploidy**. *Nat Commun 2022 131* 2022, **13**:1–13.

157. Cadart C, Bartz J, Oaks G, Liu MZ, Heald R: **Polyploidy in Xenopus lowers metabolic rate by decreasing total cell surface area**. *Curr Biol* 2023, **33**:1744-1752.e7.

158. Budirahardja Y, Gönczy P: **Coupling the cell cycle to development**. *Development* 2009, **136**:2861–2872.

159. Primmett DRN, Norris WE, Carlson GJ, Keynes RJ, Stern CD: **Periodic segmental anomalies induced by heat shock in the chick embryo are associated with the cell cycle**. *Development* 1989, **105**:119–130.

160. Eastman AE, Chen X, Hu X, Hartman AA, Pearlman Morales AM, Yang C, Lu J, Kueh HY, Guo S: **Resolving Cell Cycle Speed in One Snapshot with a Live-Cell Fluorescent Reporter**. *Cell Rep* 2020, **31**:107804.

161. Zhang L, Kendrick C, Jülich D, Holley SA: **Cell cycle progression is required for zebrafish somite morphogenesis but not segmentation clock function**. *Development* 2008, **135**:2065.

162. Ambros V, Horvitz HR: **Heterochronic mutants of the nematode Caenorhabditis elegans**. *Science* 1984, **226**:409–416.

163. Reinhart BJ, Slack FJ, Basson M, Pasquienelll AE, Bettlnger JC, Rougvle AE, Horvitz HR, Ruvkun G: **The 21-nucleotide let-7 RNA regulates developmental timing in Caenorhabditis elegans**. *Nature* 2000, **403**:901–906.

164. Monsalve GC, Van Buskirk C, Frand AR: **LIN-42/PERIOD Controls Cyclical and Developmental Progression of C. elegans Molts**. *Curr Biol* 2011, **21**:2033–2045.

165. Collart C, Allen GE, Bradshaw CR, Smith JC, Zegerman P: **Titration of four replication factors is essential for the Xenopus laevis midblastula transition**. *Science* 2013, **341**:893–896.

166. Zhu M, Cornwall-Scoones J, Wang P, Handford CE, Na J, Thomson M, Zernicka-Goetz M: **Developmental clock and mechanism of de novo polarization of the mouse embryo**. *Science* 2020, **370**:eabd2703.

167. Tadros W, Lipshitz HD: **The maternal-to-zygotic transition: a play in two acts**. *Development* 2009, **136**:3033–3042.

168. Kotsantis P, Silva LM, Irmscher S, Jones RM, Folkes L, Gromak N, Petermann E: **Increased global transcription activity as a mechanism of replication stress in cancer**. *Nat Commun* 2016, **7**:1–13.

169. Burger AM, Seth AK: **The ubiquitin-mediated protein degradation pathway in cancer: therapeutic implications**. *Eur J Cancer* 2004, **40**:2217–2229.

170. Sherr CJ: **Principles of Tumor Suppression**. *Cell* 2004, **116**:235–246.

171. Mills EW, Green R: **Ribosomopathies: There's strength in numbers**. *Science* 2017, **358**:eaan2755.

172. Cheng Z, Mugler CF, Keskin A, Hodapp S, Chan LYL, Weis K, Mertins P, Regev A, Jovanovic M, Brar GA: **Small and Large Ribosomal Subunit Deficiencies Lead to Distinct Gene Expression Signatures that Reflect Cellular Growth Rate**. *Mol Cell* 2019, **73**:36-47.e10.

173. Nakayama KI, Nakayama K: **Ubiquitin ligases: cell-cycle control and cancer**. *Nat Rev Cancer* 2006, **6**:369–381.

174. Tourtellotte WG, Milbrandt J: **Sensory ataxia and muscle spindle agenesis in mice lacking the transcription factor Egr3**. *Nat Genet* 1998, **20**:87–91.

175. Li S, Miao T, Sebastian M, Bhullar P, Ghaffari E, Liu M, Symonds ALJ, Wang P: **The Transcription Factors Egr2 and Egr3 Are Essential for the Control of Inflammation and Antigen-Induced Proliferation of B and T Cells**. *Immunity* 2012, **37**:685–696.

176. Fang F, Shangguan AJ, Kelly K, Wei J, Gruner K, Ye B, Wang W, Bhattacharyya S, Hinchcliff ME, Tourtellotte WG, et al.: **Early Growth Response 3 (Egr-3) Is Induced by Transforming Growth Factor-β and Regulates Fibrogenic Responses**. *Am J Pathol* 2013, **183**:1197–1208.

177. Li L, Yun SH, Keblesh J, Trommer BL, Xiong H, Radulovic J, Tourtellotte WG: **Egr3, a synaptic activity regulated transcription factor that is essential for learning and memory**. *Mol Cell Neurosci* 2007, **35**:76–88.

178. Umemura Y, Koike N, Tsuchiya Y, Watanabe H, Kondoh G, Kageyama R, Yagita K: **Circadian key component CLOCK/BMAL1 interferes with segmentation clock in mouse embryonic organoids**. *Proc Natl Acad Sci U S A* 2022, **119**:e2114083119.

179. Wataya T, Ando S, Muguruma K, Ikeda H, Watanabe K, Eiraku M, Kawada M, Takahashi J, Hashimoto N, Sasai Y: **Minimization of exogenous signals in ES cell culture induces rostral hypothalamic differentiation**. *Proc Natl Acad Sci U S A* 2008, **105**:11796–11801.

180. Woltjen K, Michael IP, Mohseni P, Desai R, Mileikovsky M, Hämäläinen R, Cowling R, Wang W, Liu P, Gertsenstein M, et al.: **PiggyBac transposition reprograms fibroblasts to induced pluripotent stem cells**. *Nature* 2009, **458**:766–770.

181. McWilliam H, Li W, Uludag M, Squizzato S, Park YM, Buso N, Cowley AP, Lopez R: **Analysis Tool Web Services from the EMBL-EBI**. *Nucleic Acids Res* 2013, **41**:W597–W600.

182. Waterhouse AM, Procter JB, Martin DMA, Clamp M, Barton GJ: **Jalview Version 2—a multiple sequence alignment editor and analysis workbench**. *Bioinformatics* 2009, **25**:1189–1191.

183. Mönke G, Sorgenfrei FA, Schmal C, Granada AE: **Optimal time frequency analysis for biological data - pyBOAT**. *bioRxiv* 2020, doi:10.1101/2020.04.29.067744.

184. Upham NS, Esselstyn JA, Jetz W: **Inferring the mammal tree: Species-level sets of phylogenies for questions in ecology, evolution, and conservation**. *PLOS Biol* 2019, **17**:e3000494.

185. Schindelin J, Arganda-Carreras I, Frise E, Kaynig V, Longair M, Pietzsch T, Preibisch S, Rueden C, Saalfeld S, Schmid B, et al.: **Fiji: an open-source platform for biological-image analysis**. *Nat Methods* 2012, **9**:676–682.

186. Picelli S, Faridani OR, Björklund ÅK, Winberg G, Sagasser S, Sandberg R: **Full-length RNA-seq from single cells using Smart-seq2**. *Nat Protoc* 2014, **9**:171–181.

187. Afgan E, Baker D, Batut B, Van Den Beek M, Bouvier D, Ech M, Chilton J, Clements D, Coraor N, Grüning BA, et al.: **The Galaxy platform for accessible, reproducible and collaborative biomedical analyses: 2018 update**. *Nucleic Acids Res* 2018, **46**:W537–W544.

188. Dobin A, Davis CA, Schlesinger F, Drenkow J, Zaleski C, Jha S, Batut P, Chaisson M, Gingeras TR: **STAR: ultrafast universal RNA-seq aligner**. *Bioinformatics* 2013, **29**:15–21.

189. Ewels P, Magnusson M, Lundin S, Käller M: **MultiQC: summarize analysis results for multiple tools and samples in a single report**. *Bioinformatics* 2016, **32**:3047–3048.

190. Hayashi M, Zywitza V, Naitou Y, Hamazaki N, Goeritz F, Hermes R, Holtze S, Lazzari G, Galli C, Stejskal J, et al.: **Robust induction of primordial germ cells of white rhinoceros on the brink of extinction**. *Sci Adv* 2022, **8**:eabp9683.

191. Smid M, Coebergh van den Braak RRJ, van de Werken HJG, van Riet J, van Galen A, de Weerd V, van der Vlugt-Daane M, Bril SI, Lalmahomed ZS, Kloosterman WP, et al.: **Gene length corrected trimmed mean of M-values (GeTMM) processing of RNA-seq data performs similarly in intersample analyses while improving intrasample comparisons**. *BMC Bioinformatics* 2018, **19**:1–13.

192. Robinson MD, McCarthy DJ, Smyth GK: **edgeR: a Bioconductor package for differential expression analysis of digital gene expression data**. *Bioinformatics* 2010, **26**:139.

193. Patro R, Duggal G, Love MI, Irizarry RA, Kingsford C: **Salmon provides fast and bias-aware quantification of transcript expression**. *Nat Methods* 2017, **14**:417–419.

194. Wu T, Hu E, Xu S, Chen M, Guo P, Dai Z, Feng T, Zhou L, Tang W, Zhan L, et al.: **clusterProfiler 4.0: A universal enrichment tool for interpreting omics data**. *Innovation* 2021, **2**:100141.

195. Subramanian A, Tamayo P, Mootha VK, Mukherjee S, Ebert BL, Gillette MA, Paulovich A, Pomeroy SL, Golub TR, Lander ES, et al.: **Gene set enrichment analysis: A knowledge-based approach for interpreting genome-wide expression profiles**. *Proc Natl Acad Sci U S A* 2005, **102**:15545–15550.

196. Liberzon A, Subramanian A, Pinchback R, Thorvaldsdóttir H, Tamayo P, Mesirov JP: **Molecular signatures database (MSigDB) 3.0**. *Bioinformatics* 2011, **27**:1739–1740.

197. Shannon P, Markiel A, Ozier O, Baliga NS, Wang JT, Ramage D, Amin N, Schwikowski B, Ideker T: **Cytoscape: a software environment for integrated models of biomolecular interaction networks**. *Genome Res* 2003, **13**:2498–2504.

198. Merico D, Isserlin R, Stueker O, Emili A, Bader GD: **Enrichment map: a network-based method for gene-set enrichment visualization and interpretation**. *PLoS One* 2010, **5**.

199. Theiler K: *The House Mouse*. Springer-Verlag; 1989.

200. Beaudoin S, Barbet P, Bargy F: **Developmental stages in the rabbit embryo: guidelines to choose an appropriate experimental model**. *Fetal Diagn Ther* 2003, **18**:422–427.

201. Winters LM, Green WW, Comstock RE: *Prenatal Development of the Bovine*. University of Minnesota; 1942.

202. O'Rahilly R: **Early human development and the chief sources of information on staged human embryos**. *Eur J Obstet Gynecol Reprod Biol* 1979, **9**:273–280.